Polythiophene Transistors as Gas Sensors for Electronic Nose Applications

Frank Jason Liao

Electrical Engineering and Computer Sciences
University of California at Berkeley

Technical Report No. UCB/EECS-2009-174
http://www.eecs.berkeley.edu/Pubs/TechRpts/2009/EECS-2009-174.html

December 16, 2009

Polythiophene Transistors as Gas Sensors for Electronic Nose Sensors

by

Frank Jason Liao

A dissertation submitted in partial satisfaction of the

requirements for the degree of

Doctor of Philosophy

in

Engineering-Electrical Engineering and Computer Sciences

in the

Graduate Division

of the

University of California, Berkeley

Committee in charge:

Professor Vivek Subramanian, Chair
Professor Tsu-Jae King Liu
Professor Jean Fréchet

Fall 2009

Polythiophene Transistors as Gas Sensors

for Electronic Nose Sensors

by

Frank Jason Liao

ABSTRACT

Polythiophene Transistors as Gas Sensors for Electronic Nose Applications

by

Frank Jason Liao

Doctor of Philosophy in Engineering - Electrical Engineering Computer Sciences

University of California, Berkeley

Professor Vivek Subrmanian, Chair

Electronic noses have been studied for decades, but are still relatively uncommon in commercial use because fabricating a gas sensor array, the heart of the electronic nose, is costly and difficult. Commonly, the most difficult part of fabricating a sensor array is integrating the individual sensor elements into one platform, an expensive proposition using current gas sensors like metal oxide devices. Thin film transistors (TFTs) made from polythiophene, an organic semiconductor, stand to be attractive candidates for sensor arrays because they can be easily arrayed with deposition methods like inkjet printing and they have a rich chemistry that can exploited to tune their sensor behavior. The thesis of this work is that functionalized polythiophene TFTs are compelling, and perhaps superior, candidates in sensor arrays for electronic nose applications.

First, polythiophene TFTs are demonstrated to be viable gas sensors. Basic electrical and sensing behavior is introduced and initial metrics and difficulties are addressed. Physical characterizations of polythiophene based gas sensors are carried out using Grazing Incidence X-ray Diffraction (GIXD), X-ray Reflectivity (XRR), and Quartz Crystal Microbalance (QCM) techniques. Novel in situ XRR and QCM measurements have shown, for the first time, the presence of a physical interaction between the gaseous analyte and the sensor film. These physical changes are corroborated and compared with the electrical response. Strategies for engineering better gas sensors are proposed and demonstrated. Using elegant and robust motifs, simple but powerful sensor arrays are fabricated that demonstrate discrimination between analytes even in the presence of mixtures. These arrays are capable of discriminating analytes based on the size and arrangement of their molecules, an important but previously unexplored avenue. Discrimination based on the analyte's functional groups is also presented. Based on these findings, a mechanistic model is also proposed which is consistent with experimental observations and highlights more pathways for engineering better sensor arrays.

DEDICATION

Dedicated to Daniel—friend, brother, and companion,

and to Gloria—spouse, companion, and helpmeet.

TABLE OF CONTENTS

ACKNOWLEDGMENTS

The foremost person who must be acknowledged is my advisor, Vivek Subramanian. Without him, this work would not be here, for it was he who offered me a standing invitation to return to graduate school after I initially withdrew. It was also he who encouraged me and provided moral support during a period of discouragement and directionless research. Therefore, in one sense, the fruition of this work can be attributed to him as much as it can be to me since none of this would have been possible without his support. Not only the work presented here, but much of my academic composition—my research acumen, methodology, communication skills—has come forth from his mentoring and guidance.

Besides Vivek, the contribution from my colleagues must also be acknowledged. For invaluable discussions concerning research, both content and methodology, I gratefully acknowledge Daniel Huang, Steven Volkman, Alejandro de la Fuente Vornbrook, and Paul Chang. In addition, Christopher Chen and Josephine Chang have both made significant contributions to this research project. Christopher worked alongside me as undergraduate researcher in the early days of this project and Josephine took charge of the sensors work during my absence. Besides these, the remaining members of the organic electronics research group, both present and former, have provided the community and support in which this research was conducted. I would also like to thank the support staff in the EECS department, especially Phil Guillory, Joe Donnelly, Alan Briggs, and Ruth Gjerde, for providing precious assistance that often exceeded their professional duty.

Finally, I would like to acknowledge my qualifying exam and dissertation committee members: Tsu-Jae King Liu, Bernhard Boser, Arun Majumdar, and Jean Fréchet. In particular, Tsu-Jae has been a pattern in her professional excellence and commitment to teaching including the undergraduate level as well as her personal character.

Chapter 1 Introduction

Machine olfaction is the use of electronics to simulate the sense of smell. The envisioned realization of this technology is the electronic nose, or e-nose, which is an electronic device that can sense and identify vapors. The promise of the electronic nose has been heralded since the mid to late eighties, with a formal definition published by Gardner and Bartlett in 1994 [1]:

"An electronic nose is an instrument which comprises an array of electronic chemical sensors with partial sensitivity and an appropriate pattern recognition system capable of recognizing simple or complex odors."

Since the eighties there have been many implementations of the electronic nose, but machine olfaction has yet to be realized as a widespread technology with much societal impact. Indeed, the promise of a widespread e-nose technology includes applications ranging from product spoilage detection to environmental and safety monitoring to explosives detection. Unfortunately, most electronic noses today are too expensive to penetrate these exciting areas.

In the late 90s, the cost of commercial electronic noses began to fall with the advent of microfabrication technologies that lead to low-cost integrated sensors [2], but since then prices have plateaued and remained at the same level as in 1998 [3]. While current fabrication techniques have enabled cheaper sensor elements, integration of these sensors into a single array is still a difficult proposition. These techniques rely on subtractive processes which substantially raise the price tag of the sensor array, which generally contain metal oxide sensors that are expensive to integrate onto a common substrate. The key to opening the door to many attractive applications is to lower the cost and specifically, to find a way to fabricate the sensor array much more cheaply. This key may lie in the confluence of two emerging areas of research: additive processing and organic electronics.

Additive processing is the best alternative to fabricate the sensor array since it greatly simplifies the crucial issue of materials integration. The prototypical example of additive processing is solution processing in which the materials of interest are dissolved into solution and subsequently deposited as an 'ink' onto the substrate. This allows the material to be placed on the substrate only where desired and avoids the issue of materials integration since deposited materials have no consequence on what materials are subsequently deposited. Additionally, additive processing is inherently cheaper than subtractive processing because the material is placed in one processing step rather than the several steps that are required in a subtractive approach like photolithography.

Of course additive processing via solution has a major requirement, which is that all the materials must be soluble. This brings in another field of interest, namely organic electronics. Organic electronics refers to carbon-based materials that possess conducting and semiconducting properties depending on the arrangement of bonds within the organic molecules. One of the most attractive features of many of these materials is that they can be processed by solution using printing techniques such as ink-jet or gravure [4-7]. Ink-jet printing of transistors and circuits has been demonstrated by several research groups and is even under commercial development by some companies [6,8].

More importantly, many organic materials exhibit gas sensing behavior. Several common organic semiconductors have been reported to exhibit changes in electrical behavior upon exposure to various organic solvents [9-12]. Research at Bell Labs by Crone et al was among the first to show that several organic transistors showed marked decreases in their on-current upon exposure to various solvents [12]. Additionally, early sections of this thesis provided one of the first demonstrations of the gas sensing behavior of polythiophene based transistors, a popular semiconducting polymer [11]. Furthermore, it may also be possible to tune the sensor behavior of organic materials by exploiting their rich chemistry, an attractive proposition for making sensor arrays. Considering all these factors, organic materials are certainly potential candidates for sensor arrays.

The aim of this thesis is to show that polythiophene is an attractive, if not ideal, candidate for gas sensor arrays to be used in electronic noses. Polythiophene is appealing because it possesses several important qualities of facile integration via solution processing and gas sensing behavior with the possibility of adjusting that behavior. This thesis will take a much more comprehensive approach that is currently lacking in this area of research by investigating the physical interactions during sensing and considering what properties affect the sensing behavior. Based on this understanding, it will show how useful arrays of polythiophene can be engineered, presenting some of the most original data that showcases the possibilities of leveraging the rich chemistry of polythiophene semiconductors for gas sensing.

The thesis begins in Chapter Two with an overview of electronic nose technologies. Along with reviewing the basics of an electronic nose, the historical development and ideal applications will be discussed. This chapter will also discuss commercially available products and current research on electronic noses. Chapter Three introduces organic thin film transistors (OTFTs), specifically polythiophene transistors, and discusses performance issues along with charge transport mechanisms, an important topic when considering gas sensing.

Chapter Four covers in detail the use of organic transistors as gas sensors. The basic behavior of gas sensors will be described as well as the relevant issues and challenges for making robust gas sensors. Previous work on OTFT sensors and mechanisms that have been proposed for the sensor response are also discussed. This chapter presents experimental data demonstrating the gas sensing capabilities of polythiophene transistors. Real-time extraction of multiple device parameters during sensing experiments is used to shed light on the mechanisms of sensor response transduction in OTFTs.

While many groups have since demonstrated the viability of organic materials as gas sensors, much of it is empirically-based and centered on reporting the response of a certain material to a slew of gas molecules; yet, to date, the important question of mechanism remains unanswered. This question is addressed in Chapter Five. Several techniques are employed in order to corroborate the sensor response with measurable and quantifiable changes in the physical films. This chapter will present some novel results showing how the sensing behavior is tied to physical changes in the film by using x-ray techniques.

The understanding gained in previous chapters is then used to design better gas sensors. Chapter Six is about the engineering of sensor arrays. It highlights the relevant parameters which can tune the sensor response and then demonstrates how to achieve discrimination with simple, but powerful, motifs. Different methods of discrimination are covered which are robust enough to be used with mixtures of gases. Many of results in this and preceding chapters are synthesized

into a cohesive framework that includes the sensing mechanism and highlights strategies for improving sensor arrays.

Finally, the thesis concludes with Chapter Seven, which covers future work on organic gas sensors and summarizes the salient points from this work. Appendix A contains some additional GIXD diffraction patterns not included in Chapter Five and because XRR is heavily used in this work, Appendix B presents a more thorough discussion of the basic theory behind the technique.

Chapter 2 The Electronic Nose

With the advent of increasingly powerful electronics technology, great advances have been made in the ability to process digital information. To match these gains in processing power, transduction technologies have also advanced, enabling these digital systems to interact with real-world signals in the environment. Speech recognition, image processing, touch-screens and pressure sensors, are just a few examples. These technologies have enlarged the scope and benefit of electronics. Interestingly, most of these are centered on the basic senses of sound, touch and sight, while taste and smell are usually overlooked. The latter two are closely related and, in fact, the realm of smell is a storehouse of useful information. Odors and smells are ubiquitous and biological olfaction is used everyday from basic functions like survival to evaluating the quality of foodstuffs, beverages, perfumes, and others.

If one doubts the importance of olfaction in society, consider that grain spoilage is still inspected by a human expert who sniffs the grain and rates it with four classifications: Good, Sour, Musty, or COFO (commercially objectionable foreign odor) [1]; that canines continue to be the most reliable and accurate way to detect explosives and narcotics [2]; that air quality, while important to health and comfort, is often poorly assessed; or that odor and aroma, which cannot be assessed in-line during processing or shipping, can completely invalidate consumer products such as foodstuffs, perfumes, sunscreens, carpet, wines, and more [1,3,4]. Odors are repository of useful and important information and besides all these applications there are still untapped areas in early detection of cancer, product spoilage detection and environmental monitoring.

Motivation for and Applications of the Electronic Nose

When considering the applications for machine olfaction, the specific benefits of an electronic nose should be taken into account. While electronic noses are more sophisticated than single sensor elements, the tradeoff with complexity means that single sensors still make sense for a number of applications such as oxygen sensors in automobiles. However, there are a number of exciting applications that are waiting to benefit from electronic noses that have discriminatory powers akin to mammalian olfaction. The best of these applications are those in which single element sensors offer little to no value, yet a functionally superior electronic nose would offer an unprecedented advantage over any existing technology. Examples of these include food spoilage detection, environmental monitoring and explosives detection. The first of these, spoilage detection, will be discussed at length as a motivation for electronic noses since it provides a good framework for discussing the challenges and requirements of a good electronic nose technology.

Food spoilage detection presents a very exciting opportunity for electronic nose technology because, currently, there are no satisfactory methods of detection that can be employed at critical points in the food supply chain. Food spoilage continues to pose an enormous societal burden both in financial terms as a loss of resources, as well as the time and energy invested in producing the foodstuffs and the loss in productivity associated with foodborne illnesses. It is

estimated that 25% of the world's food supply is lost through microbial activity alone [5] (For non-grain staples, such as vegetables and fruits, the World Health Organization believes the loss to be as high as 50% [6].) Food loss occurs throughout the entire supply chain, beginning on the farm and continuing throughout post-harvest storage, distribution, processing, wholesaling, retailing and use in the home and in catering [7]. Meanwhile, the Centers for Disease Control and Infections estimates that foodborne diseases cause approximately 76 million illnesses, 325,000 hospitalizations, and 5,000 deaths in the US each year [8].

While the food industry made great gains in modernization and automation during the latter half of the 20th century, the conventional methods of microbiological testing, on the whole, saw little progress [9]. Though there are over 40 methods to identify and quantify bacterial spoilage in meats [10,11], their effectiveness in detecting food spoilage is minimal because they are focused on identifying pathogens of interest using microbiological methods. These laboratory techniques are not as suited for detection since they are often time consuming, intractable and retrospective. For instance, holding times of eight hours are sometimes required for certain sterilized foods while awaiting the outcome of microbial assessment [12].

Presently the most robust identification methods are these microbiological techniques which involve obtaining a food sample and isolating the pathogen of interest. These methods are based on two different approaches; the first involves immunological techniques and the second is concerned with nucleic acid detections. The most prevalent immunological technique is the enzyme-linked immunosorbent assay (ELISA) and is based on using an enzyme label to find surface antigens of specific bacteria responsible for spoilage or contamination [10]. Of the nucleic acid detection schemes, polymerase chain reaction (PCR) is the most popular route [13]. PCR amplifies specific gene fragments and then identifies them using gel electrophoresis [14-16]. PCR has the advantages of being relatively rapid and selective but it can also introduce false positives since any intact nucleic acid sequences are amplified during the reaction. In addition to identification, quantification is carried by measuring ATP bioluminescence, impedance or using microscopy to count cell colonies [9].

Clearly, none of these techniques are sufficient to detect food spoilage at the processing or consumer level. There is still the need for rapid, in-line detection methods in food process control as well as instruments that could be used by food retailers or consumers. Current in-line methods monitor several parameters including color, using reflectance, or temperature, via infra-red thermometry [12]. The most relevant parameters to spoilage might by pH and humidity, but this is still a rather indirect measurement at best. Gas chromatography has been used for odor analysis and in some processes, gas chromatography olfactometry (GCO) has been tried, which consists of a gas chromatography (GC) instrument with an added sniffing port for the human operator (Fig. 1) [12]. Since GC can only give the chemical analysis of the odor but cannot determine the olfactory impact of the molecules, the sniffing port allows the human operator to determine the quality of the odor. At the retail or consumer level, there is no method except through human olfaction or visual clues such as discoloration or changes in texture.

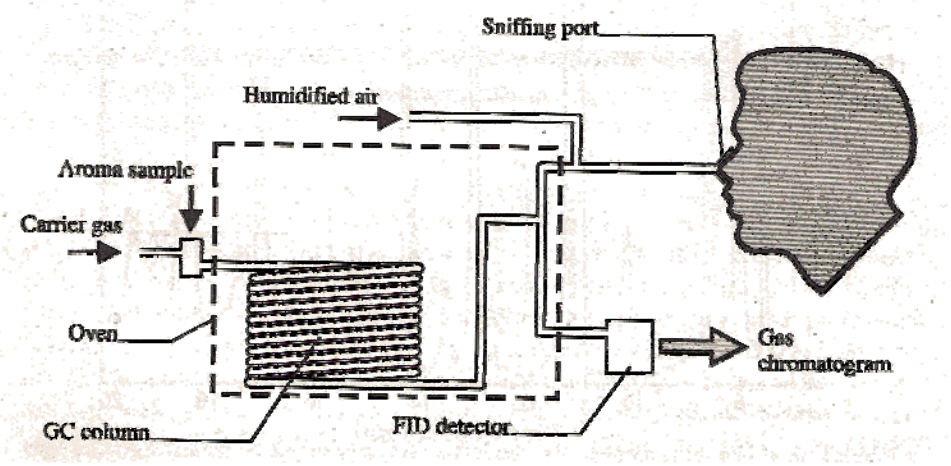

Figure 1. Gas chromatography olfactometry (GCO) configuration. The gas chromatographer accommodates a sniffing port for the human operator. Figure taken from ref [3].

Developing and employing a rapid and accurate method that detects spoilage apart from microbiological techniques poses several challenges. First, food spoilage is a macroscopic phenomenon that describes a whole gambit of microscopic scenarios involving the confluence of several microbial processes, of which there is no unique combination that produces the overall condition of spoilage. Second, within this slew of microbial processes, there is no definable threshold at which spoilage occurs. While spoilage is a categorical term, it is actually describing a whole spectrum of microscopic possibilities. These two challenges, when taken together, constitute a very difficult problem and raise the question of "false positives", cases where the detection method incorrectly designates the food as spoiled. Notice that currently existing methods employing microbiological techniques do not necessarily address these challenges either. In fact, PCR can often introduce false positives because it may amplify certain irrelevant gene fragments. Third, food spoilage varies from foodstuff to foodstuff. Obviously, the microscopic mechanisms of spoilage for meat differ from those for grains and the indicators are different as well. Besides these challenges, there is another important consideration which is cost. For the instrument to be feasible as an in-line tool or at the retail and consumer level, it should not be prohibitively expensive.

Despite these challenges, food spoilage can be detected, as many have demonstrated, by looking for the right "markers", byproducts of physical decay which are produced during the spoilage process [17-22]. In particular, biogenic amines are important markers for many decay processes [23]. Both Dainty *et al* and Edwards *et al* have monitored the concentration levels of two biogenic amines, putrescine and cadavarine, in naturally contaminated beef and found them to be good markers for bacterial metabolism and off-odor formation, respectively [24,25].

The actual markers will depend on the spoilage process. As an example, consider meat products, for which spoilage is major concern at many points throughout the supply chain. Although there are several types of bacteria that can cause spoilage, it turns out only a few species dominate the spoilage process. For refrigerated meat that is or has been exposed to air, the most dominant bacteria is Pseudomonas, a gram-negative bacterium that has evolved to excel

in aerobic environments due to its high affinity for oxygen [26-29]. Pseudomonas also has a competitive advantage because it can convert 2-oxo-gluconate and gluconate, products which are not readily assimilated by other bacteria. Therefore, after endogenous glucose, the first energy source for spoilage bacteria, has been depleted, these alternative carbon sources are reserved entirely for pseudomonas [30,31]. The byproduct of glucose conversion is an extra-cellular matrix, or slime, which aids in the bacteria's attachment to the meat. Pseudomonas has such a competitive advantage in aerobic environments that it can be found in cured meats through processing faults, such as weak vacuum or poor handling. After the carbon sources have been depleted, the dominant Pseudomonas, along with related bacteria, turns to nitrogenous sources, notably amino acids and eventually to lactic acid cause putrefactive types of meat spoilage [32-34]. In some respects, this is the onset of spoilage, at least "sensory" spoilage, since the byproducts of amino acid conversion leads to volatile amines, sulfides, and esters, molecules which are responsible for the malodors associated with spoilage [35,36]. As the decay process continues, larger amines are produced such as putrescine or cadavarine [24,25]. The first of these two aptly named biogenic amines is responsible for the putrid odor associated with decay and the second for the smell of rotting flesh.

Given these challenges, an electronic nose stands to be a very appropriate solution. While "bacterial" spoilage is complex and encompasses many scenarios, "sensory" spoilage, perceived by a human being, is relatively straightforward. This is because the human user is able to integrate and partition many complex signals in order to make a clear assessment of odor. In like manner, an electronic nose with a sensor array and a pattern recognition scheme is most equipped to deal with various scenarios and look for patterns or to cluster similar scenarios.

Another main advantage of the e-nose is that it works through odors, which is the most straightforward and closely aligned with human methods. As GC has shown, chemical analysis is not necessarily equivalent to sensor spoilage and provides no information about the olfactory impact, or flavor quality of the aroma.

Finally, if electronic noses can be made at low cost, they can be employed as in-line tools or perhaps even as embedded sensors in food packaging at the retail or consumer level. Also, if they are cheap, then they can be potentially configurable as needed by using different versions of the sensor arrays where the composition of sensors is different depending on the needs of the applications. Thus it may be possible to have different electronic noses suited for different foodstuffs or for different scenarios for a particular foodstuff. This would be a huge advantage in the relatively daunting arena of spoilage detection.

After introducing the electronic nose with its historical development, the remainder of this chapter will discuss the important components and conclude with a review of the current state of electronic noses in industry and at the research level.

Historical Development of Electronic Noses

Prior to the 1950s, research on machine olfaction was, for all intents and purposes, nonexistent. In 1954, Hartman *et al* reported an electrochemical sensor made from a polished metal wire in contact with the surface of a porous rod saturated with a dilute electrolyte [37]. By using various combinations of metal wires, electrolytes and potential biases, they constructed an array of eight electrochemical cells which gave different patterns to various odorant samples. No

attempt was made to process or interpret these patterns. During the latter half of the twentieth century, improvements in microprocessors and an increasing political awareness of environment and public health issues drove gas sensor research and many types of sensor technologies were explored [38]. These two tracks began to develop and in the early 1980s the concept of an electronic nose began to coalesce. As the processing power and the sensor transduction principles became apparent, the concept of an electronic nose seemed more feasible. The idea of putting an array of sensor transducers together into an intelligent, gas sensor system for odor recognition was first introduced by Persaud and Dodd in 1982 [39], and the term electronic nose was later coined in 1994 by Gardner [38].

The 1990s saw a period of intense research with much early progress. Several demonstrations of early systems were introduced, including electronic noses that were able to distinguish between coffee beans by the country of origin [40] or different vintages of wine [41]. In the mid-1990s, commercial products began to appear first with the MOSES, the IIT Electronic nose, and the Applied Sensor 3300 [42]. Unfortunately, further developments and advances did not continue as strongly and in the early to mid-2000s, electronic noses still remained relatively obscure, save for some niche industries like perfume or tobacco. Today, nanowires and carbon nanotubes as potential sensors suitable for electronic noses have become the subject of ongoing research [43-46].

The Components of an Electronic Nose System

From the 1990s onward, the basic architecture of an electronic nose has remained the same. In discussing the basic components and to frame this discussion, it is helpful to refer back to the definition of the electronic nose given in Chapter One [38]:

"An electronic nose is an instrument which comprises an array of electronic chemical sensors with partial sensitivity and an appropriate pattern recognition system capable of recognizing simple or complex odors."

In essence, the electronic nose is a system composed of two main components: a sensor array plus a computing or processing unit. The sensor array is responsible for the transduction of odors or gases into electronic signals which are then interpreted by the processing component of the e-nose. In addition to these two key components, there are also some peripheral systems which generally include how the gas is sampled and delivered.

Sensor Elements

In a very real sense, the sensor array is the heart of the electronic nose because the sensor elements within the array prescribe the physical limitations of the functionality and the capabilities of the electronic nose. In other words, the transduction power of the nose is only as good as the sensor elements that comprise it. This is one main reason why the experimental work in this thesis has focused so much on understanding and improving the sensor element. Recent decades have shown great gains in computation and it can be expected that further advances will be made, certainly in the area of signal processing; however, the lack of similar advances in making sophisticated and desirable sensor elements continues to hold back the progress of electronic noses.

Metal Oxide Sensors

Metal oxide sensors are the among the earliest and most popular sensor element in sensor arrays [39,47,48]. Indeed, the oxygen sensors used in every automobile are metal oxide sensors. A metal oxide sensor is an n-type inorganic semiconductor, such as tin oxide, doped tin oxide derivatives, zinc oxide, or iron oxide, heated to temperatures of 300 °C to 550 °C and used as a two-terminal resistive device. The response arises from the reduction of the gas species at the surface of the semiconductor which increases the electron carrier concentration, resulting in higher conductivity. Notice that the gas species is consumed as the sensor operates.

The sensor was traditionally constructed by using a ceramic support tube containing a platinum heater coil and the metal oxide is coated onto the outside of the ceramic tube with the appropriate electrical leads connected to the film (Fig. 2). In recent decades, newer implementations of the metal oxide sensor have been constructed with planar configurations using conventional microfabrication techniques [49]. While using microfabrication methods is generally advantageous, there is a significant challenge with integration of multiple sensor elements into a single array. The procedure can be difficult and expensive due to extensive subtractive processes arising from materials compatibility across the different elements.

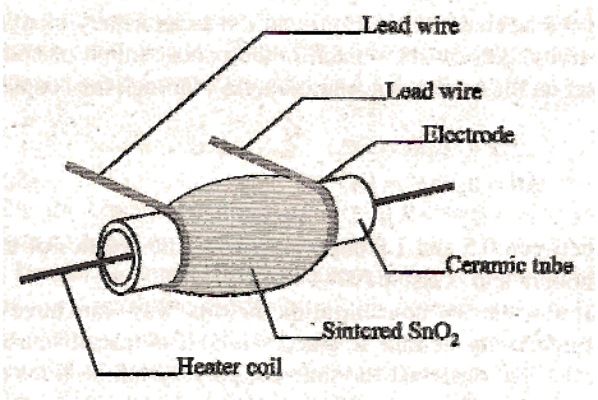

Figure 2. Traditional construction of a metal oxide sensor. Diagram taken from ref [3].

Another disadvantage of the metal oxide is power consumption. Because the sensing response depends directly on the reduction reaction, which is very sensitive to the temperature, the sensor must be heated to at least 300 °C since the reaction is too slow below 200 °C, and resulting power consumption is typically around 800 mW; although with silicon micromachining, Corcoran *et al* demonstrated a planar version with reduced power consumption of 75 mW [49]. Also, another disadvantage includes a general lack of discrimination since the combustion mechanism limits the sensitivity of the device and is not reliant on the chemistry of the gas species itself.

Despite the main disadvantages of power consumption and integration, the metal oxide is by far the most commonly used gas sensor in commercially available electronic noses. The sensor is rugged and rather versatile and is already used in many other industrial settings, such as detecting various gases. Of those that are often used for industrial applications, the tin oxide

sensor doped with palladium or platinum is the most popular. However, if the electronic nose is to be improved or adopted more widely, the use of metal oxides continues to pose a fundamental problem of difficult integration.

Conducting Polymer Sensors

A conducting polymer sensor is based on a polymer material possessing electrical properties that can selectively absorb specific odorants. Exposure to a gas analyte induces changes in the electrical behavior of the sensor. The sensor response arises from intermolecular interactions between the sensor and the analyte. These interactions are the result of hydrogen bonding, dipole-dipole or dipole-induced dipole dispersions, and hydrophobic forces [3]. For this reason, conducting polymer sensor array may be considered the most similar to the olfactory sensor of a biological nose [50].

The most popular materials is poly(pyrrole), which was first prepared electrochemically by Dall'Olio *et al* in 1968 [51]. Figure 3 shows a pyrrole unit and polymer molecule. A key feature of the polymer is the repeating and alternating arrangement of double bonds throughout the molecule; this feature, known as a conjugated pi-electron system, gives rise to the electrical behavior and will be discussed in detail in the next chapter. Reduction and oxidation of the polymer can subsequently modify its charge conducting behavior and it is surmised that the sensor response may result from reduction and oxidation processes or similar interactions involving partial charge transfer [52,53]. Polypyrrole is most often deposited using electrochemical polymerization in order to avoid solvent compatibility issues [54]. The properties of the film are strongly affected by the growth conditions but with careful control, purified and reproducible films can be achieved [3].

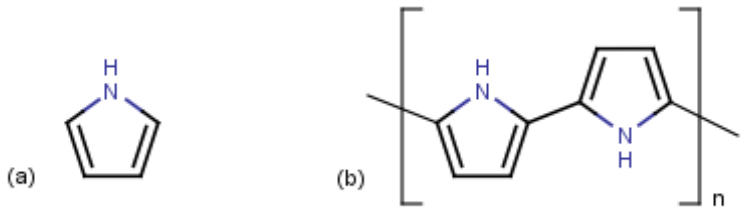

Figure 3. Conducting polymers that are used as gas sensors. (a) A single pyrrole molecule; (b) a polypyrrole molecule

Conducting polymer sensors have several advantages. In general, they respond to a broad range of organic vapors and there is a large spectrum of materials that can be synthesized allowing for a wide range of selectivity [3]. There are synthesized using relatively low cost materials and the sensor element can be fabricated with an attractive form factor. Unlike metal oxide sensor, conducting polymer sensors operate at room temperature, reducing power consumption and providing for longer lifetime [3].

A major disadvantage of a conducting polymer sensor is the susceptibility to poisoning by strongly oxidizing gases [54]. They are also sensitive to humidity and show a long-term drift in

their performance. While their sensitivities are lower than metal-oxide sensors, measurements at the ppm and sub-ppm levl are achievable [55]. Unfortunately they do not display high specificity to individual gases, but they can be chemically tailored to enhance differences to response to classes of molecules. [1]. However overall, sensor elements based conducting polymers have great promise as evidenced by the fact that the first commercially available electronic nose was based on array of conducting polymer gas sensors [3].

The most common implementation of the conducting polymer is the chemiresistor, in which conductivity or resistance is measured. Figure 4 shows the structure of the chemiresistor. The figure makes apparent the greatest advantage of the chemiresistor: its simplicity. Usually gold is used as the electrodes and the final resisitivity depends on the polymer, device geometry and film thickness. It is relatively easy to construct an array of discrete polymer devices. Besides the chemiresistor, other implementations have been demonstrated [3]. One of these, conducting polymer composite sensors, will be discussed later in this chapter and another implementation, a gated field-effect structure, is the major topic of this thesis and will be treated thoroughly in the next chapter.

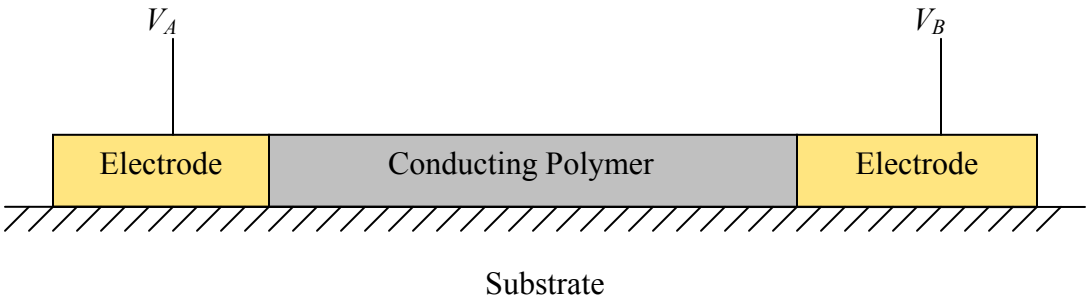

Figure 4. Basic configuration of a chemiresistor. An applied voltage, V_{AB}, is applied to the electrodes. The electrodes may also be located underneath the polymer film.

ChemFET Sensors

Chemically sensitive FET (ChemFET) sensors also employ conducting polymers but in the more traditional paradigm of a field effect transistor. A ChemFET is the structural analog of a MOSFET, with the polysilicon gate replaced with a chemically sensitive layer, usually a specific metal like Palladium [56] or a conductive polymer [57] in the case of gas sensing. The gate is chosen such it reacts with the gaseous species to cause a work function shift that can be detected through FET operation. In the case of metal gate like Palladium, the ChemFET is amenable to microfabrication methods and largely compatible with integrated devices since they are essentially MOSFETs [56], although the range of gases they can respond to are limited. With a conducting polymer as the gate material, there is a wider range of gases that the ChemFET is sensitive to, but fabrication is less straightforward since most polymers are electrochemically deposited.

Piezoelectric Sensors

The last type of sensor element that will be discussed represents an entire category of sensors that are based on piezoelectrics. These sensors rely on mass changes to detect the analyte. The adsorption of the analyte onto the sensor results in a mass change which is registered through the wave velocity or resonant frequency of the sensor. A surface acoustic wave (SAW) device is an example of a piezoelectric sensor that detects changes in its wave velocity. SAW devices typically operate between 30 and 300 MHz [3], higher frequencies than quartz crystals, which rely on changes in its resonant frequency. The sensor is usually coated in order to modulate its selectivity to different gaseous species. While interesting, they have been slow for adoption and since they use similar materials as metal oxide sensors, also suffer from the same issue of integration.

Data Processor

After the sensor array, the data processor is a major part of the electronic nose. The function of the data processor is to not only collect and integrate the responses from the array, but to ultimately recognize and classify the odor. While a single sensor element may respond to the presence of a particular alcohol and a sensor array may reveal the composition of alcohols in a particular sample, but it is the data processing of the electronic nose that ultimately identifies the sample as wine, determines that it is a Merlot, and even judges its freshness. This ability to recognize and classify odors is the hallmark of the electronic nose.

In its complete implementation, the data processor works by collecting and integrating the signals and using pattern recognition techniques to determine the identity of the odor. To carry out odor identification, the data processor employs pattern recognition techniques on the integrated response of the sensor array. Fortunately, modern advances in computing have enabled the use of very sophisticated recognition techniques, including non-parametric techniques with artificial neural networks.

The data processor receives its signals from a front-end preprocessor, whose job is to condition the signals prior to analysis. The preprocessor handles a number of issues with the sensor elements, such as transient responses, background subtraction, or initial transients. Usually the preprocessor will also convert or normalize the signals either using a simple difference, relative difference, or fractional difference technique.

Once the signals are received, the data processor integrates the signals and can interpret them using pattern recognition techniques. These techniques fall into two broad categories. Linear techniques, also known as parametric techniques, are based on statistical analysis and interpret the signals according to residuals and dimensionality. The most popular of these is Principal Component Analysis (PCA), although other schemes such as Cluster Analysis (CA) or Discriminant Function Analysis (DFA) can be used.

PCA works by reducing the dimensionality of the signals. It does this by reconstituting the response as a linear sum of components with the components ordered by the amount variance; in other words, the first component possesses the greatest amount of variance, second the next greatest amount, and so forth. This is done by first normalizing the signals, assuming a normal distribution. (If this assumption is not valid, the analysis can still be carried out as long as the standard deviation is appropriately accounted [58]. In this case, the components are treated more

generally as eigenvectors and they are ordered according to their eigenvalues, with the first eigenvector exhibiting the largest eigenvalue.) Once the signals are normalized, the first component is determined by rotating the signals around the empirical mean in order to find the largest variance, and the process repeats. This essentially reduces the dimensionality of the signals by throwing as much variance into the first few dimensions. Since the remaining dimensions are highly correlated, the response is characterized with a few principal components which can reveal patterns and be used for recognition.

The second category of pattern recognition techniques comprises non-linear methods. These non-linear, or non-parametric, techniques usually employ artificial neural networks that are inspired by the human cognitive process. Though they require some training, neural networks are highly parallel constructs that can handle signal noise and drift and require few assumptions about the data [1].

The neural network is a lattice of individual processing elements called neurones. Inputs coming into the neurone from the sensors as well as from other neurones are weighted with a synaptic coefficient are processed using a non-linear activation function to produce the appropriate output (Fig. 5). The number of outputs usually corresponds to the number of possibilities, which are determined through training. The connectivity of the neurones is prescribed by the architecture of the neural network with the most common being the two layer back-propagation. As the name suggests, this network is composed of two levels of neurones, a hidden layer and output layer, along with the input layer, and works reasonably well for many electronic noses [59].

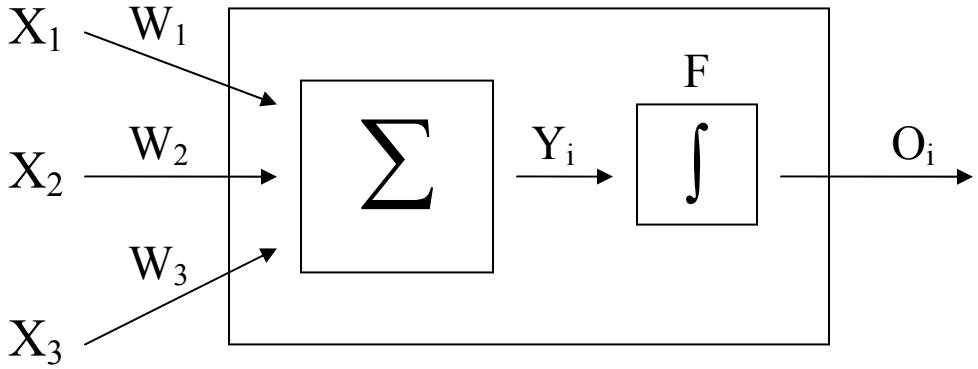

Figure 5. Schematic of an artificial neurone. The neurone takes inputs, $\mathbf{X_n}$, and produces an output $\mathbf{O_i}$. Each input is weighted by a factor, $\mathbf{W_n}$, integrated them and then applied to an activation function, **F**.

Artificial neural networks require a significant training period in order to determine the synaptic coefficients. During this extensive phase, reference inputs are used and the parameters are adjusted until the correct outputs are achieved. The process can be quite labor intensive, but once trained the neural network is capable of identifying responses very quickly [3]. Since artificial neural networks are also very good at dealing with signal noise and baseline drift and

few assumptions are required for the data, they may be the best data processing route for current sensor arrays [1].

A great advantage of these data processing techniques, whether linear or non-linear, is that they can be employed with varying degrees of sophistication. In the case of PCA, the level of dimensional reduction can be lowered in order to trade off sophistication with ease of implementation. Such versatility is useful for low-cost implementations where the operating environment of the sensor is constrained to a limited number of analytes. Similarly, with artificial neural networks, a very simple library of a few analytes greatly simplifies the necessary training and complexity of the neural network.

Auxiliary Components: Gas delivery, Sampler and Pre-concentrator

Besides these two main components, a complete electronic nose requires some auxiliary components to deliver the gas to the sensor array. Sample preparation instruments are already used for many analytical techniques like gas chromatography or mass spectroscopy and can be readily applied for an electronic nose system. The process requires extracting a sample, called headspace, from around the material of interest. Extraction of the headspace can be done directly although in some cases the headspace can be adsorbed onto a solid substrate and then thermally desorbed for analysis. The headspace is then transferred to the sensor array for analysis. The two main methods of delivering the headspace are generally known as headspace sampling, which involves direct injection, and as flow injection. Headspace sampling has been advantage of being relatively simple to implement and if the injection is automated, then sample delivery is not only fast but also reproducible [60]. On the other hand, flow injection, where the analyte is continuously delivered, allows for a greater range of analyte concentration and tolerates environmental fluctuations such as changes in temperature or humidity, but gives a much slower response time [3]. For a low-cost implementation, direct exposure may be the best route since it is simpler and is often better in field applications where a rapid response time is important.

Present State of Electronic Noses: Commercial Products and Current Research

Commercial products began appearing in the mid-1990s and in 2003 there were at least 17 companies manufacturing and selling electronic nose instruments. The most popular sensors have been and continue to be metal oxide sensors, usually fabricated from doped tin oxide (SnO2) or sometimes palladium oxide (PdO2). As mentioned earlier, metal oxide sensors exhibit robust and well-characterized sensor responses [39,47,48].

Table I lists various companies that offer electronic noses along with the sensor technology. This table represents a sample of the commercially available electronic noses. Some companies like Electronic Sensor Technology, the electronic noses uses a hybrid of sensing technologies and others like Alpha MOS offer a different product lines that each use a different technology. (The two bottom companies, ChemSensing and Cyrano Science will be addressed in a moment.)

Company Name	Sensor Technology	# of Sensors	Company Website
Air Sensor Analytics	Metal Oxide	10	www.airsense.com
Alpha MOS	Metal Oxide	6 to 24	www.alpha-mos.com
Electronic Sensor Technology	SAW/GC		www.estcal.com
Lennartz Electronic	Metal Oxide/QCM	16	www.lennartz-electronic.de/Pages/Homepage_english.html
Smart Nose	Mass Spectrometry		www.smartnose.com
Cyrano Sciences (now Smiths Detection)	Polymer	32	www.smithsdetection.com/eng/index.php
ChemSensing	Metalloporphyrin	36	www.chemsensing.com

Table I. A partial list of companies that sell electronic nose products.

Unfortunately, the use of metal oxide sensors drives up the cost because integration of the metal oxide sensors into a single array is expensive. In general, most commercial e-nose systems cost about $60k to $175k [61]. While many aspects of these electronic noses have improved over the years, prices have stayed at relatively the same level since 1998 because the fabrication of the sensor array remains the key hurdle to lowering the cost. If the cost of arrays could be drastically lowered, then it is likely electronic noses would be found in many more applications.

For this reason, several groups have explored alternatives to the metal oxide sensors for the purposes of making sensor arrays. Two of these groups are represented as the last two companies in Table I, Cyrano Science and Chemsensing. The former is the commercial venture of Lewis's work from Caltech using conducting polymers and the latter is derived from Suslick's work at UIUC using modified metalloporphyrins.

The work done by Lewis uses conducting polymer composites which are composed of a conducting material such as carbon black or polypyrrole dispersed in an insulating organic polymer [62]. The approach is like that of using a regular conducting polymer as a gas sensor, but the use of a composite avoids the need to simultaneously optimize several different properties of solubility, conductivity and chemical sensitivity. The chemical sensitivity is determined by the appropriate polymer, which can be electrically insulating, thus enlarging the pool of available materials. The sensor is implemented as a chemoresistor with enough carbon black or polypyrrole dispersed in the polymer to reach the percolation threshold, where the density of the conducting material barely supports conduction. Upon exposure to the analyte, the polymer absorbs some of the gas and subsequently swells. Because the composite is at its percolation threshold, this physical expansion results in a large decrease in conductivity as the

conducting material becomes more dispersed. Table II shows the polymers that are used in a typical conducting polymer arrays.

Sensor Number	**Polymer**
1	poly(4-vinyl phenol)
2	poly(styrene-*co*-allyl alcohol), 5.7% hydroxyl
3	poly(α-methylstyrene)
4	poly(vinyl chloride-co-vinyl acetate), 10% vinyl acetate
5	poly(vinyl acetate)
6	poly(carbonate bisphenol A)
7	poly(styrene)
8	poly(styrene-co-maleic anhydride), 50% styrene)
9	poly(sulfone)
10	poly(methyl methacrylate)
11	poly(methyl vinyl ether-*co*-maleic anhydride), 50% maleic anhydride)
12	poly(vinyl butyral)
13	poly(vinylidene chloride-*co*-acrylonitrile), 80% vinylidene chloride
14	poly(caprolactone)
15	poly(ethylene-*co*-covinyl acetate), 82% ethylene
16	poly(ethylene oxide)
17	poly(4-vinyl phenol)

Table II. The polymers use in a conducting polymer sensor array from reference [62].

Instead of conducting polymers, Suslick uses metalloporphyrins, cyclic molecules with a metal ion core, to detect the presence of different vapor molecules. These metalloporphyrins show a dramatic color change upon ligation of the vapor molecules to their metal ions [63]. The magnitude of the spectral shift depends on the polarizability of the ligand so it is possible to fabricate an array of metalloporphyrins by varying their metal centers. Since the response is directly proportional to the analyte concentration up to a saturation point, Suslick has demonstrated arrays that exhibit a unique color signature for a variety of vapors (Fig 6). The response of the sensor array is measured by using software to perform image processing on the arrays before and after exposure; the color difference is calculated and used in pattern recognition schemes. A major benefit of metalloporphyrins is that their response is insensitive to moisture.

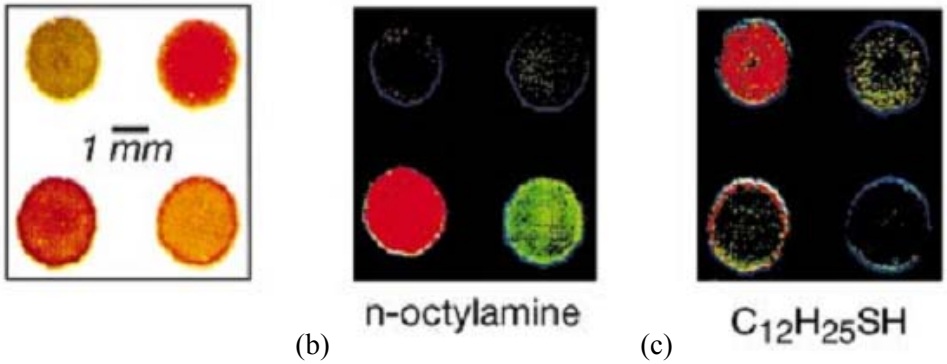

(a) (b) (c)

Figure 6. Example of metalloporphyrin arrays demonstrated by Suslick. The (a) four element metalloporphyrin array shows different spectral responses to (b) octylamine vapor and (b) hexanethiol vapor. From ref [63].

Both of these approaches show considerable promise, though there are some disadvantages. The conducting polymer composites have similar issues as regular conducting polymers, including drift and specificity. A major disadvantage is that the sensor mechanism is based on bulk swelling which limits the discrimination power because it relies on partitioning of the gas molecules within the polymer composite. In fact, Zellers *et al.* have shown that for sensors whose responses rely on equilibrium vapor-polymer partitioning, the discrimination power of the array levels off after six sensors [64]. At the other end, the metalloporphyrins are extremely selective, but signal processing is more difficult because of the need for image processing. In order to work with the signals, it is necessary to introduce another transduction event to convert the optical signal into an electrical one. As the arrays become larger, the need to process the optical signal may become a larger hurdle and limiting factor as has become the case with DNA arrays.

There is another approach which will be introduced in the next chapter, thin film transistors as gas sensors. Using thin film transistors avoids the need for additional signal conversion. Since their response is electrical, their output can be directly processed by the data processor making it easier to work with larger and denser arrays. Meanwhile, the interaction of the analyte occurs at the charge transport interface and is not simply related to bulk swelling, making it possible to leverage chemical interactions with the analyte and the polymer since the response is not purely physical. Additionally, since this response is dependent on the interface and leverages the transistor action of the device, it stands to be much more sensitive than a volumetric response due to bulk swelling.

Chapter 3 Organic Thin Film Transistors (OTFTs)

Since Alan Heeger won the Nobel Prize in Chemistry for his seminal work on polyaniline, conducting polymers and organic electronics have garnered increasing interest, much of which continues to this day. One of the earliest polymers of interest was polyaniline, a conducting polymer that can be doped with various additives to tune its oxidative properties. Polyaniline is still an important material today for conductive coating applications. Some time later, semiconducting polymers such as polythiophene were investigated and by the 1990s, the scope of interest had enlarged to include small molecules or oligomers such oligothiophenes, as well as organic crystals. Today, organic light emitting diodes, organic solar cells, and organic transistors are the subjects of considerable research.

This chapter will specifically discuss polythiophene as semiconducting material including its structure and properties as well as its use in transistors. Rather than simply cover these matters generally, it will consider them from the viewpoint of sensing. Electrical characteristics and charge transport models will also be considered. Finally, the chapter concludes by covering non-idealities that are germane to sensing.

Background on Organic Semiconductors

The electrical properties of an organic semiconductor completely arise from its underlying chemistry. In particular, the semiconducting behavior is derived from a specific bonding arrangement which is known a conjugated pi system. The conjugated pi system is most easily described as a series of alternating double and single bonds within a molecular system. The alternating arrangement means that the double bonds are strongly associated with specific atoms and as a consequence, the electron participating in these double bonds are said to be delocalized. These delocalized electrons, which are located in the higher energy pi orbitals rather in the lower energy sigma orbitals (Figure 1), have their wave function spread over many atoms. As a consequence, these delocalized carriers are responsible for charge transport within the molecular system. The presence of conjugated system is a critical feature of semiconducting polymers and conducting polymers.

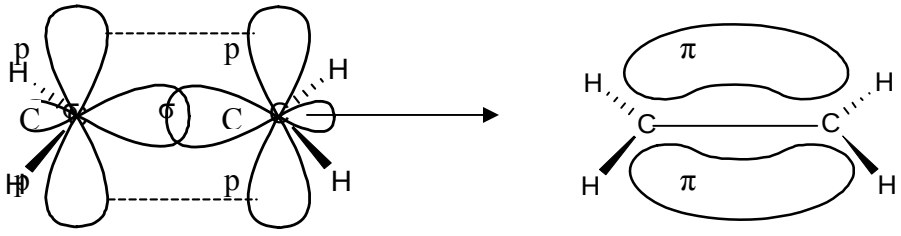

Figure 1. p orbitals becoming a delocalized π orbital

Since organic semiconductors are composed of discrete molecules, as opposed to a single crystal, the degree of conjugation can only extend as far as each discrete molecule. Conjugation length is used to characterize the extent of conjugation through the entire material. In terms of charge transport, the conjugation length is the average distance a charge carrier can travel before it is trapped or encounters an energy barrier [1]. For oligomers, the conjugation length has been shown to correlate to the length of the molecule; in the case of polymers, the conjugation length is much smaller than the entire length of the molecule due to physical or chemical defects which breaks the conjugation length into smaller segments [1]. Many semiconducting oligomers possess fused ring structures and many polymers also have ring structures which provide a degree of planarity and rigidity to minimize defects and extend the conjugation length.

In fact, the conjugation length is related to various properties. Not only does the presence of a planar backbone improve the conjugation length, but twisting and strain can affect it, as do the presence of long-range ordering, temperature and bias. Conjugation length also gives rise to optical properties since it is directly related to the absorption length. The sensitivity of the conjugation length to a variety of factors provides the capacity for organic semiconductors to be good sensors. The introduction of a molecule into the conjugated system has the ability to perturb this length which will then affect the electrical or optical properties.

Common types of organic semiconductors are shown in Figure 2. Semiconducting molecules can be polymers like polythiophene (Fig. 2a) or an oligomer, such as pentacene (Fig. 2b). Typical polythiophene molecules will have ca. 500 repeating units. Notice the presence of the conjugated system which results from the alternating double bond arrangement and as well as a planar backbone from the presence of rings. In both cases of these molecules they exhibit sensing behavior.

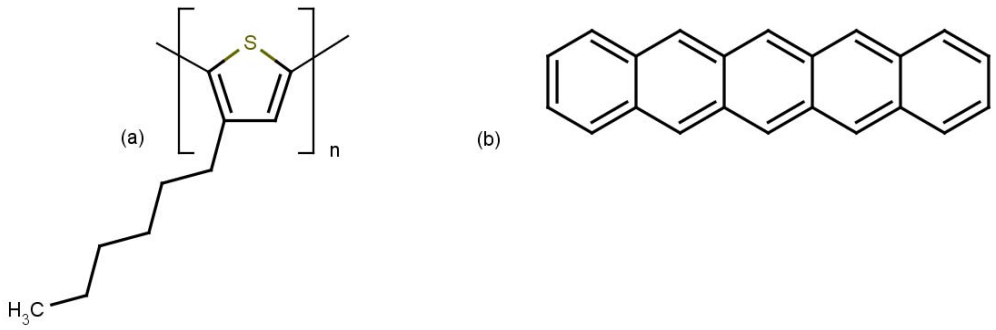

Figure 2. Common types of organic semiconductors include polymers like (a) polythiophene and oligomers like (b) pentacene.

An alternate perspective when considering the electrical behavior and sensing is density of states, which is taken from the traditional framework concerning inorganic crystalline semiconductors. In an inorganic semiconductor that possesses long range ordering, the interaction of the crystalline lattice gives rise to the valence band and the conduction band, with a forbidden energy bandgap, E_g, between them. Within the bandgap there are no allowable energy states with a sharp transition occurring at the edge of the valence and conduction band, E_v

and E_c, respectively. As one moves away from these band edges, the density of allowable states increases (Fig. 3a).

The situation is quite different with an organic semiconductor. The delocalization of the pi electrons creates a spread of molecular orbital energy levels not unlike the bands of an inorganic system. In this case, the energy bandgap, E_g, is defined as the energy between the highest occupied molecular orbital (HOMO) and the lowest unoccupied molecular orbital (LUMO), which are somewhat analogous to valence band edge, E_v, and the conduction band edge, E_c, respectively. However, one major difference is that E_g is determined by the interaction of several discrete molecules, as opposed to a large crystalline lattice. The inhomogeneities of the system result in a gradual transition at the band edges known as bandtails (Fig. 3b). These bandtails are usually modeled with a Gaussian or exponential profile. The magnitude of E_g is a function of nature of the pi bonding in the system, the immediate environment of the molecule, and its conjugation length [1,2]. The capacity for sensing can also be seen in the density of states profile, since variability in E_g depends on the local environment.

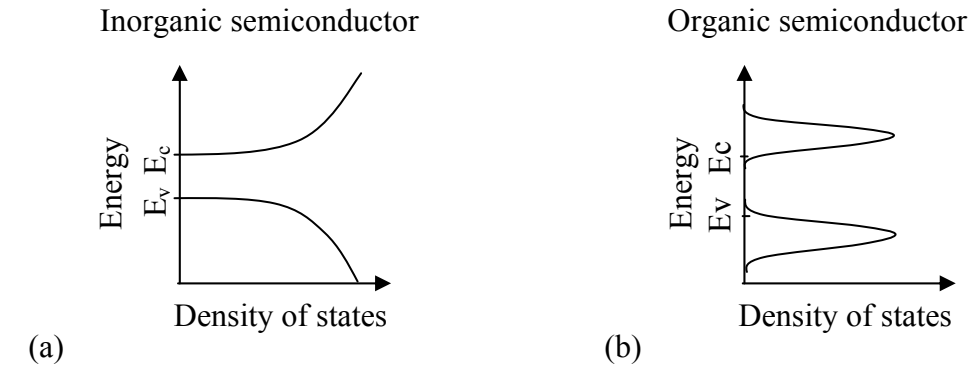

Figure 3. Density of states for (a) an inorganic semiconductor compared to (b) an organic semiconductor. Notice the presence of the band edges, or bandtails, in the organic semiconductor

With inorganic devices, the position of the Fermi level dictates the dominant carrier in the system. An n-type material, where the Fermi level is close to the conduction band, conducts current with electrons as the majority carrier while in a p-type material the Fermi level is closer to the valence band and holes the majority carrier. With organic devices, p-type and n-type do not bear the same meaning as with inorganic semiconductors. In organic devices, the preferred polarity of mobile charge is determined by the position of the HOMO and LUMO levels of the material and the mobility of one type of carrier will be much higher than the other. Generally, this means that an organic device is limited to one polarity of operation. This polarity is affected by the contact electrodes, whose work function will align either with the HOMO or LUMO of the semiconductor and dictate the type of injected carrier. Therefore n-type materials usually have high LUMO levels and p-type materials have low HOMO levels [3]. Other research has shown that the composition of the dielectric can also dictate the charge polarity because it may selectively trap one type of charge at the interface [4,5]. Chua *et al* have shown that using a fluorinated dielectric instead of silicon dioxide can result in n-type behavior [6].

Thin Film Transistors (TFTs) Based on Organic Materials

Many of the unique properties discussed thus far give rise to differences in the electrical characteristics of organic transistors from those of inorganic devices. The most common incarnation of the polythiophene transistor is the thin film transistor (TFT). Unlike inorganic materials, where the substrate becomes the active device, organic transistors are derived from thin films that are usually fabricated on top of a substrate. In order to examine the I-V characteristics of polythiophene TFTs, the fabrication of these devices will first be discussed.

Since organic semiconductors are not bulk crystals, the device structure and the processing are different than that of traditional integrated circuits. Because organic TFTs are derived from a film that is deposited on top of the substrate, there are several derivations of OTFTs characterized by their different gate configurations. As depicted in Figure 4, OTFTs may be top-gated, back-gated, or bottom-gated. The top-gated configuration most closely resembles the traditional MOSFET structure with the gate placed on top of a dielectric which is on top the organic semiconductor film. The patterned back-gated configuration is when the gate and gate dielectric are placed below the active film. The bottom-gated configuration is similar to the back-gated configuration except that the gate and gate dielectric are incorporated into substrate. In terms of sensing, the bottom-gated configuration is most advantageous configuration because the active film is entirely exposed and can interact with the gaseous species in the atmosphere. Besides the gate configuration, the device may have top contacts or bottom contacts as shown in Fig. 4c and d. These refers to the position of the contacts relative to the semiconductor film and this distinction can also be applied to the other gate configurations.

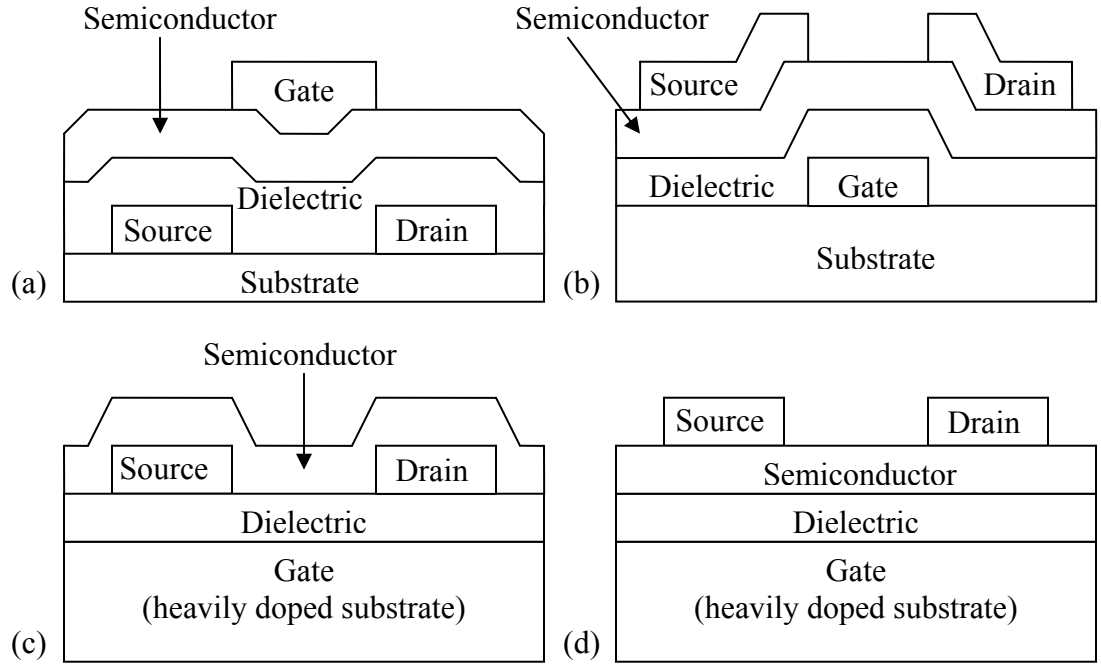

Figure 4. Different gate configurations of an organic TFT. (a) top-gated configuration; (b) patterned back-gated configuration; (c) bottom-gated configuration with bottom contacts; (d) bottom-gated configuration with top contacts

Electrical Characteristics of Organic TFTs

The operation of an organic TFT resembles that of silicon FETs with similar biases and currents, absent the body contact and potential. The three important contacts are the gate, source, and drain, with the latter two being designated by the applied biases rather than any physical denotation. Consistent with convention, currents are defined to be positive entering into the electrode or terminal. Figure 5 shows the transistor configuration and related biases. Channel length and width are defined by the geometries of the source and drain pads and the thickness of the gate dielectric is the oxide thickness. At sufficiently high gate voltages, current passes laterally through the film between the source electrode and the drain electrode and is modulated by the gate voltage. Electrical characterization can be performed by sweeping the drain voltage for discrete values of V_G (I_D-V_D) and by sweeping the gate voltage for discrete values of V_D (I_D-V_G).

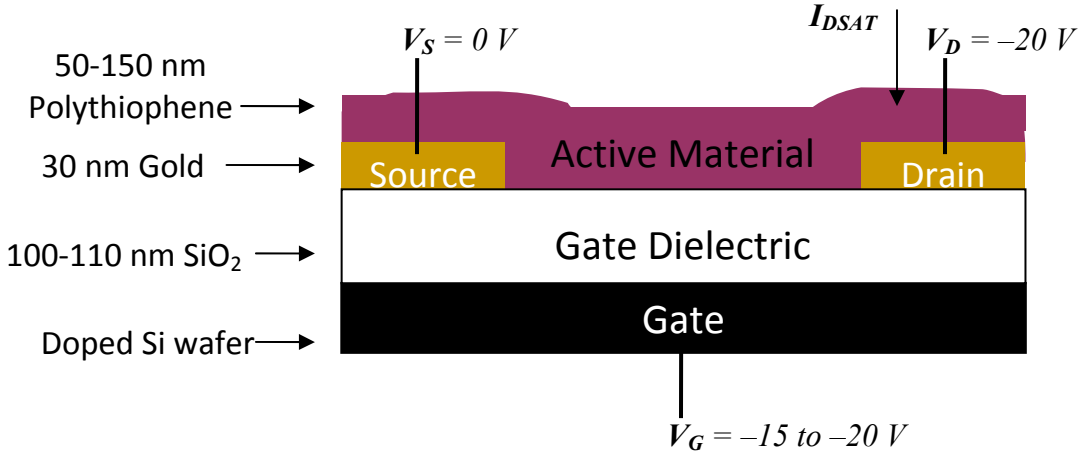

Figure 5. The basic configuration of an organic TFT as a gas sensor showing the applied biases, V_G, VD, VS, and I_{DSAT}.

Figure 6 shows the I_D-V_D and the I_D-V_G characteristics of a polythiophene transistor. As noted before, the devices are p-type so the currents are negative. Overall, the behavior bears resemblance to that of a transistor made from an inorganic semiconductor like silicon. From the I_D-V_D curve, overall transistor behavior is observed and the I_D-V_G characteristic shows the familiar turn-on characteristics and gate modulation present in field-effect transistors.

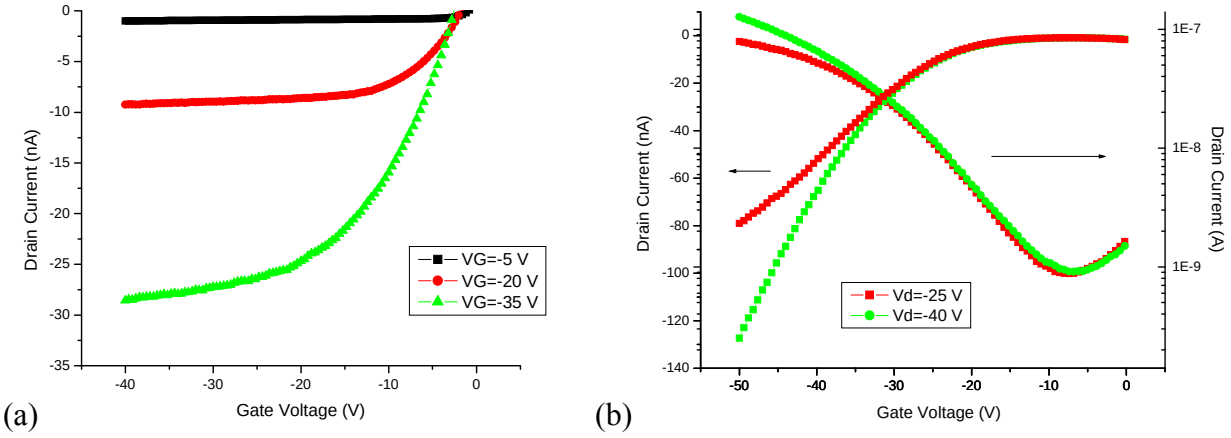

Figure 6. The (a) I_D-V_D and the (b) I_D-V_G characteristics of a polythiophene transistor with gold source and drain contacts on an oxidized silicon substrate. The applied biases are shown on the figure; W/L = 250/10 μm; oxide thickness is 100 nm.

While the general behavior looks similar to more traditional FET behavior, there are some important differences that are apparent upon closer inspection. The fundamental distinction is that organic TFTs do not obey the square law and this has several implications in the electrical behavior.

First, these organic TFTs operate in the accumulation mode rather than inversion. The presence of the band tail results in a high trap density making inversion in organic transistors extremely difficult. In this case, these devices are p-type so a negative bias applied to the gate results in positive charge carriers accumulating at the dielectric interface. As the gate voltage increases, number of carriers continues to increase until there is a dramatic rise in conductivity between the source and drain.

It is not surprising that a gradual turn-on characteristic is a main feature of organic devices. Specifically, organic devices exhibit an extended subthreshold region which is bounded by two voltages: the turn-on voltage, which is the voltage when current first appears and the threshold voltage, which is the voltage at which the device is considered 'on'. In an ideal situation, the turn-on voltage and threshold voltage should be nearly identical. However, the presence of traps and defects in the organic semiconductor often translates into an extended subthreshold region because trap filling and charge screening is necessary before a sufficient charge layer is generated at the dielectric interface [7]. This means that the turn-on voltage is distinct from the threshold voltage.

While inorganic devices have a well-defined inversion point at which the concentration of inversion charge in the channel is the equal to the concentration of the majority carrier charge in the bulk at equilibrium, threshold voltage is not as clearly defined in organic devices. Currently, the most commonly used definition for the V_T of an organic TFT is derived from the ideal square law model. Under those assumptions, V_T can be extracted by taking the square root of I_D-V_G characteristics and extrapolating the horizontal intercept from the linear (high V_G) portion of the curve. This is illustrated in Figure 7. An alternative method is to use the linear regime and

extrapolate the linear portion of the I_D-V_G curve to the horizontal intercept and setting that value to $V_T + V_D/2$ [2].

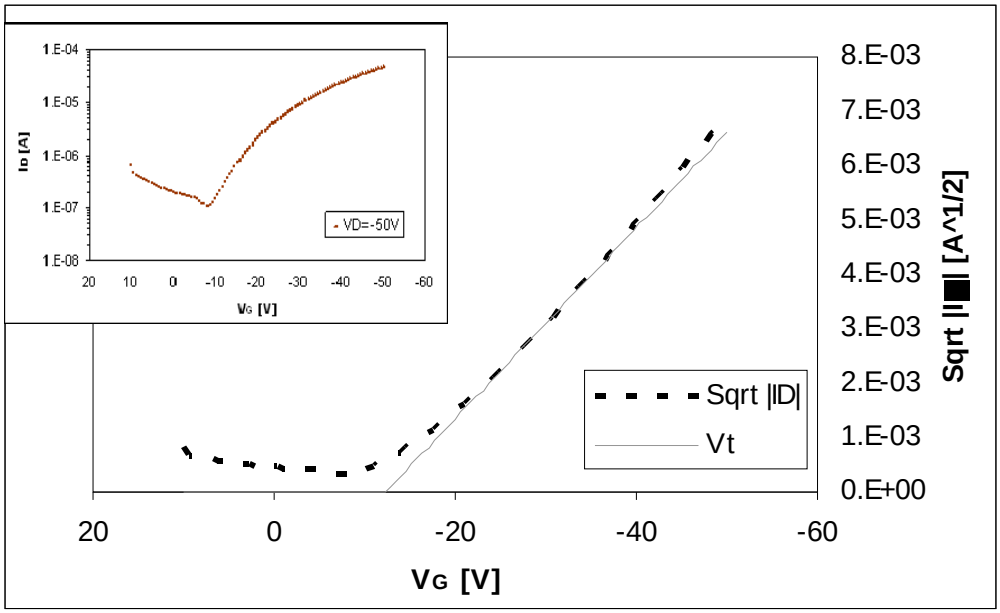

Figure 7. Showing the extraction of threshold voltage, V_T, by taking the intercept of the square-root of the I_D-V_G curve (shown in inset).

Beside the gradual turn-on characteristics, one of the most notable differences is that the field effect mobility of organic TFTs is dependent on the gate bias. Field effect mobility, μ_{FET}, is different than the intrinsic mobility, μ_0, of the material and is a measure of the velocity of charge carriers, v, under the influence of an electric field, E (Eqn. 3.1).

$$\mu_{FET} = \frac{v}{E} \qquad \text{Equation 3.1}$$

μ_{FET} is extracted from the I_D-V_G characteristic under the assumption of square-law behavior. Under this assumption, mobility is calculated from the transconductance, g_m, which is the slope of the I_D-V_G curve (Eqn 3.2). Although, this assumption of square-law behavior is invalid, this extraction is still used because it provides a relatively intuitive and consistent metric for evaluating the performance of organic TFTs. Currently, mobilities for organic devices range from the order of 0.1 to 2 $cm^2/V/s$ [8]; outstanding mobilities >10 $cm^2/V/s$ are reported for devices made from evaporated, single crystalline materials like rubrene [9,10] or naphthalenetetracarboxylic diimide [11,12].

$$\mu_{FET} = \frac{\frac{\partial I_{DS}}{\partial V_{GS}}}{\left(\frac{W}{L} C_{ox} V_{DS}\right)}$$ Equation 3.2

Figure 8 shows the extraction of mobility with a typical I_D-V_G curve and the dependence of mobility upon the gate voltage. Here the mobility decreases at higher gate biases, an effect that is not always observed but can be attributed to high series resistance that results in a smaller extracted μ_{FET} [2]. As seen in the figure, the mobility varies between the two regimes of saturation and linear; often only the higher, saturation mobility is usually reported as μ_{FET}.

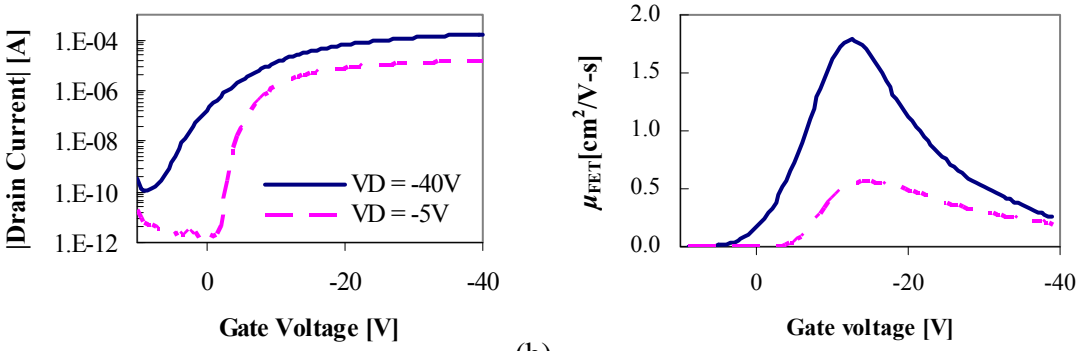

(a) (b)

Figure 8. Extraction of field effect mobility, μ_{FET} [2]. (a) The I_D-V_G curve of an organic TFT; (W/L = 500/50 μm); (b) the gate dependence of mobility is clearly visible.

This kind of dependence underscores the charge transport behavior which is certainly different for organic devices. Charge transport is also important for sensing applications because it will give a better understanding of the working principle or mechanism for sensing behavior. Originally, it was believed that the gate dependence arose because charge transport was based on the Poole-Frenkel mechanism but this was discounted by Dimitrakopoulos *et al*. The Poole-Frenkel formalism prescribes an exponential dependence on the electrical field, *E*, but Dimitrakopoulos *et al* separated the effect of charge carrier concentration, *N*, and electric field, *E*, and showed that the mobility increase is due to increases in *N* [13].

Charge Transport Models for Organic TFTs

The remaining explanations for the origin of gate dependence in μ_{FET} broadly fall into two categories, representing the two major approaches to modeling charge transport in organic

devices. These two approaches will be characterized by a representative model, though many models may be grouped in each approach. The first approach is represented with the Multiple Trap and Release (MTR) model and the second with Mott's Variable Range Hopping (VRH) model. The first approach includes other models like the Grain Boundary Trapping (GBT) model and the second includes Ambegaokar's percolation networks. Fundamentally, these two approaches represent differences in how to treat the disorder of an organic semiconductor, which is the central issue with organic TFTs. The first approach is to borrow from the inorganic framework and to treat these organic devices like amorphous or polycrystalline TFTs with high trap or defect densities. The second approach is to reconsider the whole issue from the bottom up and think about charge transport in discrete molecules as taking place through hopping events.

The MTR model takes the phenomenological approach as treating transport as occurring through extended states as in inorganic semiconductors [14]. In order to deal with the disorder, the band tail gives rise to a shallow trap density. Unlike deep traps which are located closer to the middle of the gap between the Highest Unoccupied Molecular Orbital (HUMO) and the Lowest Unoccupied Molecular Orbital (LUMO), shallow traps are only a few k_BT away from the edge of the HOMO or LUMO energy level so that carriers are trapped for a finite time and can be released by thermal excitations. In this way the carriers spend some time moving in the HOMO or LUMO and then are trapped in the shallow traps and then released again, hence the name of the MTR model. This behavior effectively reduces the field effect mobility of the carriers which can be modeled either two ways both of which produce the same result. The first is to assume that all the carriers spend some amount of time in the shallow traps, using a time τ, and the other is to assume that only a fraction of carriers are moving at a given time. Since conductivity is directly proportion to the effective mobility and the number of free carriers the net effect is the same.

MTR is consistent and handles well some of the hallmarks of charge transport in organic devices: a gradual turn-on characteristic, since the filling of traps is required before a conductive layer is formed; thermally activated transport, since thermal energy means that carriers more easily escape the traps or spend less time in the traps; gate-dependent mobility since the position of the Fermi level will determine the effective trap density.

The outstanding characteristic of the MTR model therefore lies in the bandtail and how the shape or density is modeled. In the simplest sense the trap density can be simplified into a single localized state at energy E, a few k_BT, away from the band edge. More sophisticated models will provide ways of treating the width and shape of the band tail. In terms of sensing; it may be that sensing affects the trap density by influencing the width and shape of the tail. The presence of an analyte species may introduce a new energy level that effectively increases the residence time of free carriers in defect states which originate from the analyte molecules.

A second major approach is the semi- phenomenological approach which is considers discrete charges as hopping through the material. Two of the models in this approach are known as the VRH model, developed by Mott [15], and the percolation network proposed by Ambegaokar *et al*. These models ignore transport through extended band-like states. Instead, VRH considers the statistical probability of a single carrier hopping from a localized occupied state to an empty state. The most important parameter in constructing the hopping rate is the width of the band tail, where too small a width results in too low a density of states and too large a width incurs an energy premium for hopping. The final expression for variable range hopping is very similar to MTR and shows the same dependencies. Ambegaokar *et al* approach the

hopping problem with perhaps a more intuitive approach and look at it as a percolation network [16]. For an analytical expression, this hopping system can be modeled as a resistor network for which hopping occurs at or near the Fermi level, resulting in a strong dependence on the Fermi level. This is because resistivity is determined from occupancy so that hopping at states far away from the Fermi level is associated with high resistance. The last step in converting the resistor network is to employ the "lazy-charge principle" and remove the higher resistance values, usually done by removing the conduction paths below a conduction threshold, G_c, as defined by the density of states [17]. Note that a major assumption is that the DOS is slowly changing over energy, since hopping is close to the Fermi energy.

From the VRH standpoint, sensing behavior can be incorporated as a change in the charge hopping rate; the analyte has an electric permittivity which affects the dielectric permittivity of the material and changes the charge hopping rate.

While the approach is different, VRH accounts for many of the same dependencies as MTR, such as temperature and Fermi level dependence, making it difficult to ultimately distinguish between the two based on empirical results. Perhaps the biggest difference is the degree of disorder accounted for in the models but it is difficult to take advantage of this using empirical methods [18].

Saleo *et al* report that both VRH and MTR models provide a good fit for a fairly extensive set of experimental polythiophene OTFT data, noting that the two models are indistinguishable within the temperature range accessible for organic materials. They reject the VRH in favor of the MTR model solely on the basis of a more physical interpretation of the final parameter values [18].

Non-idealities in the Electrical Behavior of Organic TFTs

Besides non-square law behavior, organic TFTs demonstrate several non-idealities, including the bias stress effect (BSE) and oxidative degradation, both of which will be discussed here because of their impact on sensor behavior.

Bias Stress Effect (BSE)

Bias stress effect is the reduction in the drain current during prolonged operation of the device due to trapping of charge at the semiconductor-dielectric interface [19]. The reduction is a result of a shift in the threshold voltage that begins immediately upon application of a bias. The current reduction exhibits logarithmic behavior and its rate is commensurate to the duration and frequency of the applied bias so that a constant bias produces the fastest reduction in on current. Upon removal of the bias, recovery begins immediately and is also logarithmic in nature (Fig. 9) [20,21]. Therefore, the bias stress effect is not destructive and suggests that the origin is electronic in nature. In fact, some groups have demonstrated that recovery can be accelerated with opposite polarity biasing [22] or exposure to light [23].

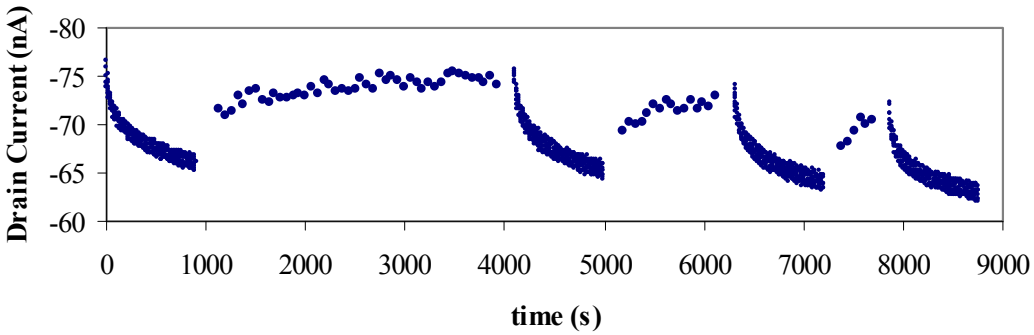

Figure 9. Example of the BSE in a polythiophene TFT (W/L = 500/20 μm). A bias of $V_G = V_D$ = -20 V was alternately applied and released. Figure from ref [24]

The origins of bias stress are thought to lay in charge trapping from deep, mid-level traps with very long time constants within the semiconductor channel and at the dielectric interface. This would be consistent with the time scales of the bias stress effect, the recovery of the current over time after removal of the bias, and the fact that mobility does not decrease with repeated biasing since shallow traps would degrade mobility. Since there is a shift in the threshold voltage, it is also believed that these traps are located within the channel or near the semiconductor-dielectric interface [19]. However, Chang and Subramanian have reported that the BSE also shows a dependence on the active layer thickness [24]. The reason for the thickness dependence cannot be definitively proven given the experimental evidence, although a plausible explanation is that band bending of organic semiconductors extends significantly into the active material [25]. Thus, the charge responsible for the threshold voltage shift need not only be present at the dielectric interface [24,26]. Another possible explanation is that the activation energy for trap creation at the semiconductor-dielectric interface decreases with increasing thickness of the active layer.

BSE is present not only in polythiophenes but in many other organic materials, such pentacene [19,27,20], thiophenes [28,20,29], and polyarylamines [30]. However, the rate of decay is different for different types of active materials [20].

Addressing BSE is necessary because it can convolute the sensor response. Yang *et al* has demonstrated that the bias stress effect is actually superimposed upon the sensor response [31]. This implies that the traps associated with the bias stress effect are not the same as those associated with sensors. The easiest way to deal with BSE is to use differential sensing architecture [32] and/or use pulsed measurements to allow the transistors to recover from the bias-stress during the interrogation [20]. The former method employs a differential amplifier with an active load to remove the reduction from BSE through common-mode rejection. In this architecture, two organic TFTs are used to form a differential pair but one of the devices is isolated from any vapor exposure. Since reduction from BSE is common to both transistors the use of a differential pair means this reduction is rejected like other common modes like electromagnetic noise or ground line variations. Besides rejecting the reduction from the BSE, the differential pair provides an enhancement of the sensor response, since it amplifies only the difference between the two transistors.

Using a differential architecture requires one extra device, though more likely several devices for an active load architecture along with supporting circuitry, and these devices need to be well matched to achieve an adequate common-mode rejection ration (CMRR), defined as the differential gain divided by the common-mode gain. This is a still a new and developing issue with organic devices and variation is well-known but studies are still required. Many errors are related to processing or processing faults like unintentional doping; these may be reduced through further refinements. However the differential sensing architecture has been successfully demonstrated by Subramnian *et al* who used it to distinguish between alcohol vapors as a way to detect wine spoilage [32].

As mentioned earlier, pulsed measurements are also extremely effective in mitigating the BSE. Since the bias stress effect is exacerbated by continually applied bias, the use of pulse measurements allows for partial recovery in between applied biases. Since the current reduction and recovery are both logarithmic in nature, employing a reasonable duty cycle mitigates the BSE and allows for a negligible reduction of the current from its initial value. This effectively removes the BSE from the steady-state behavior, making it an initial transient phenomenon. Figure 10 from reference [20] demonstrates the use of pulsed measurements. As expected, a longer duty cycle causes a greater and longer initial decrease in current. The figure shows that for a 3% duty cycle, the current is only slightly reduced and it retains a steady state value that is close to the original device current. This is the technique employed for all sensor measurements, which will be described in more detail in the next chapter.

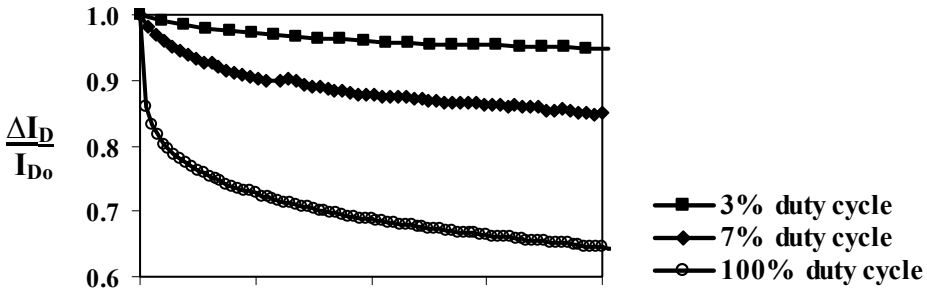

Figure 10. Pulsed measurement technique for reducing BSE. A 3% duty cycle marginally reduces the drain current. Figure from ref [2].

Oxidative Degradation

Besides BSE, another non-ideality is oxidative degradation. Most organic materials possess a HOMO level in the range of 4.5 to 5 eV which makes them susceptible to oxidative doping. This doping causes an unwanted increase in conductivity, which reduces the semiconducting character of the material by degrading the on/off ratio of the transistor. This conductivity increase also leads to a commensurate increase in leakage current.

Early on, this mechanism of oxidative doping in organic materials has been well known and there have been efforts to develop air stable materials. Much of the work done on thiophene and polythiophene has been focused on modifying the side chains of the thiophene unit[33]. The aim

is to affect the conjugation length along the polymer backbone either by "pushing in" or "pulling out" electron density with these modified side chains. This push/pull causes shifts in the HOMO and LUMO level of the molecule and can lower the material's sensitivity to air. Yet another route to making air stable compounds is to adopt a synthetic perspective and remove the oxidatively susceptible sites in the molecule. The conjugation of semiconducting materials unfortunately leaves certain sites open because the delocalized pi electrons can become susceptible to oxidation by electronegative molecules such as oxygen. Therefore, air stability can be achieved by removing these sites or blocking them with more robust atoms or molecular motifs, such as steryl groups [34] or fluorine atoms [35]. Care must be taken to make modifications without disrupting the conjugation of the original molecule. Figure 11 shows some examples of air stable molecules, including fluorinated 5,11-bis(triethylsilylethynyl) anthradithiophene. (diF-TESADT) and poly (didodecyl-2,2'-bithiophene-4,4'dicarboxylate-co-2,2'-bithiophene) (P1). In terms of sensing, Chang *et al* used P1 to show that the air stability does not affect the sensing behavior of the molecules [2]. Moreover, these approaches bear great interest to sensing because they demonstrate that by modifying the material the interaction of the semiconductor with its environment can be changed and the degree to which the behavior can be tailored.

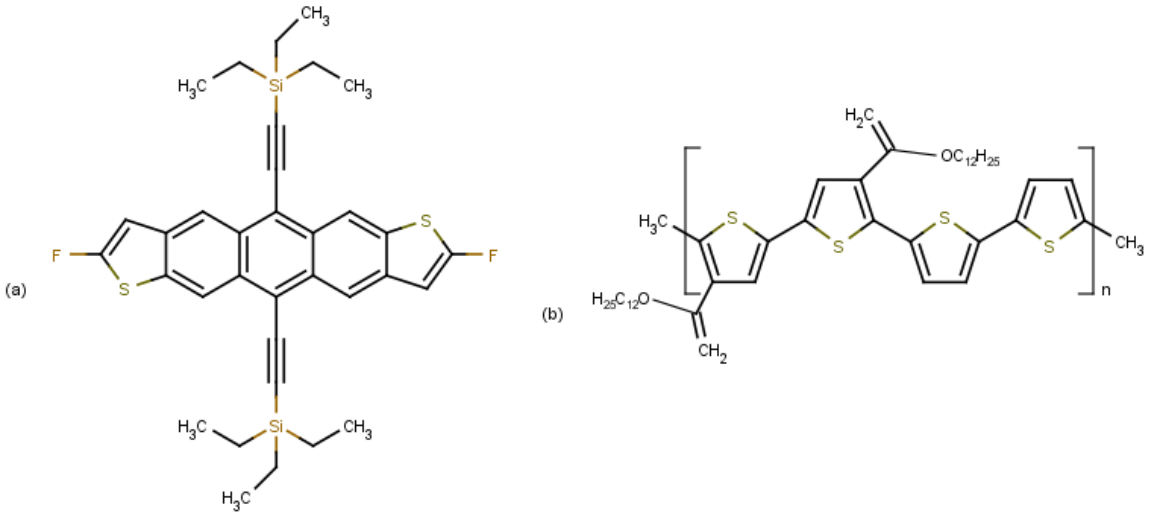

Figure 11. Air stable organic semiconductors the presence of the fluorine atoms and ester groups stabilize the overall molecule; (a) fluorinated 5,11-bis(triethylsilylethynyl) anthradithiophene. (diF-TESADT) and (b) poly (didodecyl-2,2'-bithiophene-4,4'dicarboxylate-co-2,2'-bithiophene) (P1)

Another way of addressing oxidative doping is to again use the differential sensing architecture. In this case, the gas delivery must be done properly so that only the sampled vapor is the difference between the two transistors of the differential pair.

Conclusion

An overview of organic TFTs was presented, highlighting the particular aspects that are important to gas sensing. The basic configuration and fabrication of a polythiophene TFT was also presented, both of which will be referred to for the remainder of the thesis. Charge transport mechanisms were discussed at length which will provide useful background when considering the sensing behavior. Finally, two non-idealities, BSE and oxidative degradation were covered both of which are important for gas sensing.

Chapter 4 Organic TFTs as Gas Sensors

The promise of organic electronics has come in many forms from plastic compatible electronics to ubiquitous radio frequency identification (RFID). One of the first of these to come to market was organic light emitting diodes (OLED) displays. In the early 2000s, Motorola followed by a few other companies began offering cell phones that featured OLED displays. These displays took advantage of the facile processing of organic materials in order to make cheap, large area displays.

Organic based sensor technologies have been among these heralded applications of organic transistors. Like organic displays, organic sensors also leverage some properties of organic materials. What is most attractive about an organic sensor technology is that is complements silicon electronics rather than competes with it. Organic sensors may go where their silicon counterparts cannot go by surmounting a plethora of physical and economic barriers. Substrate free processing means sensors may be incorporated in novel places and low cost devices could break through the barriers of many sensing paradigms like environmental monitoring or ubiquitous monitoring. Modern integrated circuits are capable of processing large amount of data and could easily handle the data stream from a ubiquitous network of embedded sensors. What is lacking is a sensing technology that cheap enough to be placed "everywhere" with a low-cost form factor. If organic sensors can be improved in their performance and processing, they may usher in new applications of sensing, computing, and processing.

This section introduces the concept of organic transistors as gas sensors. It begins with the motivation for organic gas sensors, followed by a discussion of the prior art. Then the basic and principles of sensor operation is discussed followed by a thorough characterization of sensors.

Motivation for Gas Sensors Based Organic TFTs

Organic TFTs have several features that make them attractive for sensing applications. They are able to simultaneously provide chemical sensing capabilities with the possibility of low-cost manufacturing. Some of these advantages will now be discussed in detail.

Solution processing. Since they are soluble in common solvents, organic materials do not require traditional IC processing techniques and can be processed using solution-based techniques such as inkjet printing [1-4]. The advantage of the printing technique is that material is deposited only where desired. This type of approach, known as additive processing, is much simpler than the fabrication methods employed with modern ICs, which can be described as subtractive processing. Subtractive processing means that the material of choice is deposited uniformly over the entire substrate and undesired portions are removed using lithography, which involves another blanket deposition of a photopolymer that can be subsequently patterned with light. Addition and removal of this photopolymer means that the deposition of one layer requires a total of five steps: deposition of the layer, deposition of the photoresist, patterning of the photoresist, removal of the unwanted material, and removal of the photoresist. These additional processing steps translate into higher complexity and ultimately higher costs associated with

yield as well as materials and abatement costs. The alternative approach of using additive processing, involving only one step, becomes a substantially simpler and cheaper route [2]. This means that an organic TFTs stand to be much cheaper to fabricate. Even with moderate performance, there may be a number of applications where a low-performance but low-cost sensor makes sense [1,3].

Integration. The method of additive processing also brings in some important benefits for developing an attractive sensor technology. First, additive processing nearly trivializes the fabrication of a sensor array [5]. Since material is deposited only where desired, printing a sensor array is comparable to printing a photograph or documents. The absence of any blanket deposition during additive processing avoids issues of cross-compatibility between dissimilar materials.

Second, the active material is no longer restricted to the substrate. This is attractive for many sensor applications since the sensor is no longer bound to a specific platform. Such freedom would be ideal for food spoilage detection, since the sensor can be integrated into the packaging, as well as general environmental monitoring applications. In practice, there may still be some requirements on the substrate, with the most important being the temperature resistance. Currently, many printed organic materials require an annealing step so the substrate should possess a modest thermal budget.

Functionalization. Another important advantage of organic gas sensors, which will be exploited in the work presented here, is the possibility to functionalize the active material with the intent of tailoring the sensor response. It has been shown that changing the functional group can make a material more or less sensitive to a specific analyte or gas [6]. This enhances the discrimination power of the sensing material and thus several sensors can be integrated together, each possessing different functionalization motif. Since many organic materials can be functionalized with great variety and with relative ease, they are ideal candidates for sensors. Specifically, polythiophene has side chains which can be functionalized as shown in Figure 1. There are well known experimental methods for functionalizing polythiophene and some varieties are already commercially available.

All of the advantages described above apply to any kind of sensor derived from organic materials. However, there are unique benefits to using organic transistors as opposed to an implementation such as a chemiresistor. Namely, organic TFTs are more sensitive since their sensor response is derived from a surface effect and the amplification of the transistors provides enhancement of the sensor response over that of a bulk conductivity measurement [7]. As mentioned in the previous chapter, another advantage of using transistors is to ability to construct a differential pair. A differential sensing architecture rejects the BSE and oxidative degradation while isolating and amplifying the sensor response [5].

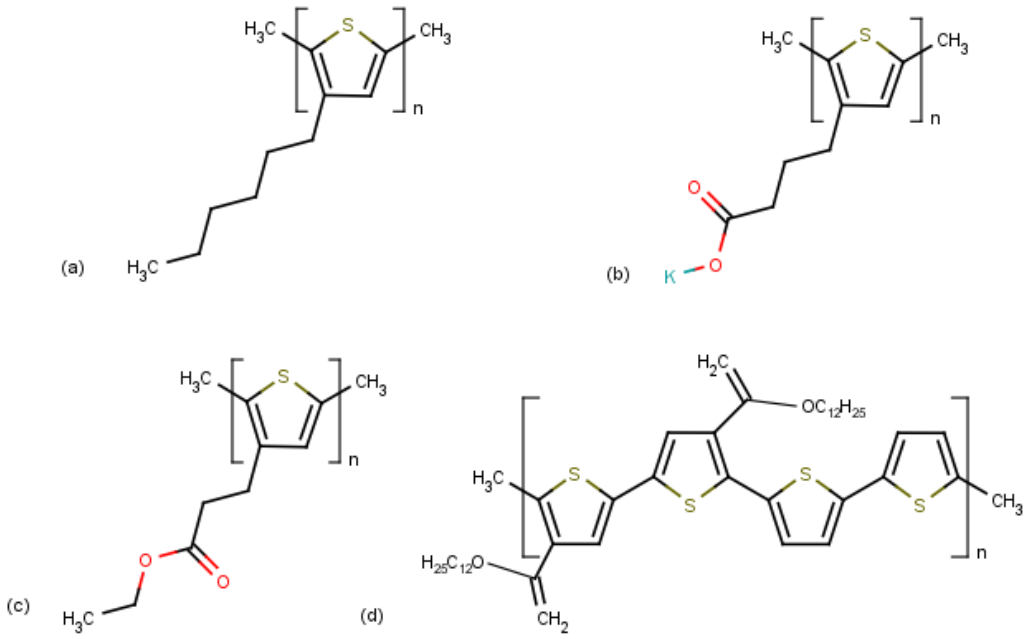

Figure 1. Examples of polythiophene derivatives with various side chain functionalities referred to throughout this thesis; (a) poly-3-hexylthiophene, (b) poly-3-(potassium-4-butanoate)thiophene-2,5-diyl, (c) poly-3-(ethyl-4-butanoate), (d) poly (didodecyl-2,2'-bithiophene-4,4'dicarboxylate-co-2,2'-bithiophene)

Prior Art of Organic Gas Sensors

Some of the most original work in the area of organic based gas sensors is presented in the seminal paper by Crone *et al* from Bell Labs [8]. This paper was the among the first to duly investigate the possibility of using organic TFTs as gas sensor arrays. The group reported many promising results by using a variety of organic semiconductors with a variety of laboratory solvents as the analytes. Figure 2 shows a chart summarizing their results.

Since then, similar results have been reported by many other groups using various materials exposed to a range of analytes, usually a battery of common laboratory solvents. However, the reports have all been typical of the original paper and usually report shifts in current when an organic based device is exposed to a certain analyte. To illustrate, consider the most recent work reported by Huang *et al*, including Katz from the original Bell Labs paper, showing a material that is sensitive to DMMP, an important compound in nerve gas [9]. The experimental results are thorough and the sensor response is well characterized but there is little reporting on the interaction of the active material with the analyte or on the methodology of choosing the particular semiconductor, in this case, 5,5'-bis(4-*n*-hexyl-phenyl)-2,2'-bithiophene (6PTTP6). These results may be said to be indicative of a larger trend in this area, where there is a general lack of research on the understanding of the interaction or form-function relationships that would encourage the development of better sensors.

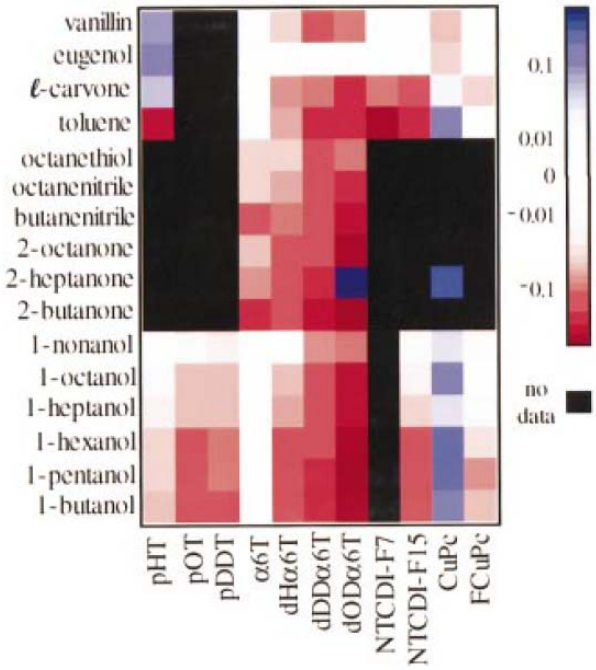

Figure 2. Chart summarizing the sensor responses of different organic semiconductors to various volatile vapors. Figure reproduced from ref [8].

There is one area, the functionalization of the active material, that has been explored more systematically by a few groups. Torsi *et al* showed that by substituting the alkyl side chains of polythiophene with alkoxy groups, the resulting devices exhibited a selective response to analyte vapors in terms of the analyte dipole moment [10]. Another contribution was made by Chang *et al* who showed that functionalization of the terminal hydrogen in polythiophene molecules lead to differences in the sensing of acids and bases [6]. This work investigated a number of different polythiophenes that were end-functionalized with an acidic or basic group, showing that functionalization of the polythiophene can induce changes in the sensor response (Fig. 3). End-functionalization means that the sole, terminal hydrogen of the polythiophene chain was replaced with a functional group. Both these result confirm some of the benefits to using organic materials, and specifically polythiophene. If polythiophene can be functionalized in this way, one can easily see how sensor arrays with substantial discrimination power can be generated simply out of one active material polythiophene, with each polythiophene sensor possessing a different functional group. The use of a single class of active material can simplify processing as well as synthesis and fabrication considerations.

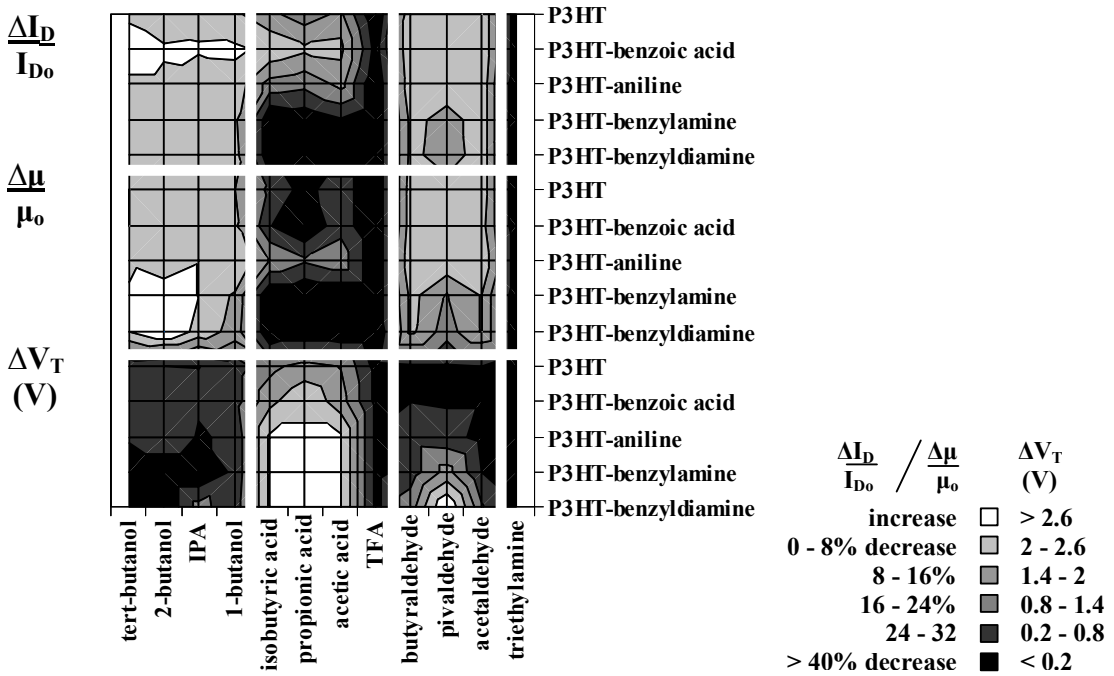

Figure 3. Sensor response of end-functionalized polythiophene to different acidic and basic vapors. Figure from ref [6].

Basic Principles of Sensor Behavior

An organic TFT operating as a gas sensor is essentially a chemical transducer element, where the chemical reactivity of the material is tied to its electrical behavior. Therefore in the presence of a chemical species like a gas analyte, the material undergoes changes in its electrical behavior. These changes can be monitored as shifts in the drain current, or I_D, of the transistor, the carrier mobility and the threshold voltage [8,11,12]. Each of these suggests different mechanisms of analyte transduction, none of which are mutually exclusive.

The process of gas sensing begins with the analyte adsorbing into the bottom-gated TFT, followed by diffusion of the analyte into the active material [13]. As the analyte is absorbed into the film and interacts with the charge carriers, it causes the aforementioned changes in electrical behavior. Removal of the analyte generally causes desorption of the analyte and a return to its previous operation.

The adsorption of analyte onto the surface of the semiconductor film is characterized using the partition coefficient, κ:

$$\kappa = \frac{C_A}{C_v}$$

Equation 4.1

where C_A refers to the concentration of the sorbent phase in the polymer film and C_v refers to the concentration of the vapor phase in the ambient.

The partition coefficient itself depends on temperature and the affinity between the analyte and the polymer as well as the analyte mass. Lighter analytes will generally exhibit lower κ values and heavier compounds possess higher values. Under ideal conditions the sensor response will be linearly proportional to C_A with a maximized partition coefficient, κ.

After adsorption, the analytes diffuse into the film, most likely through the grain boundaries [14-16], and interact with the semiconductor producing changes that are detectable in the transistor's electrical behavior. There are several proposed mechanisms for analyte transduction, none of which are mutually exclusive. One mechanism is that analyte affects the charge transport behavior either by trapping of free carriers [17] or by causing a change in the dielectric constant of the material which affects the charge hopping rate of the carriers [13]. While the use of either mechanism depends on how one models charge transport through the film, in either case, the main effect is to decrease the mobility of the carriers. This translates into a lower slope on the I_D-V_G characteristic of a transistor.

Another possible mechanism is that the analyte acts a dopant causing complete or partial charge transfer into the semiconductor [18]. The presence of these additional charges will affect the turn-on behavior of the device and will appear in the semiconducting sensor as a change in threshold voltage, V_T, which will shift in the I_D-V_G curve.

Charge transport may also be affected by physically-based mechanisms. Drawing from the behavior of chemiresistors, it is also hypothesized that uptake of the analyte causes the semiconductor film to swell increasing the film's electrical resistivity. It is conceivable that this resisitivity change occurs on top of the mobility effect, but it can be modeled either as a change in the charge hopping rate [13] or as a decrease in effective mobility as the conjugation length of the material changes.

The net effect of all these mechanisms is to cause a decrease in the drain current, I_D. In practice, all three parameters of mobility, threshold voltage, and drain current, respond to the presence of an analyte. The actual mechanism of transduction is still uncertain and has yet to be definitely proven [19]. It is possible that more than one interaction is present, especially since multiple parameters are affected in the sensor.

Experimental Setup and Measurement Technique

The bottom-gated configuration is the most ideal for sensing applications and is quite amenable to fabricate via solution-based techniques. Printing techniques offer the greatest advantages in terms of manufacturing cost but for research purposes, spin casting a film onto an oxidized, doped silicon wafer is the simplest and most reproducible method. The oxide and doped substrate become the dielectric and gate, respectively, thus reducing the number of fabrication steps. The entire procedure for fabricating a polythiophene TFT that was used as the standard method for this work is as follows:

- Start with heavily doped Silicon wafer, (usually p-type)
- Thermal oxidation for gate dielectric (nominal thickness of 100 nm)
- Lift-off process:
    - Spin-coat wafer with I-line photoresist
    - Expose photoresist with contact printer
    - Develop photoresist
    - Thermally evaporate gold onto wafer (target thickness of 300 Å); 15 Å of crome is used as an adhesion layer
    - Remove photoresist and unwanted gold with acetone bath
- Thorough cleaning of wafer:
    - O_2 plasma clean for 10 minutes
    - RCA clean (5:1:1 mixture of DI water/NH_4OH/H_2O_2 heated at 70 °C) for 5 minutes
    - Rinse with DI and air dry
- Spin-cast polymer film (these steps were performed in an inert, dry environment):
    - Dissolve polythiophene in anhydrous chloroform; most often used weight percent is .08 wt. %
    - Vortex for 1 hour at 1000 rpm
    - Optional: continue dissolving overnight
    - Filter spin solution with 0.45 μm filter
    - Bake wafer at 120°C for 20 minutes to remove residual moisture
    - Spin coat substrate at 6000 rpm for 60 sec; (solution is deposited at 15 rpm)
    - Post-spin bake at 120°C for 5 minutes to remove residual solvent

Unless otherwise stated, a W/L ratio of 500/20 μm and a gate oxide thickness, T_{ox}, of 100 nm of SiO_2 was used for all devices. Several concentrations of spin solutions were used throughout this work, with 0.08 wt. % being the most common. This resulted in a film thickness of 70 nm. Other concentrations were: 0.01 wt. %, 0.02 wt. %, 0.04 wt. %, 0.16 wt. %. The corresponding film thickness scaled linearly with weight concentration, with more dilute concentrations producing thinner films. This relationship, as well as other dependencies of processing parameters on device performance, is discussed in a later chapter.

Once fabricated, the organic TFTs were characterized as gas sensors using a custom setup that was designed, built, and modified over the course of several years. The picture shows the most recent configuration, which is outlined with the schematic in Figure 4. The main features are the sensor chamber, the gas delivery system, and the characterization assembly. The sensor chamber is composed of a custom glass chamber that was fabricated by a local glass blower (Pacific Flame; Emeryville, CA). This chamber has a special feedthrough to allow electrical connections for a 40 pin ribbon cable and the power supply for a small fan, which is used to stir the air inside the chamber. Caulk is used to seal the area around the feedthroughs. For gas delivery, the chamber has inlet and outlet connections that are designed for Swagelok ultra-torr fittings that create an air tight seal. The chamber is closed with a clamp assembly that seals against a rubber o-ring to produce an air tight seal, confirmed through mass flow measurements. Custom fabric is used to cover the entire sensor chamber so that the measurements are performed in the dark. The number of sensor chambers can be increased up to three to allow for parallel testing.

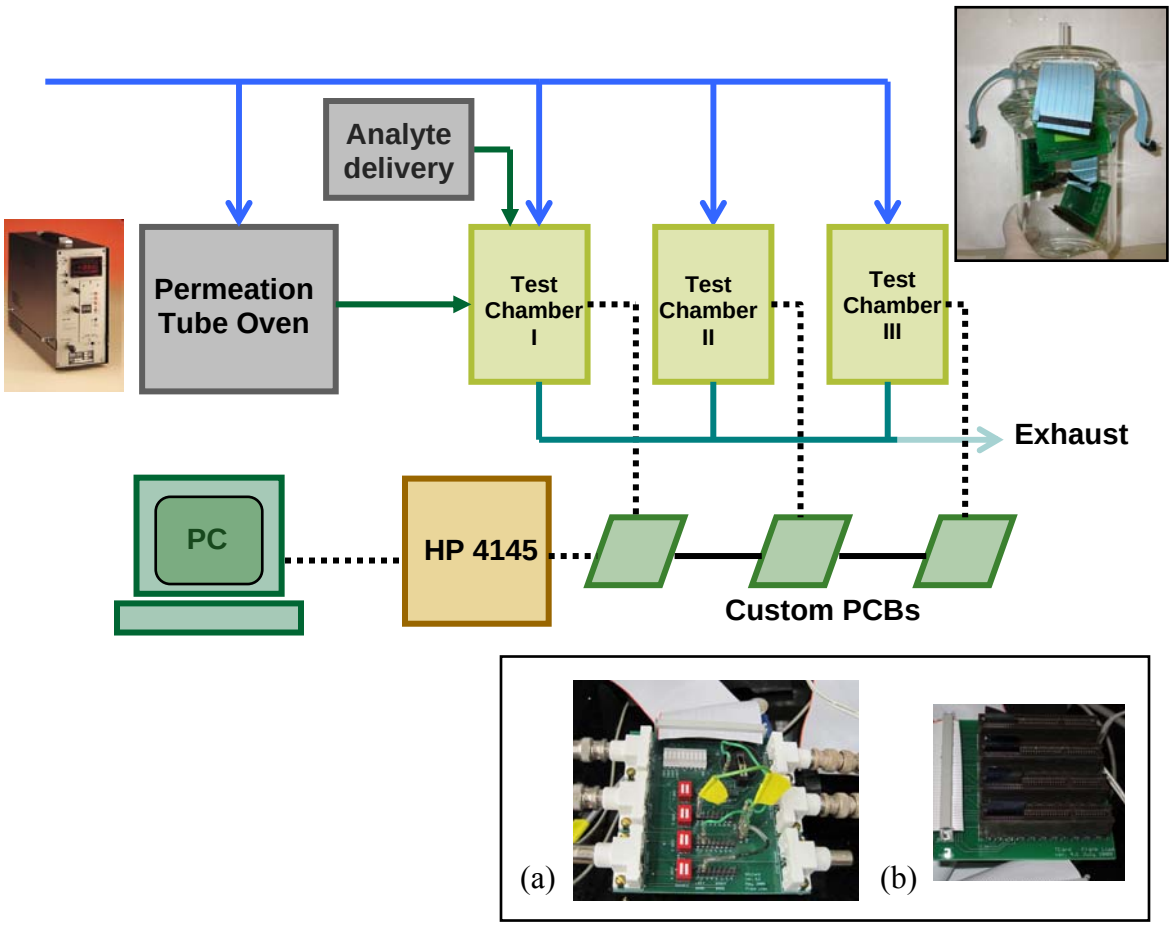

Figure 4. Schematic of experimental setup used to characterize gas sensors made from organic TFTs. The test chamber is shown in the top right inset; the (a) SELCard and (b) TCard are shown in the bottom right inset.

The gas delivery system is composed of poly pipe with several Swagelock two-way and three-way valves, a mass flow meter, pressure regulators, and an air dryer. These serve to deliver either dry nitrogen or dry air into the sensor chambers. The valves are designed such that the lines can be flushed to avoid any introduction of unwanted air or contamination into the chamber. The mass flow meter dynamically confirms that the entire system is extremely air-tight, with a discrepancy of less than 1 sccm.

Delivery of the analyte is accomplished using two techniques, each with its own advantages and disadvantages. The first method is direct injection of analyte vapor. Several sources of analyte vapor were generated using saturated vapor pressures. These sources were maintained under dry nitrogen and were replenished before each experimental run. The exact concentration of analyte was introduced using a syringe which delivered a set volume of saturated vapor pressure. By monitoring the temperature and controlling the volume, the exact concentration of analyte is introduced. This method allows for the characterization of multiple analytes within an experimental run and it is capable of accommodating different types of analytes. It eliminates

any transient effects associated with analyte delivery as well as any contamination of the gas delivery lines or cross-contamination with previous analytes. Due to the high the dilution factor of anywhere from 100 to 1000, any error in the analyte concentration is minimized to about 1% to 0.1%.

The second method overcomes these disadvantages by delivering precise amounts of analyte using a permeation tube oven. The permeation tube oven is very accurate and well-calibrated oven that houses something called a permeation tube. The permeation tube contains the analyte of interest and is made of a semi-permeable membrane. For a given length of the tube and at a given temperature, the tube emits a NIST-calibrated concentration of analyte that is then picked up with gas and delivered to the sensor chamber. The disadvantage is that each tube must be specially purchased and calibrated and there is a substantial waiting time of weeks before each tube is ready. Also, the flow used to deliver the analyte is relatively low and thus the introduction of the analyte is extremely slow, resulting in gross transients. The custom sensor setup has been designed to easily accommodate both types of delivery systems depending on the needs of a particular experimental run.

Electrical characterization is carried out with an HP4145 Parameter Analyzer that is connected to a dedicated PC. The HP Parameter Analyzer interfaces with the sensor through a series of custom printed circuit boards (PCBs). One PCB, called a TCard, contacts the sensors using an edge connector and is used inside the sensor chamber. It interfaces with another PCB, called the SELCard, which selects up to four actives devices to be interrogated. Since the HP4145 has four SMUs, it is capable of measuring four drain currents, while the two VMUs are used for the gate voltage and the source voltage. The SELCard also has LED indicator lights to ensure that the devices are properly contacted with the pins. The PC runs Matlab scripts that automate the electrical testing, while recording electrical data and extracting various parameters such as mobility, V_T, and saturation drain current, I_D. These parameters were extracted using the methodologies presented in the previous chapter. Mobility is derived from the slope of the I_D-V_G curve; V_T is defined as the horizontal intercept of the square root of I_D versus V_G plot; and I_D is defined as the drain current when $V_{GS} = V_{DS}$.

Operation of Organic TFT Based Gas Sensor

With the correct experimental setup, the sensor operation is relatively straightforward. Figure 5 shows the sensor configuration with the corresponding biases that are applied during operation. The bottom gated configuration facilitates sensing since the analyte diffuses directly into the film, which constitutes the active material of the device. As the analyte is introduced into the sensing chamber, electrical changes in the behavior of the TFT are detected and monitored via an I_D-V_G sweep of the device as demonstrated in Figure 6, which shows the I_D-V_G sweep of a polythiophene TFT. Upon introduction of an analyte vapor, the organic TFT undergoes an immediate change (in this case, a decrease) in drain current at all gate voltages, V_G. The shift is immediate and is often reversible depending on the analyte. Besides a decrease in current, the devices exhibit a corresponding decrease in the slope of the I-V characteristic and change in the threshold voltage. Thus the sensor parameters can be the saturation drain current, I_{DSAT}, defined as the value of drain current at the highest V_G, as well as the mobility, μ, and the threshold voltage, V_T.

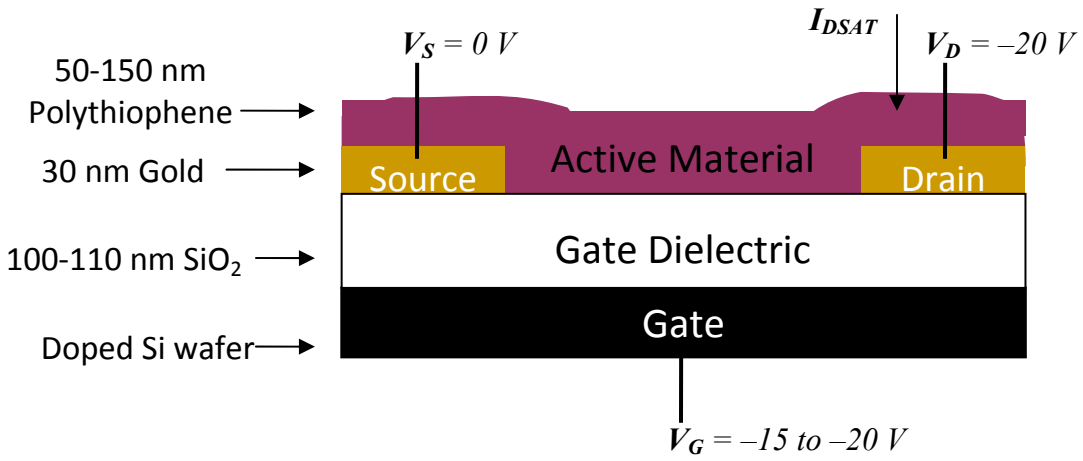

Figure 5. The basic configuration of an organic TFT as a gas sensor showing the applied biases, V_G, V_D, V_S, and I_{DSAT}.

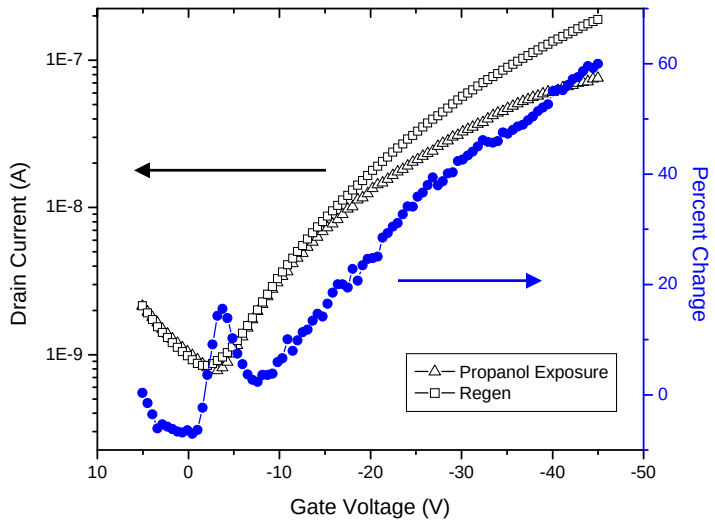

Figure 6. I_D-V_G characteristic of an organic TFT sensor and the sensor response as a function of gate voltage

As Figure 6 also shows, the sensor response increases with increasing gate voltage, which is made apparent by extracting the percentage change in current as a function of gate voltage. The transistor action means that the conductivity is a function of mobility, which is proportional to the carrier concentration and scattering, both of which are affected by the interaction with the analyte and are also dependent on the gate voltage. Thus the gate of a TFT can attenuate and amplify any response of the sensor which is a major advantage of using OTFTs as sensors [7].

In practice, the sensor devices will be interrogated repeatedly over a certain time period. This runs into the problem of the bias stress effect (BSE) introduced in the previous chapter. The BSE can interfere with proper characterization of the sensor response and can convolute the sensor response if it is severe enough. As mentioned earlier, this can be addressed using pulsed measurements [20]. In this work the sensors are interrogated on a 3% duty cycle, which entails a partial sweep of -15 to -20 V on the gate voltage (with V_D kept at -20 V) every sixty seconds. A warm-up period of at least 5 minutes was employed so that the decrease associated with the 3% duty cycle would reach steady-state.

Figure 7 shows how this technique was implemented. The figure shows a polybutylthiophene device exposed to 80 ppm of butanol analyte at around the 900 seconds mark of the experiment. The sensor response is monitored by recording the saturation current of each partial sweep which is normalized to its baseline value. Upon exposure to the butanol vapor, there is a marked and immediate decrease in the drain current. Upon removal of the analyte with fresh nitrogen, the current is restored to its previous value. In this case, there is an overshoot of the drain current but this is usually not observed. The ability to recover is dependent on the analyte with a full and complete recovery observed for the majority of analytes, though some vapors can cause a permanent decrease.

At each time point, the partial sweeps provides enough information to extract the field effect mobility, μ_{FET}, and the threshold voltage, V_T, in addition to the saturation drain current, I_{DSAT}. All three parameters can be monitored as a function of time in order to observe the sensor response. For example, the response to butylamine vapor at a concentration of 79 ppm, is shown in Figure 8. Upon butylamine exposure, all three parameters, I_{DSAT}, mobility, and V_T, respond immediately. These plots of sensor response over time are used extensively in this thesis.

As previously discussed, each parameter points to a possible sensor mechanism and it is possible that several mechanisms are simultaneously present. A shift in the threshold voltage, V_T, may indicate that the analyte is acting like a donor with partial or complete charge transfer, while a decrease in carrier mobility may indicate the analyte acts as a trap or scattering site [15]. Both of these shifts contribute to a decrease in saturation drain current. The actual mechanism of transduction is still unclear [19]; but the fact that all three parameters shift indicate that the three mechanisms may be occurring in the device.

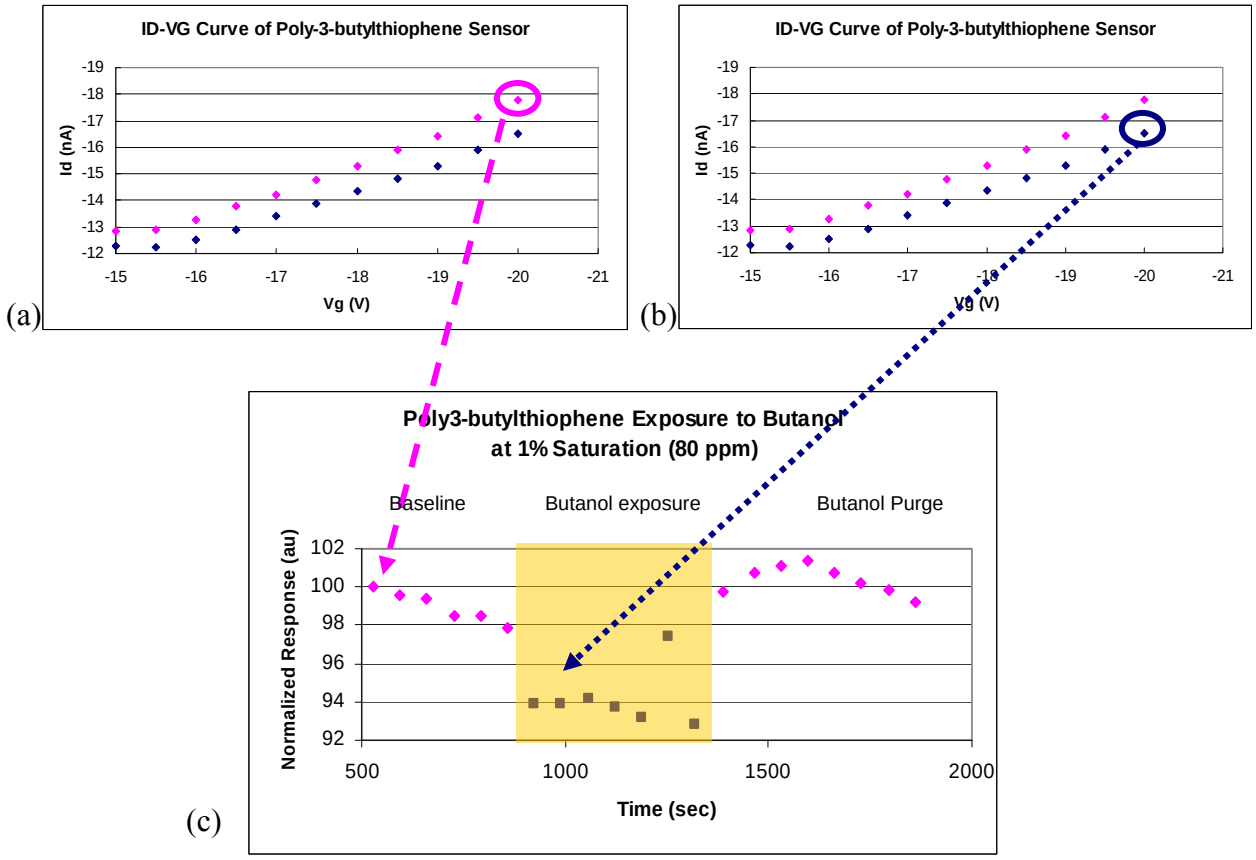

Figure 7. Characterizing the sensor response by monitoring saturation drain current, I_{DSAT}, as a function of time. I_{DSAT} comes from a partial I_D-V_G sweep of the sensor.

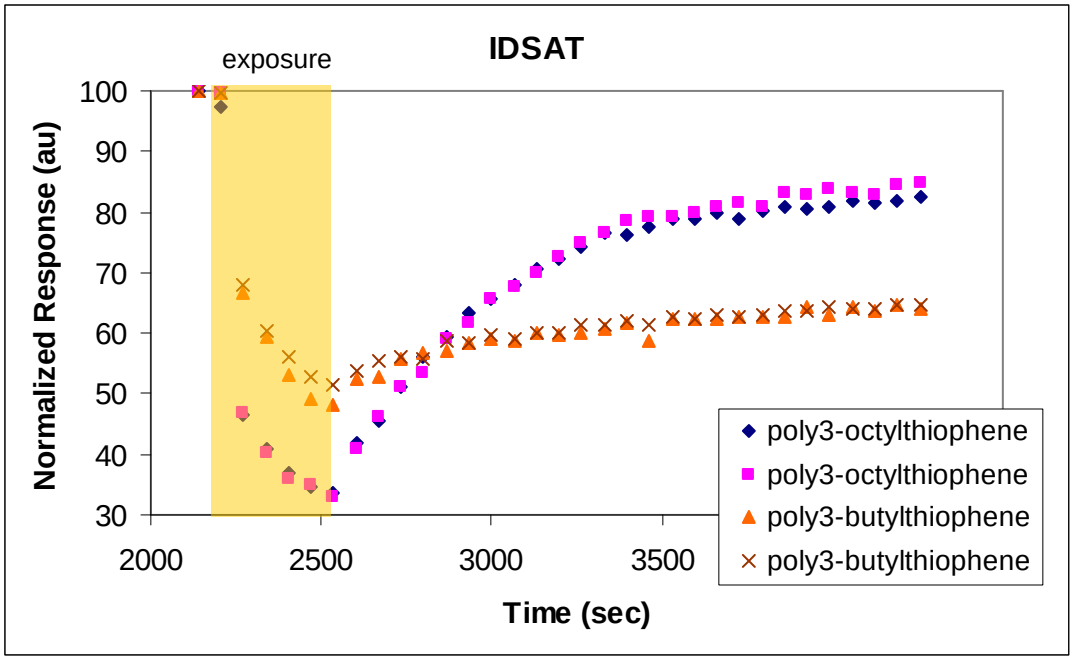

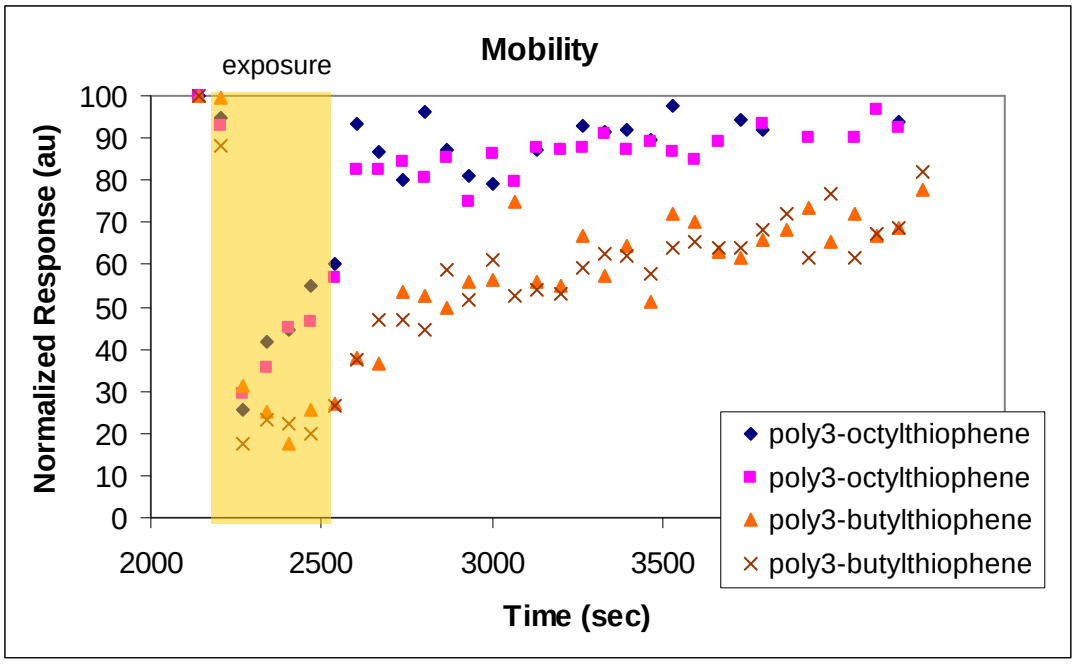

(b)

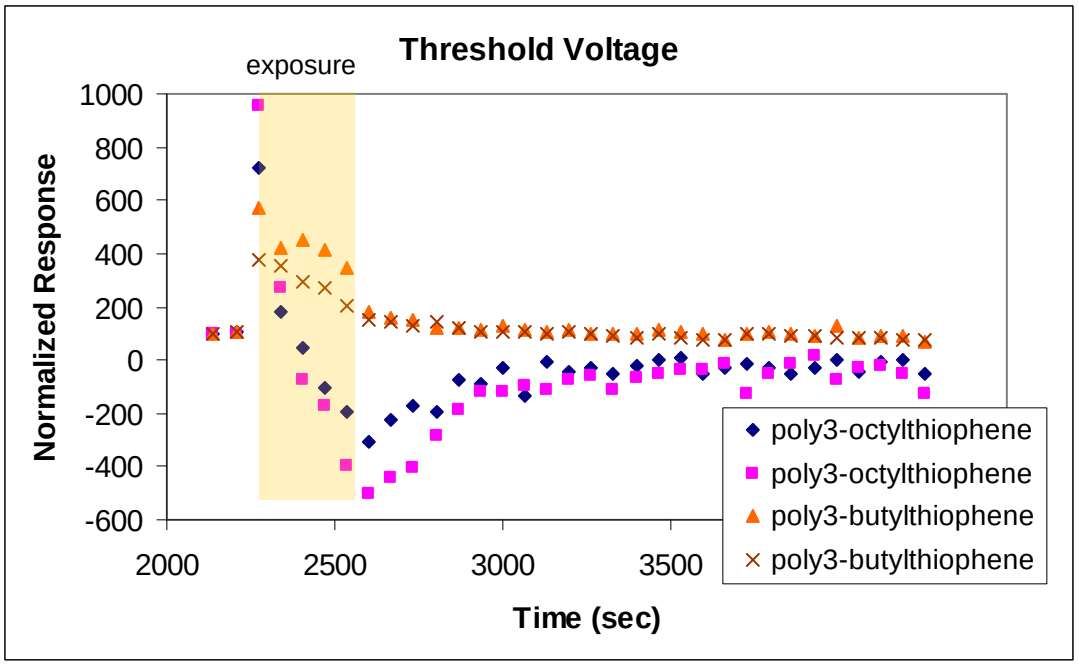

(c)

Figure 8. The sensor response to butylamine analyte (79 ppm) in terms of, saturation drain current, I_{DSAT}, mobility, μ, and threshold voltage, V_T.

Sensor Response to Gaseous Analytes

By testing the sensor with a number of different analytes, the range of the sensor response can be explored. Polythiophene sensors show immediate and definite response to a number of

analytes including toluene (shown in Fig. 9), ethanol, propanol, eugenol, acetic acid, octanoic acid, water, and even milk [11].

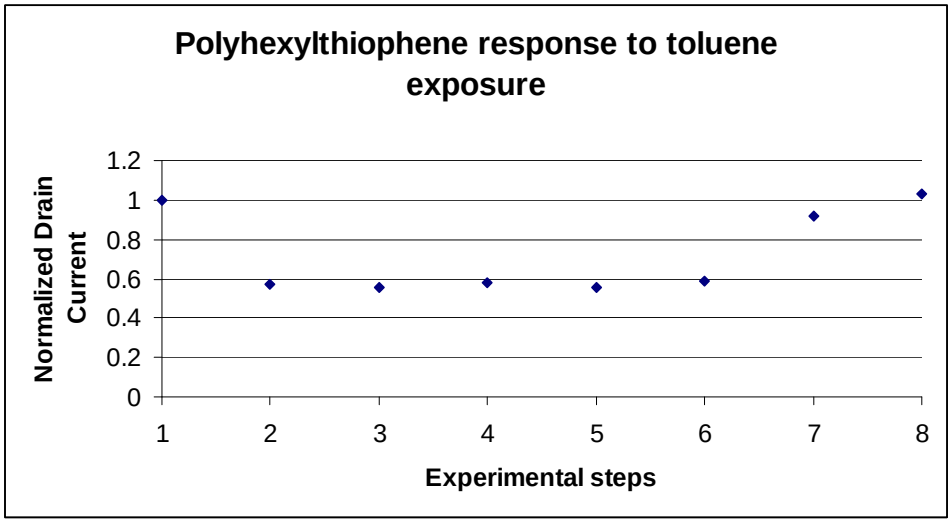

Figure 9. Polythiophene TFT response to toluene vapor. The response is plotted in terms of discrete experimental steps instead of time. At step 2, toluene is introduced and at step 7 it is purged with dry N_2.

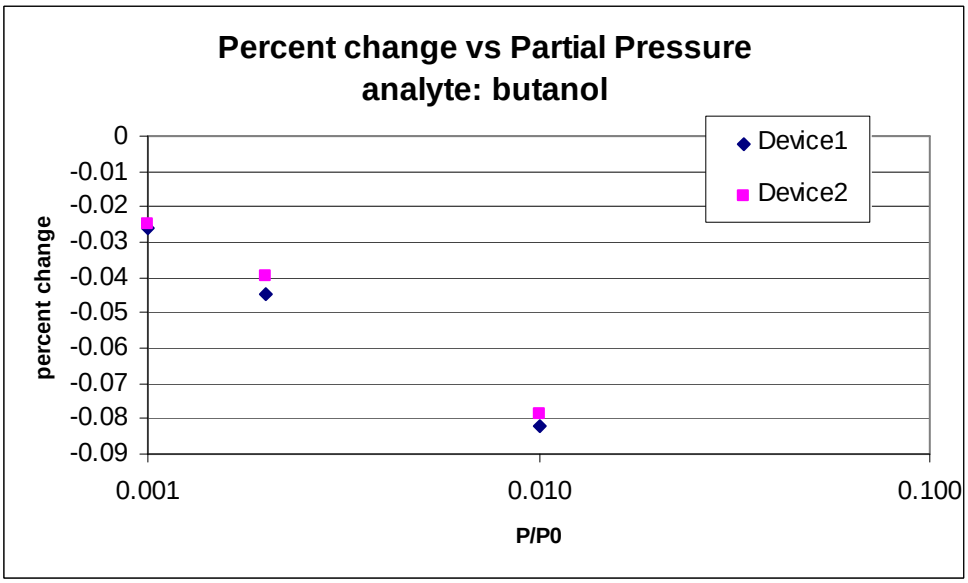

Figure 10. Polythiophene sensor response increases with increasing analyte concentration, characterized as the partial pressure of analyte within the sensor chamber.

One interesting class of analytes to which polythiophenes respond is alcohols as was shown in Figure 6. Not only are alcohols found in many applications for environmental or product monitoring, but many common gas sensors, such metal oxide sensors, are poisoned when

exposed to alcohols. As with many analytes, the polythiophene response to alcohols is reversible (Fig. 6). Figure 10 shows the concentration dependence of the alcohol response. Here polythiophene TFTs were exposed to butanol vapor for varying partial pressures and showed a corresponding decrease in the drain current of the TFT upon exposure.

While the majority of analytes, like alcohols, cause a reversible response, there are a few analytes which cause an irreversible response. One of the most interesting is amines because they are an important class of compounds found in many natural processes. Biogenic amines, or amines of biological significance, are often byproducts of decay mechanisms and are indicative of spoilage [21,22].

Figure 11 shows the response of polythiophene sensor to a butylamine vapor at a concentration of 10 ppm. As with the alcohol, the polythiophene sensor shows a marked decrease upon exposure to amines. However the effect is permanent with the current staying at decreased levels even after removal of the analyte using dry nitrogen at 25 minutes. Under a constant flow of nitrogen for an extended period of time, a very small recovery is sometimes observed. Like the alcohols, the amines also show a concentration dependence with higher concentrations of amines causing larger shifts. It is difficult to ascertain the cause of irreversibility, given that the exact mechanism of sensing is still unknown.

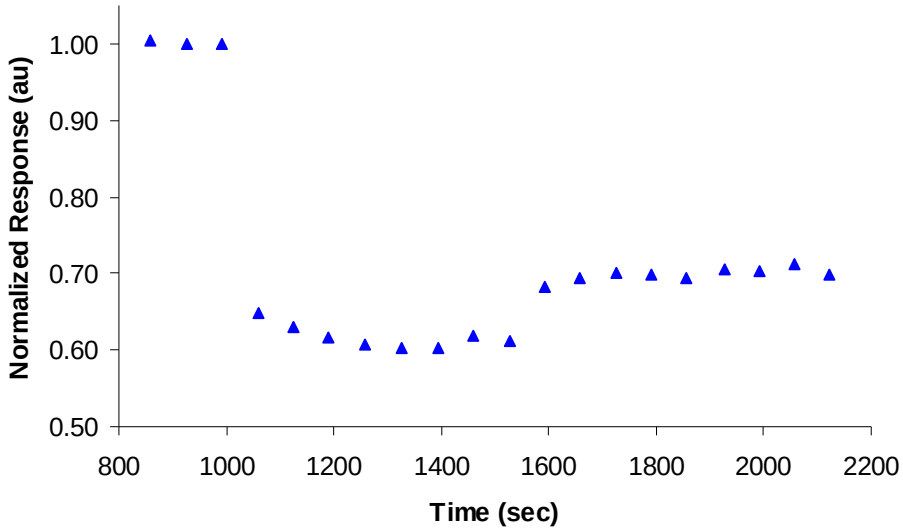

Figure 11. The sensor response of a polyoctylthiophene TFT to 9 ppm of butylamine vapor.

The final class of compounds that will be explicitly mentioned here are nitroalkanes. From an applications perspective, nitroalkanes are also interesting because nitro-based compounds are the main material used for explosives. With the exception of peroxide explosives, all explosives contain nitro-based compounds such as trinitrotoluene (TNT), cyclotrimethylenetrinitramine (RDX), or pentaerythritol tetranitrate (PETN). Not only are is the unstable nitro group associated with the high energy, but the elemental composition of nitrogen, oxygen, and carbon leads to very stable products; this combination means that combustion releases large amounts of energy,

making nitro compounds excellent materials for explosives. Polythiophene sensors show a relatively mild and reversible response to nitroalkanes. The sensor response, which was confirmed through multiple experiments, can be seen more easily in the instantaneous change in current (Fig. 12). In this case, the variation in the drain current in each measurement is about a tenth of a nanoamp; when the sensor is exposed around the 29 minute mark, the sensor exhibit a current decrease of 1 nanoamp.

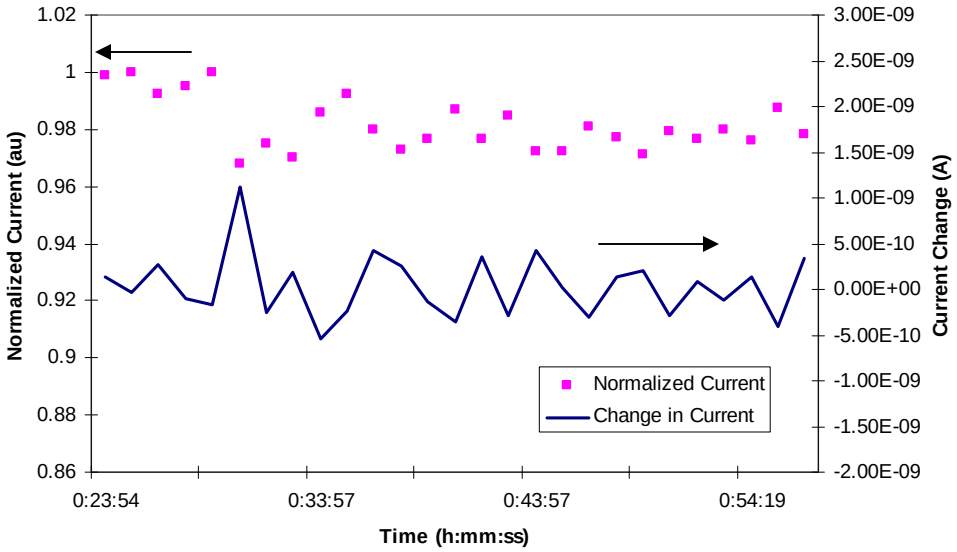

Figure 12. The sensor response of a polyhexylthiophene TFT to nitrohexane at a partial pressure of 0.01. The response is clearer when the current difference is also plotted. The analyte was introduced at ~29 minutes

Conclusion

Organic TFTs as gas sensors were introduced in this chapter. Experimental and characterization methods were presented in great detail. Principles of the sensor behavior mechanism were also discussed including possible mechanisms for the transduction. The basic sensor operation and was reported for a number of interesting analytes. In each case, the materials show an unequivocal and sometimes reversible decrease in drain current, I_D, mobility and threshold voltage, with the amount of decrease is depending on the analyte concentration. Despite these encouraging results, the sensor response is still of limited value—a better understanding of the mechanism is required and there must be a way to attenuate the response.

Chapter 5 Mechanistic Investigations

To properly engineer good sensing materials, it is necessary to have a mechanistic understanding of the sensor-analyte interaction. Unfortunately, this interaction has been poorly understood and proper studies to determine its nature have been lacking. To date, much of the work involving organic gas sensors is centered on reporting and characterizing the sensor response. Concerning organic transistors, as far as can be determined, there has only been one paper by Torsi et al that sought to corroborate the sensor with physical measurements [1]. If organic TFTs are to be a viable sensor element in sensor arrays, the understanding to the underlying interactions is extremely important.

This chapter will present several approaches that were taken to understand the physical properties of the organic TFT as a gas sensor. Since the purpose of elucidating the physical mechanism is to engineer better sensors, the first approach was to understand how physical parameters affect the sensor morphology. This was accomplished using Grazing Incidence X-ray Diffraction (GIXD). The next approach is to verify and monitor the sensor-analyte interaction; X-ray Reflectivity (XRR) proved to be a successful technique for these purposes. This section will present some enlightening and novel in-situ characterization of polythiophene gas sensors. Finally, the last approach is to definitively corroborate the interactions observed in XRR and to relate physical changes to electrical ones, by using quartz crystal microbalance (QCM) measurements to monitor frequency, and subsequently mass, changes in the films.

Grazing Incidence X-ray Diffraction (GIXD) Measurements

In recent decades, GIXD has become a popular technique to analyze the structure of thin-films. While x-ray techniques are not traditionally though of as a surface technique, GIXD is a technique, made possible by synchrotron light sources, that can be used for surfaces, monolayers and ultra thin films [2]. As the interest in organic thin films and monolayers has increased, so has the use GIXD as a characterization technique.

The theory behind GIXD will be briefly covered here. GIXD is a diffraction technique where the penetration depth of an incident beam of X-rays is restricted to a thin film by using incident angles that slightly exceed the critical angle for total external reflection of a given material. The low angle of incidence also provides for a long path length of the incident X-rays on the sample in the plane of the film (ca. 2 – 6 mm, depending upon the diffraction angle), thereby producing sufficient diffraction intensity for structural characterization. Diffraction of the evanescent wave from crystalline regions of the film enables characterization of the in-plane structure.

Figure 1 shows the setup for a typical GIXD experiment. A beam of X-rays strikes the sample as wave vector, $\mathbf{k_i}$, and the diffracted beam, $\mathbf{k_f}$, is depicted with momentum transfer $\mathbf{q} = \mathbf{k_f} - \mathbf{k_i}$. The scattering vector, $\mathbf{q}$, has an in-plane ($\mathbf{q_{xy}}$) and out-of-plane ($\mathbf{q_z}$) component. Conditions for in-plane diffraction are met when any in-plane scattering vector $\mathbf{q_{xy}}$ corresponds to a reciprocal lattice point of the two-dimensional lattice of the crystalline film [3]. Because of the two components, diffraction data from GIXD measurements are two dimensional with the in-

plane ($\mathbf{q_{xy}}$) component usually on the x-axis and the out-of-plane ($\mathbf{q_z}$) component on the y-axis, with color indicating the intensity of the diffracted beam.

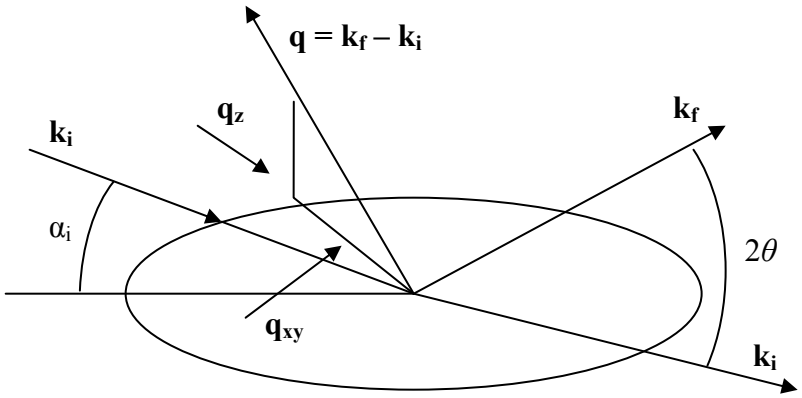

Figure 1. Schematic of GIXD experimental geometry

The two dimensional diffraction data are particularly useful for gas sensors based on organic TFTs because both components may have some physical bearing to the operation of the device. As a gas sensor, the device is a stacked structure since the gas analyte interacts with the entire surface of the film and diffuses vertically into the film. As such, the out-of-plane data, associated with traditional XRD, is helpful in understanding how the morphology may affect the sensor interaction. As a TFT, charge conduction occurs laterally in the plane of the film, so in-plane diffraction data can relate how morphology is affecting the charge transport characteristics.

This section will present how varying important parameters, the most notably the side chain length, affects both the out-of-plane and in-plane morphology of the film. Understanding the changes in the morphology both to the sensor and the charge transport behavior, can elucidate routes for engineering the device to produce better gas sensors.

The side chains of a polythiophene molecule are interesting sites for engineering good gas sensors. To begin with, there is the flexibility of accommodating many more functional groups than would be on the thiophene ring. Swapping out the sulfur or one of the carbons in the ring would be an extremely difficult synthetic challenge. Not only so, but the side chain also offers many more motifs—not only can the functional group be changed along with the length of the side chain, but a single or multiple functional groups can be accommodated at different points along the side chain and branching is also possible.

Silicon wafers having an oxide layer with a thickness of ca. 100 nm were used as a substrate. Polythiophene samples were prepared by spin coating solutions of polythiophene dissolved in chloroform at 0.08 weight percent at a spin speed of 6000 rpm. The films were then annealed at 120 °C for either 5 minutes or 24 hours and then samples were cleaved into 1” by 1” squares for GIXD characterization. The GIXD measurements were conducted at Stanford Synchrotron Radiation Lab (SSRL) on Beamline 11-3 using a Mar345 Area Detector, with a wavelength of 0.976 angstroms, and sample-detector distance of 400 mm. The incident angle was approximately 0.12degs.

The sample films are listed in Table I. The parameters investigated were the side chain functionality and length and the anneal time of the film. The latter two have been known to affect the film morphology as indicated in the literature. Using traditional XRD, Prosa *et al* have shown that side chain length can affect the out-of-plane crystalline spacing, with longer side chains setting longer d spacing [4,5]. Yang *et al* have shown that annealing spun-cast polythiophene films can improve crystallinity of the film [6].

Material	Side Chain Functionality	Side Chain Length	Anneal Time
poly-3-butylthiophene	Alkyl	4	5 min
poly-3-butylthiophene	Alkyl	4	24 hours
poly-3-octylthiophene	Alkyl	8	5 min
poly-3-octylthiophene	Alkyl	8	24 hours
poly-(3-ethyl-4-butanoate)thiophene	Ester	4	5 min
poly-(3-ethyl-4-butanoate)thiophene	Ester	4	24 hours
poly-(3-ethyl-4-heptanoate)thiophene	Ester	7	5 min
poly-(3-ethyl-4-heptanoate)thiophene	Ester	7	24 hours

Table I. The parameters of the different polythiophene materials investigated with GIXD.

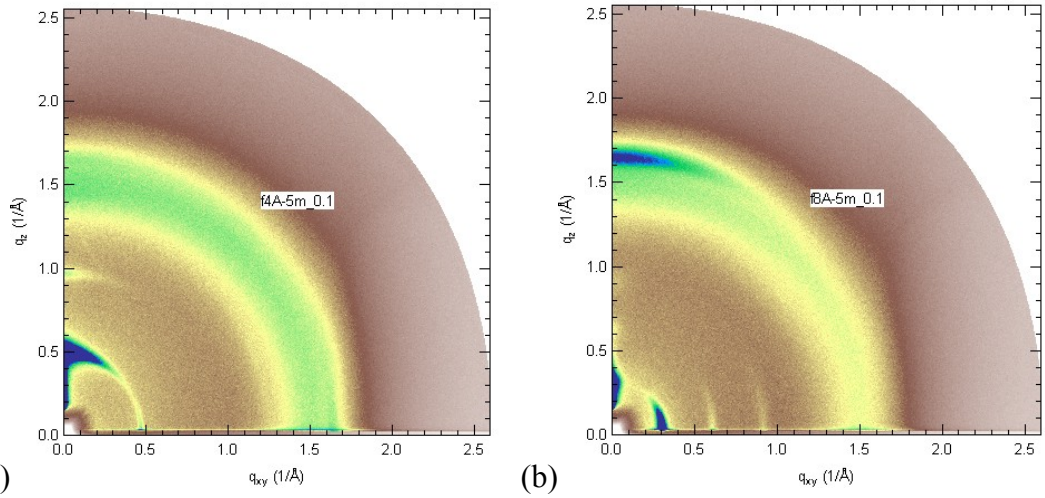

Figure 2. GIXD patterns of poly-3-butylthiophene (a) and poly-3-octylthiophene (b), both annealed for 5 minutes.

Figure 2 shows two dimensional 2D-GIXD patterns for a poly3-butylthiophene and polyoctylthiophene film, both annealed for 5 minutes. The pattern is a 2D plot with $\mathbf{q_z}$ on the vertical axis and $\mathbf{q_{xy}}$ on the horizontal axis; the color indicates the intensity of the diffracted beam, with dark blue being the most intense. The blue feature along the $\mathbf{q_z}$ axis indicates the direction of the pi-orbital that occurs orthogonal to the thiophene backbone. In-plane spacing is extracted by examining the periodicity of the intensity peaks along the $\mathbf{q_z}$ direction and out of

plane spacing is determined by the periodicity of peaks along the $\mathbf{q_{xy}}$ direction; the orientation of the pi-stacking peak, which is orthogonal to the side chains, is also extracted. These values are extracted using automated scripts.

Material	In-plane spacing (Å)	Out-of-plane spacing (Å)	Pi-stacking spacing (Å)	Pi-stacking direction
poly-3-butylthiophene	13.10	13.17	3.78	Weak In-plane
poly-3-octylthiophene	20.59	19.78	3.81	Strong Out-of-plane
poly-(3-ethyl-4-butanoate)thiophene	15.86	16.24	Noisy	Weak In-plane
poly-(3-ethyl-4-heptanoate)thiophene	22.71	21.53	3.79	Strong Out-of-plane

Table II. Extracted parameters from the GIXD diffraction patterns of the polythiophene films. All these films were annealed for five minutes. The pi-stacking spacing for poly-(3-ethyl-4-butanoate)thiophene was difficult to extract due to noise.

Table II summarizes the d-spacings for the films of polythiophene possessing both alkyl and the ester-functionalized side chains that were annealed for five minutes. (The diffraction patterns of the ester-functionalized polythiophene as well as the samples annealed for 24 hours are not shown here, but are included in Appendix A.) Since the samples annealed for 24 hours show nearly identical plane spacings, it appears the anneal time does not affect the spacing; however it does reduce the intensity of the signal so it may affect the proportion of crystalline to amorphous regions within the film.

From this data, it is clear that the length of side chain sets the out-of-plane d-spacing of the film, as consistent with previous literature, as well as the in-plane (d) spacing, as the GIXD technique is able to reveal. This relationship is preserved even with ester functionalized polythiophene units, which show a slightly larger d-spacing most likely due to the additional ethyl motif in the side chain. This means that the presence of the functional group in the side chain does not significantly impact the physical morphology.

Interestingly, the GIXD data show that there is a change in the direction of the pi-stacking peak between the two polythiophene of differing side chain lengths. The longer polyoctylthiophene films also have a pi-stacking direction that is strongly oriented orthogonal to the film surface, unlike the shorter butylthiophene films that show a pi-stacking weakly oriented in the plane of the film. This is illustrated in the in-plane and out-of-plane patterns obtained from the 2D-GIXD in Figure 3. The images show the lamella (L) and pi-stacking (P) peaks and their associated (d) spacing The pi-stacking peaks are denoted by the letter ‘P’ and d-spacing peaks are denoted by the letter ‘D.’ The broad background near the pi-stacking peaks are from background scattering caused by the thick oxide substrate.

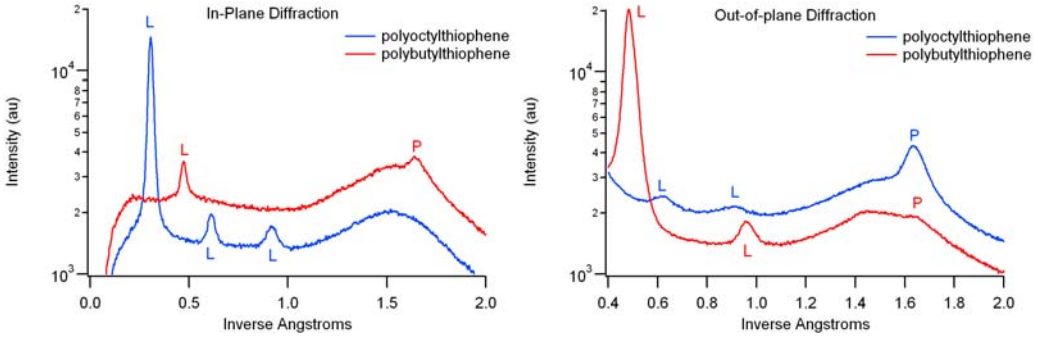

Figure 3. In-plane diffraction (left) and out-of-plane diffraction (right). The pi-stacking peaks are denoted 'P' and lamella peaks are 'L.'

The GIXD data are able to reveal the effect of changing different physical parameters on the film morphology. In particular, the results reveal that plane spacing of the film, both in-plane and out-of-plane, can be determined by the length of the side chain and that the functional group does not affect the morphology.

The next most logical step is to examine the interaction of the film with the analyte and to understand how film morphology is related to this interaction. In this case, the GIXD may be of limited value since it is likely that the sensor-analyte interaction is "invisible" to the technique since the interaction is not likely to be a periodic phenomenon and/or the analyte most likely diffuses through the grain boundaries of the film. Even if the former is not true, the latter will preclude the use of diffraction since the grain boundaries will not present in the measurement. While it is possible that certain shoulder analyses of the diffraction peaks could be used to detect aperiodic changes, this work will turn to a more robust method of monitoring the interaction.

X-Ray Reflectivity (XRR) Measurements

Although the sensor behavior is relatively well-reported, it is still empirically based and the underlying mechanism of transduction is still unclear [7]. This section will present in situ thickness changes in polythiophene films by monitoring the film thickness during exposure to gas vapors. This is the first time that the sensor-analyte interaction has been corroborated with physical changes in the film. The main technique used is X-ray reflectivity (XRR), an analytical technique that probes the structure of thin films. XRR simultaneously measures a film's thickness, electron density, average roughness, and the roughness correlation function. It is extremely accurate in measuring film thickness with Ångstrom resolution. XRR involves constructive and destructive interface of X-rays reflected from interfaces and can be applied to multilayer films.

While XRR has never been used for polythiophene films or with in situ exposure, it has been employed successfully for ultra thin polymer films [8-10], polyelectrolyte films [11]and metal nanoparticle/polymer superlattices [12]. Some previous work on polyalkylthiophene doped with iodine groups has been reported by Prosa *et al* and Tashiro *et al* [4,13], but these involved x-ray

diffraction of the film structure. Since XRR is used extensively in this section, a thorough treatment of the theory and procedure of XRR is covered in Appendix B. However for the reader's sake, a brief introduction will be given here.

Theory of Reflectivity

The basic principle of XRR is depicted in Figure 4. The incident beam impinges the surface of the film with depth, D, at a small angle, θ, and the intensity of the reflected beam is measured

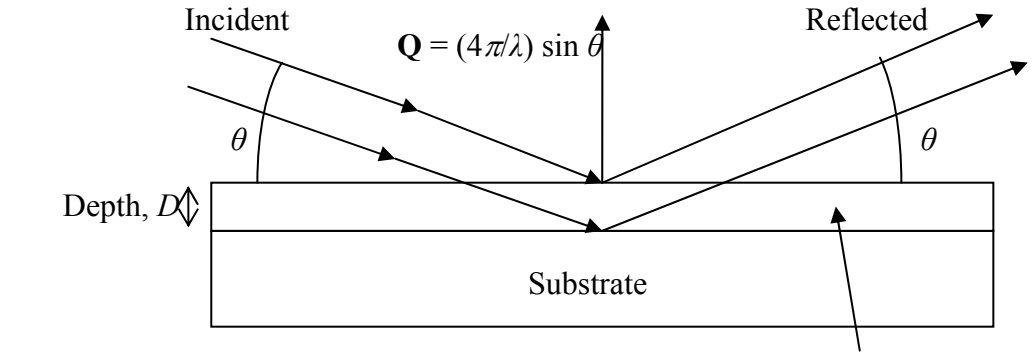

(a)

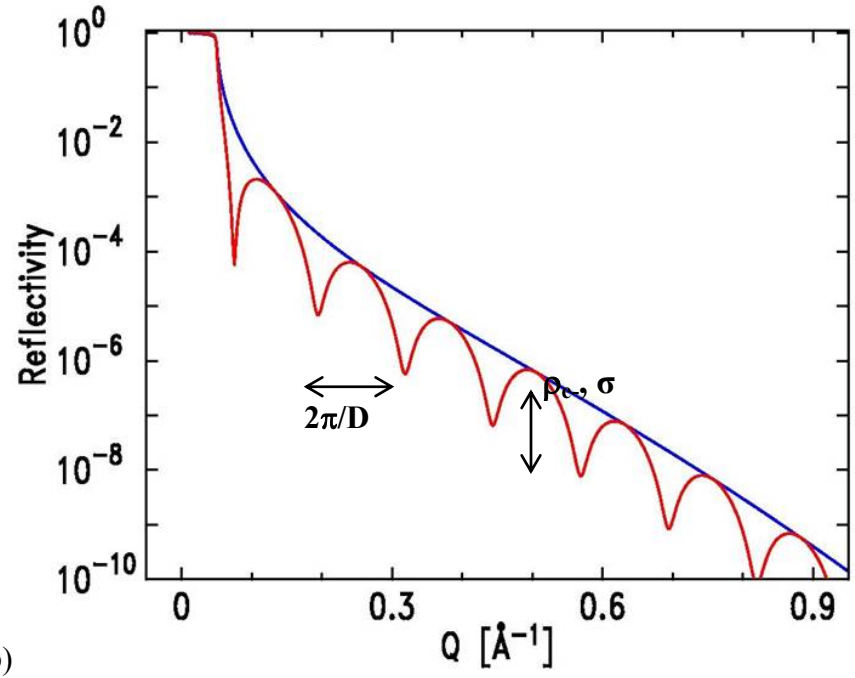

(b)

Figure 4. (a) Basic principle and geometry of XRR measurement. (b) Corresponding XRR curve of thin film on a substrate. The blue line indicates the reflectivity off the substrate without the thin film; the red line is the reflectivity curve from the film with the substrate. The peaks arise from constructive interference of the two layers.

at the specular condition, where the reflected angle equals the incidence angle. The scattering angle is 2θ and the scattering vector is normal to the surface. Data are collected as function of θ or equivalently $\mathbf{Q} = (4\pi/\lambda) \sin \theta$. The corresponding, hypothetical XRR curve is shown in Figure 4b. The spacing of the fringes is determined by D and their feature size is determined by the electron density of the film, ρ_{e^-} and the film rms roughness, σ. Specular reflectivity data are analyzed to determine the depth dependence of the electron density of the material of interest. The thickness of the sample is basically determined from the subsidiary maxima of the reflection curves, while the electron density of the film gives rise to the intensity profile [14,15]. Reflectivity can also be done in the diffuse or off-specular condition, where the incidence angle is $\theta - \omega$, while the reflected X-rays are detected at an exit angle of $\theta + \omega$ from the surface. The diffuse technique was not employed in this work.

Specular reflectivity data are analyzed with a multilayer model analogous to that employed in standard optics. The data are fit using the Parratt method which is based on Fresnel optics; this model incorporates several variable parameters (e.g., film thickness, density and roughness) and can be described with the recursive equation describing the reflectivity of the nth layer of the film:

$$R_{n-1,n} = a_{n-1}^{4}\left[\frac{R_{n,n+1} + F_{n-1,n}}{R_{n,n+1}F_{n-1,n} + 1}\right] \qquad \text{Equation 5.1}$$

where R_n and F_n are the Fresnel and reflectance coefficients for the nth layer or medium, respectively and a is the amplitude factor of the electric vector. The reflectance, R, is related to the square root of the ratio of intensity of the reflected beam to the incident beam. Thus this recursive equation can be solved iteratively to determine the film morphology for a given XRR scan.

Using XRR reflectivity, the films were examined under a number of conditions. First the film morphology, in this case thickness, was characterized as a function of the processing parameters. Once the basic morphology is established, in situ scans were employed to dynamically monitor the change in film thickness during an analyte exposure. These changes were monitored for both cases of analyte absorption as well as desporption, in order to fully verify the response. Not only do these in situ scans confirm the physical interaction of the analyte with the sensor but they elucidate a number of important dependencies in the sensor-analyte interaction.

Experimental Methods and Techniques

Polythiophene films for the XRR scans were prepared by spin-casting onto oxidized silicon wafers. The oxide thickness was 100 nm for polythiophene TFTs in order to act as a suitable gate dielectric and 10 nm for XRR measurements in order to optimize sensitivity to thickness changes. For polythiophene TFTs, lithographically patterned gold source and drain pads (30 nm) were deposited onto the substrate using a standard lift-off process prior to spin-casting. Polythiophene of different varieties were purchased from Rieke Metals and used as received. They were dissolved in chloroform according to various weight percent solutions for an extended

period, filtered with 0.45 μm filter, and spin cast at 6000 rpm, and subsequently annealed at 120 °C for five minutes.

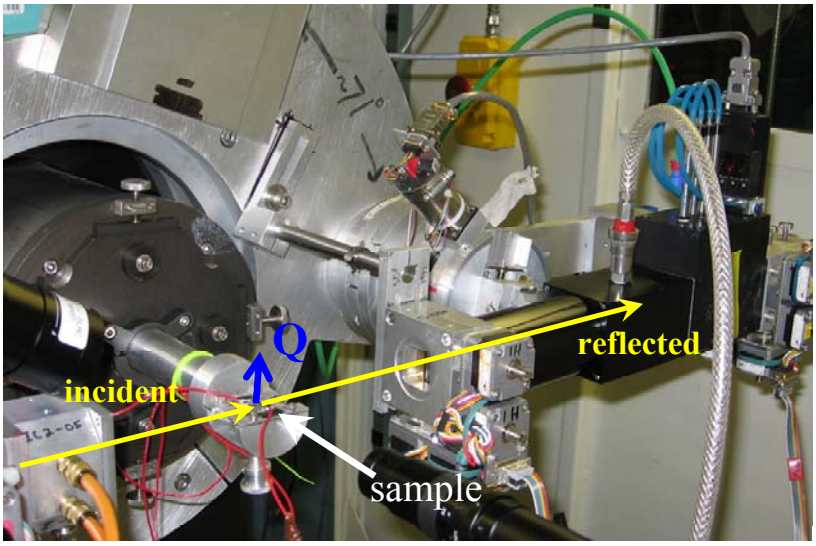

(a)

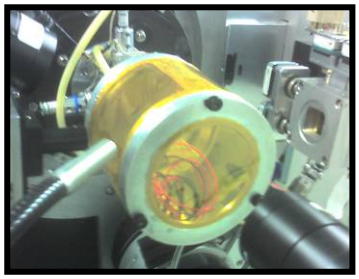

(b)

Figure 5. (a) Experimental setup of XRR measurement (b) Schematic representation of the custom beamline set up for in situ exposure. The custom x-ray sample chamber is shown in the inset (top).

In-situ measurements were carried out using a custom setup that was constructed on the 2-1 beamline at Stanford Synchrotron Radiation Lightsource (SSRL). The X-ray energy was 8 keV and all data are reported as a function of the scattering vector $\mathbf{q} = (4\pi/\lambda) \sin \theta$, where λ is the X-ray wavelength and θ is half the scattering angle [16,17] The scattering geometry was vertical and incident beam was collimated with an 0.05 mm vertical slit. Two 1mm slits collimated the reflected X-ray beam. The custom setup was capable of purging the sample chamber and introducing pure nitrogen for proper baseline calibration, remote gas delivery of the analyte species while the beam was delivered to the sample, and in situ electrical characterization in parallel with the reflectivity measurement. A schematic representation is shown in Figure 5. The setup utilizes a gas sampling tube (500 mL), a syringe pump for delivery of the gas analyte, several mass flow controllers and meters, an HP4145 parameter analyzer, a computer to interface the parameter analyzer and syringe pump, and a custom sample chamber equipped with gas inlet/outlet ports, electrical feedthroughs and an internal fan to stir the chamber gas.

The procedure for in situ XRR measurements is as follows: the gas lines are first purged to remove any residual analyte and oxygen followed by baseline reflectivity measurements. The syringe pump then collects a precise volume of saturated analyte vapor from the analyte vapor reservoir and injects this volume into the sample chamber. The final concentration is set by the dilution of the saturated vapor by the analyte volume and the temperature of the x-ray hutch, which is constant at about 25 °C. Because the syringe pump is accurate to better than 0.01 mL and the injected volume is diluted by a factor of 100, any errors in concentration are minimal at less than <1%. A fan inside the chamber ensures adequate and swift mixing. Since the injected volume is 0.1% to 0.5% of the total volume, ideal and fast mixing can be assumed, avoiding issues like condensation. The injection is followed by a reflectivity measurement on the same spot on the sample. Physical thickness changes are immediately detected by this procedure.

Results and Discussion

Thickness Measurements of Spun Polythiophene Films

The first XRR scans were measurements of polythiophene films under different processing conditions. Figure 6 shows a sample reflectivity curve for a polybutylthiophene film. Although the polymer films are thicker and less smooth than a typical inorganic film, the curve showed nice oscillations indicating a smooth film of reasonably high quality. The presence of fringes can easily be seen indicating that the film thickness is within the range of the technique. The data are analyzed using the Parratt32 program which employs the Parratt method of fitting the data to film thickness, electron density and surface roughness [16]. The fit gives a thickness of 189 Å, with a roughness of 2.3 Å and an electron density of 1.01E-5 electrons(e-)/Å^2. For comparison, Figure 7 shows a scan of a polybutylthiophene film spun at a higher weight percent of the spin solution and the associated fit. The smaller fringe spacing shows a thicker film as expected with using a higher weight percent. As with the previous scan, the regular oscillations indicate that the film quality is smooth enough for the XRR technique despite being a softer polymer film.

Several polythiophene films were analyzed producing similar scans. The data were all fit using the Parrat method and the fitting parameters are tabulated in Table III.

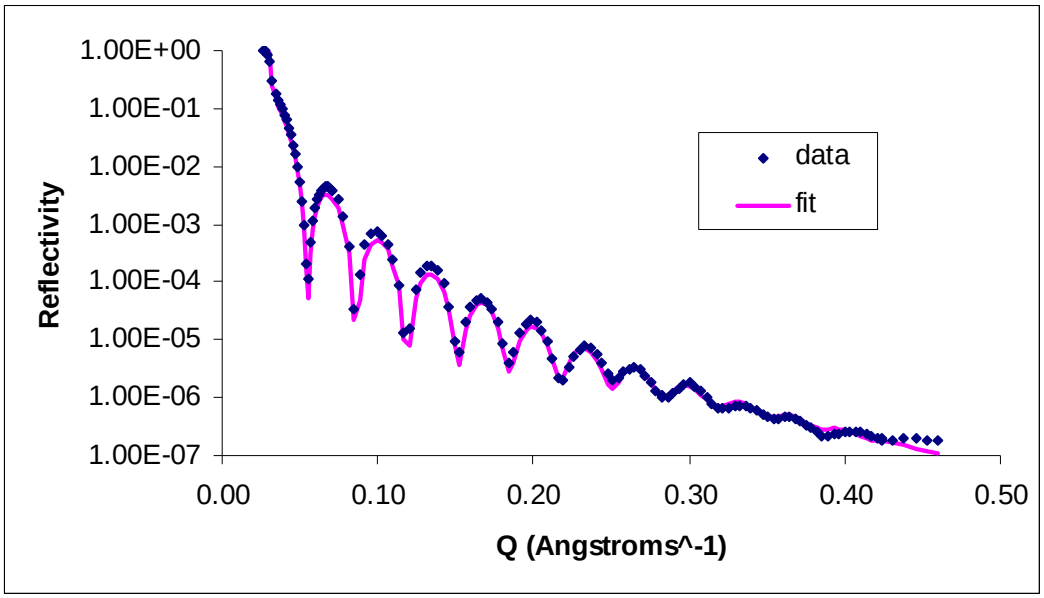

Figure 6. XRR scan of a polybutylthiophene film (blue line) spun at 0.02 weight percent along with the Parratt32 fit (pink points).

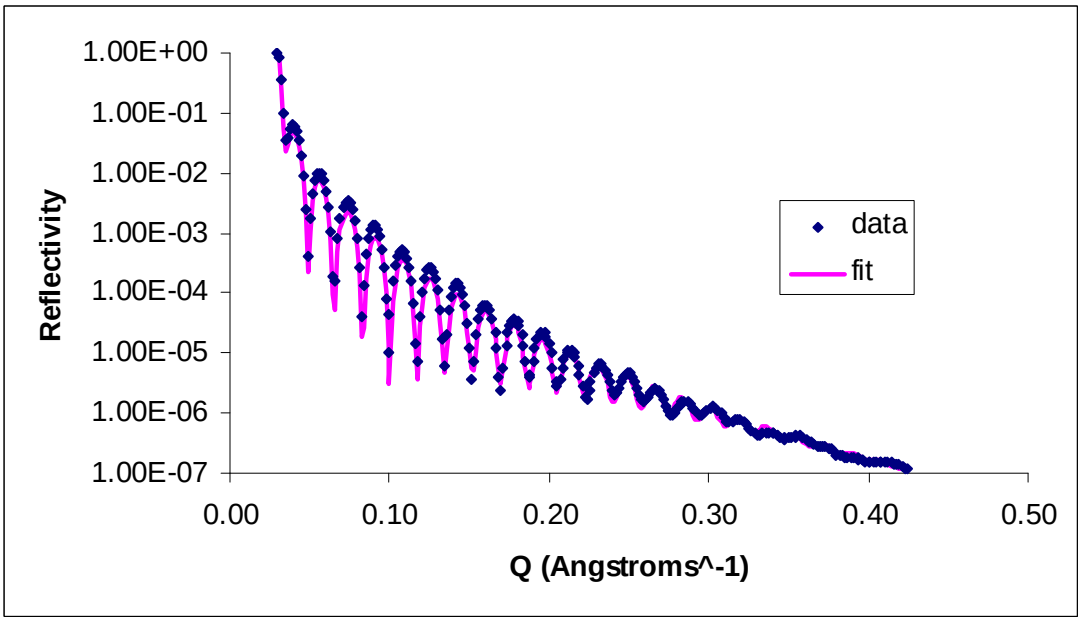

Figure 7. XRR scan of a polybutylthiophene film (blue line) spun at 0.04 weight percent along with the Parratt32 fit (pink points).

From these values it is clear that film thickness is nearly a linear function of the weight percent of the spin solution (Fig 8). Comparing the thickness between a polybutylthiophene film and polydecylthiophene film of the same weight percent, there is a slight difference in thickness. Although polydecylthiophene has a side chain length of more than double that of polybutylthiophene, the polydecylthiophene film is only about 30 Å (16%) thicker than the corresponding polybutylthiophene of the same weight percent.

Material	**Weight Percent**	**Thickness (Å)**	**Roughness (Å)**	**Electron Density (e-/Å^2)**	**χ^2 value**
poly-3-butylthiophene	0.01	118.0 ± 0.1	3.4 ± 0.2	1.02E-5 ± 2E-7	0.1520
poly-3-butylthiophene	0.02	188.9 ± 0.1	2.4 ± 0.2	1.01E-5 ± 2E-7	0.04642
poly-3-butylthiophene	0.04	355.2 ± 0.1	2.8 ± 0.2	1.00E-5 ± 2E-7	0.06569
poly-3-butylthiophene	0.08	754.6 ± 0.1	3.9 ± 0.2	1.14E-5 ± 2E-7	0.05917
poly-3-decylthiophene	0.02	219.0 ± 0.1	3.4 ± 0.2	9.53E-6 ± 2E-7	0.1985

Table III. Parameters fit to the XRR data using the Parratt method. All the fits gave reasonable χ^2values, which measures the goodness-of-fit.

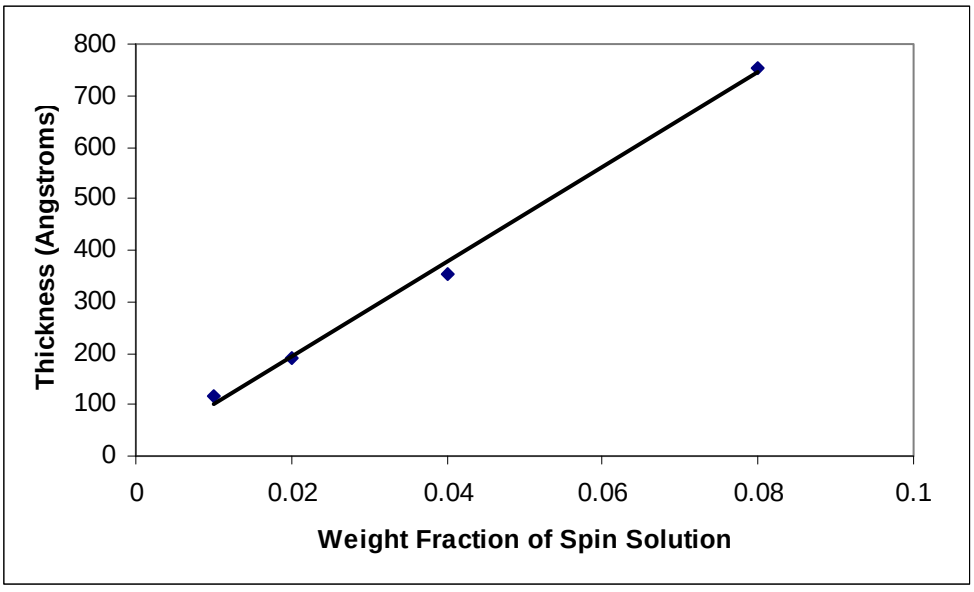

Figure 8. Film thickness as a function of weight percent of the spin solution. The line is a guide to the eye. The error bar estimate is 0.1 Å and is too small to see on the graph.

In Situ Measurements of Film Thickness during Exposure

The great advantage of XRR for this work is that it is amenable to the introduction of gaseous species during measurement. This allows for in situ characterization of the physical interaction between the analyte molecules and the polythiophene films. Specifically the uptake of the analyte by the films can be confirmed and the relationship between analyte uptake and film thickness can be elucidated. XRR scans were performed on several films while the gas analyte was introduced as described in the experimental section. Physical thickness changes are quickly detected.

Before the swelling change can be determined, the effects of possible beam damage and thickness stability of the sample thicknesses must be assessed. Multiple scans reveal a baseline drift as seen in Figure 9. Here a short scan was performed in order to monitor the position of two fringes. Over time, the sample becomes nominally thicker as the fringes shift to lower **q**. This baseline drift is likely due to absorption resulting from degassing in the environment, including the custom sample chamber which contained epoxy, or due to uptake from residual volatile organic compounds in the ambient. The same scan is performed on another part of the sample while the gas analyte is delivered. As Figure 9 shows, when the gas analyte is introduced after the second scan, there is an immediate and marked shift that is much more pronounced than the baseline drift.

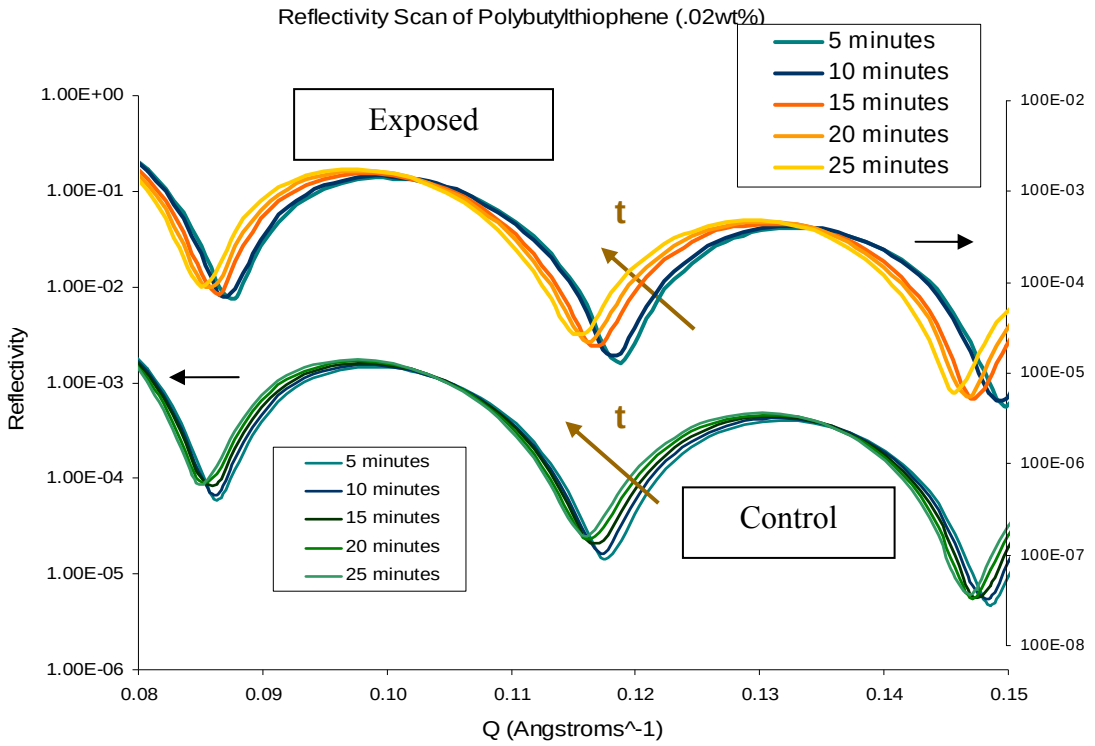

Figure 9. XRR scan depicting the baseline drift (control) and the clear shift due to analyte exposure (exposed). Both scans were performed on the same film but in different spots. Each scan represents a five minute data acquisition time. For the analyte exposure, the analyte was added after 5 minutes.

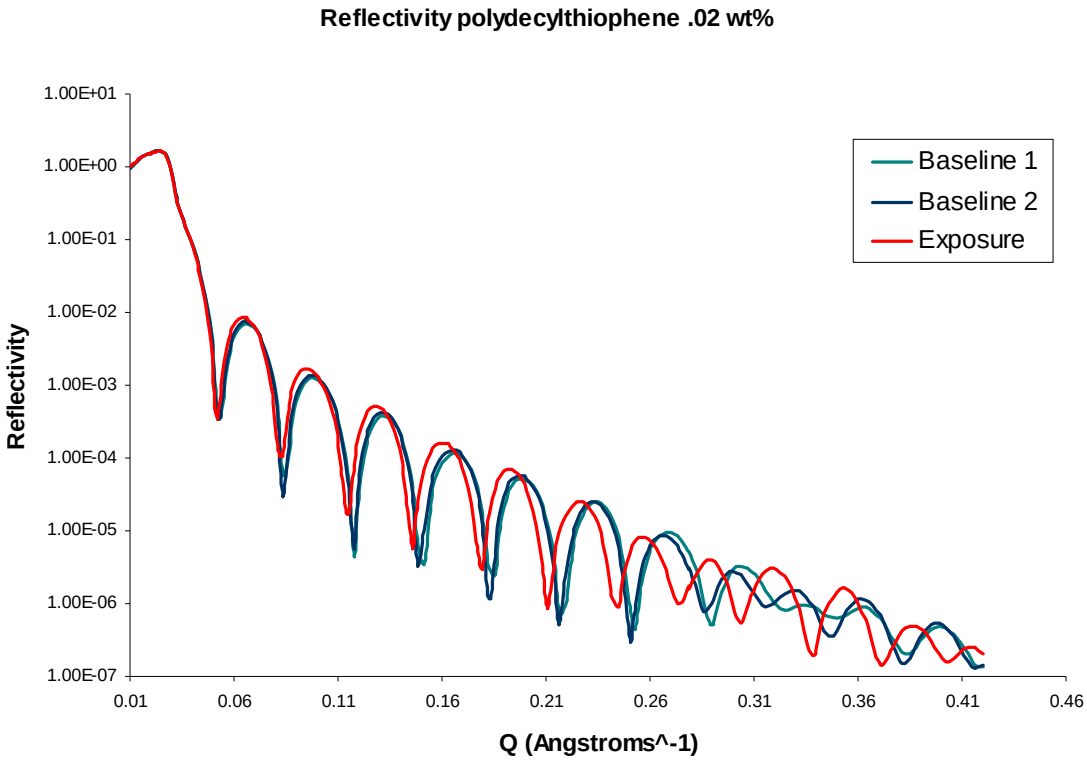

Figure 10. Successive scans of polydecylthiophene. The scans are performed in fifteen minute increments and the butylamine analyte (50 ppm) is introduced after the second scan. Notice the shift in fringes between second (blue) and third (red) scan.

Scan	Thickness (Å)	Roughness (Å)	Electron Density (e-/Å^2)	χ^2 value
Baseline 1	184.7 ± 0.1	3.1 ± 0.2	1.08E-5 ± 2E-7	0.1762
Baseline 2	186.0 ± 0.1	3.1 ± 0.2	1.07E-5 ± 2E-7	0.1743
Exposure	192.0 ± 0.1	3.4 ± 0.2	1.19E-5 ± 2E-7	0.1710

Table IV. Fit parameters from the scan of the polydecylthiophene exposed to butylamine analyte.

The partial scans in Figure 9 confirm the physical uptake and swelling of the polythiophene films in response to a gas analyte. The amount of swelling cannot be calculated from these partial scans, so full scans are necessary. Figure 10 shows a full scan of polydecylthiophene film exposed to 50 ppm of butylamine vapor. There are three scans performed on the same spot in fifteen minute increments, with the first two baseline scans being used for drift calibration. The fit parameters show the original thicknesses to be 184.6 Å and 186.1 Å respectively (Table IV), which indicates a 2% drift at a rate of 0.1 Å/min. The third scan shows a marked shift as a result of butylamine exposure. The final thickness is now 192.0 Å, which gives thickness increase of 4.4 Å, accounting for drift. In addition, to a thickness increase, there is also an increase of 0.12± 0.02 E-5 e-/Å^2 in the electron density. Since electron density is directly related to mass density of

the film [17,18], this is most likely due to the introduction of material into the film and corroborates mass uptake of the analyte by the film.

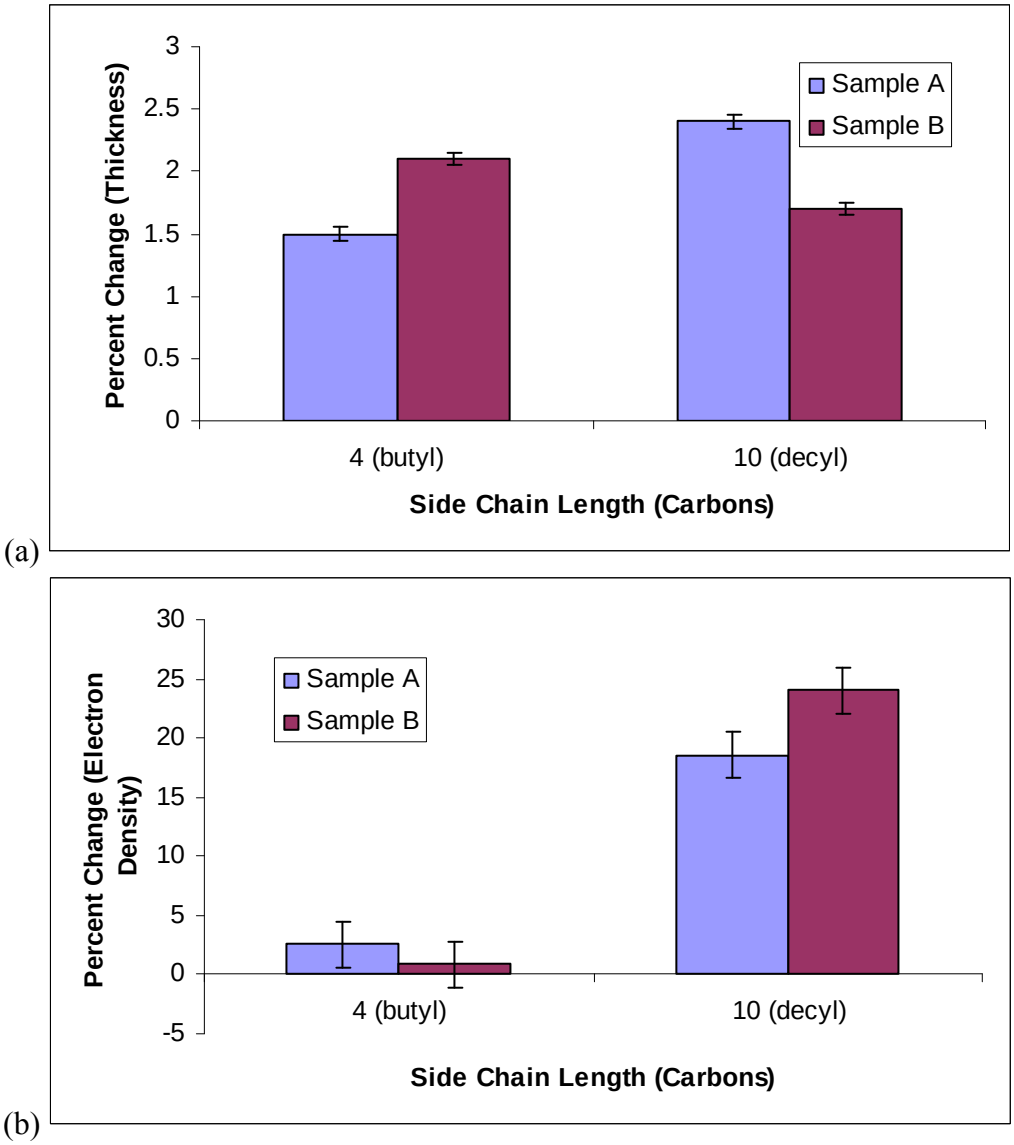

Figure 11. Percent change in thickness (a) and electron density (b) as a function of side chain. While side chain length does not have a strong effect on thickness change, it strongly affects electron density. Sample A and B are two different films and were run to verify consistency.

Similar scans were also performed for films of polybutylthiophene and of polydecylthiophene. It appears that the length of the side chain does not play a strong role in the swelling response of polythiophene films (Fig. 11a). Both polybutylthiophene and polydecylthiophene films showed about the same percent change in thickness. However there is large difference in the change in electron density between the types of polythiophene (Fig. 11b). The electron density of polydecylthiophene films increases by ca. 20%, while

polybutylthiophene show only a few percent increase in electron density. The most plausible explanation for arise from the larger lamellar layer spacing of the polydecylthiophene film than that of the polybutylthiophene film, a seen in the GIXD measurements from the previous section. The larger d-spacing may mean that the polydecylthiophene film is able to incorporate more of the butylamine analyte which leads to a larger increase in mass density and hence electron density.

Varying analyte concentration had only a mild effect on the swelling response. Meanwhile, when the film thickness was halved, the percent change in thickness also halved. Both of these effects are discussed more in the next section.

Thickness Changes due to Blanket Exposure

To investigate the limits of the swelling response, samples were subjected to a blanket exposure of the analyte. Note that these exposures were not performed in situ, rather the sample was removed and placed in a completely saturated analyte chamber for several minutes, removed and immediately re-characterized with XRR. Since desorption takes about 30 minutes (see below), the analyte induced swelling can be characterized. Although the same spot is not scanned, consistency scans have shown the thickness is uniform across a film.

Figure 12 shows the scan of a polybutylthiphene film spun at 0.02 wt% before and after the blanket exposure of butylamine analyte (125 ppt). The exposure of butylamine introduces a clear shift in the XRR scan.

These exposures allow us to examine the swelling response for a range of analyte concentrations. Interestingly, varying the analyte concentration only has a mild effect on swelling response as indicated by Figure 13 which shows the percent change in thickness of a 190 Å thick polybutylthiophene film. The threshold for the swelling response is about 10 ppm for butylamine; however, for this concentration there is no measurable thickness change (<0.5%). Increasing the analyte concentration to about 50 ppm produces a swelling response of about 2-3%. Further increase to 125 ppt (parts per thousand) - four orders of magnitude about the 10 ppt threshold - causes a more significant 7 percent increase in thickness.

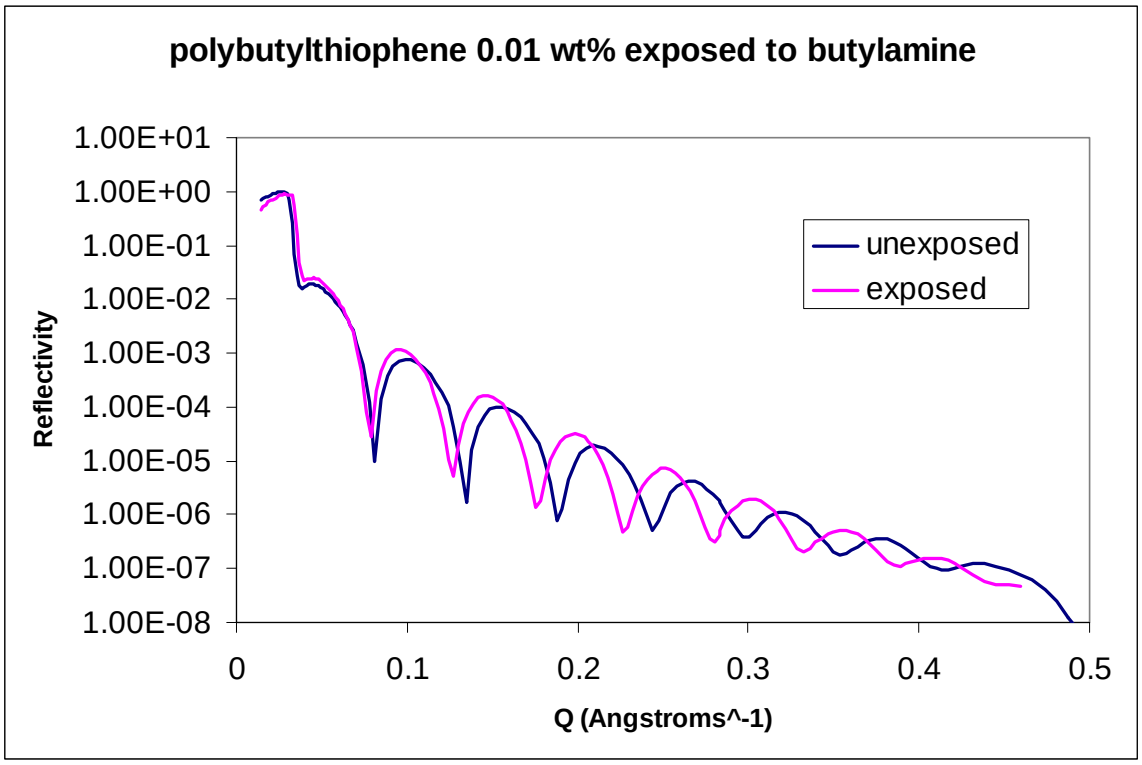

Figure 12. XRR scan of a polybutylthiphene film spun at 0.02 wt% before and after the blanket exposure of butylamine analyte (125 ppt).

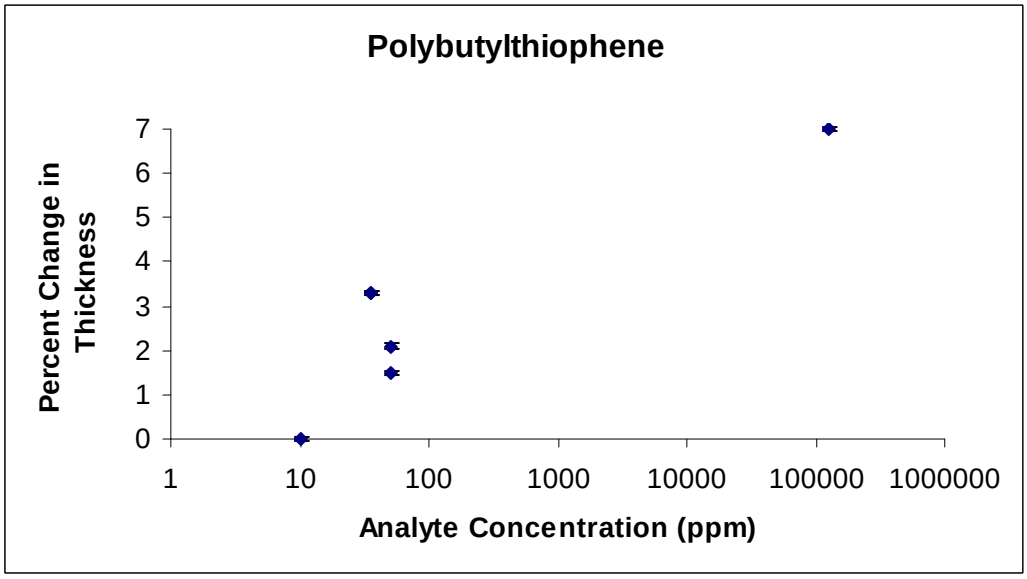

Figure 13. Thickness change of a 190 Å thick polybutylthiophene film as a function of analyte (butylamine) concentration from 10 ppm to 125 ppt (parts per thousand). (Note that the error bars are about the size of the data point symbol and that the analyte concentration is plotted logarithmically.)

For analyte concentrations from 10 ppm to 125 ppt, the XRR shows small changes in film thickness (less than 2-3%). In contrast, the electrical response for these concentrations is more pronounced showing a large percent change at concentrations as low as 10 ppm. This can be seen in Figure 15 which plots the electrical response of a 180 Å thick polydecylthiophene sensor as a function of time for an exposure to 10 ppm of butylamine vapor. Upon exposure to the butylamine vapor at the 385 second mark in the experiment, the saturation drain current decreases by 40 percent. Polybutylthiophene films also show electrical responses of comparable magnitude. While the electrical response does depend on other factors, it is more pronounced than the physical swelling response. The important point is that the sensor response depends on more than just the film swelling, since this is below the measurement limit of about 1 Å.

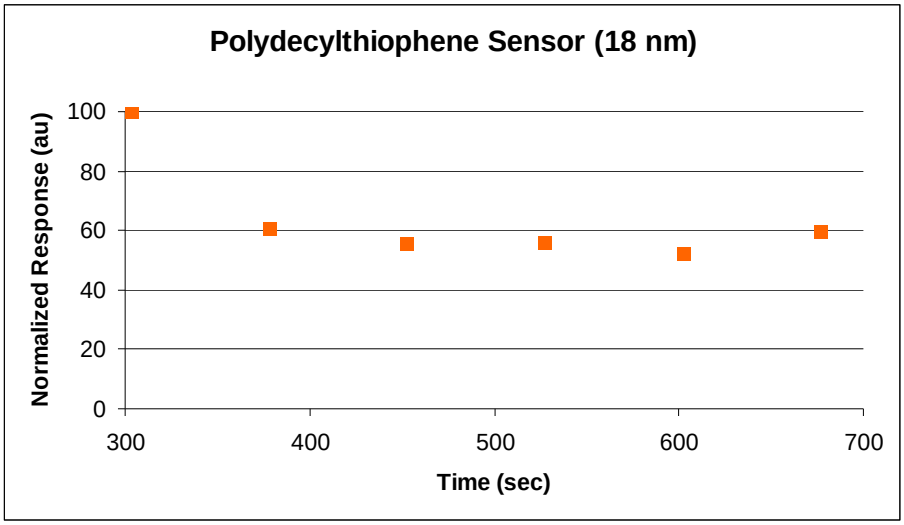

Figure 14. The electrical response to 10 ppm of butylamine. While the electrical response shows about a 40%, the swelling response for the same concentration is <1 %.

Figure 15 shows a comparison of the swelling response for films of different thicknesses. As Fig. 15a shows the relative thickness change is dependent on initial thickness. As is apparent (Fig. 15b), the absolute thickness changes are about 4-6 Å and are relatively independent of film thickness. While not definitive, this is suggestive of an interface accumulation, which will be discussed in more detail below.

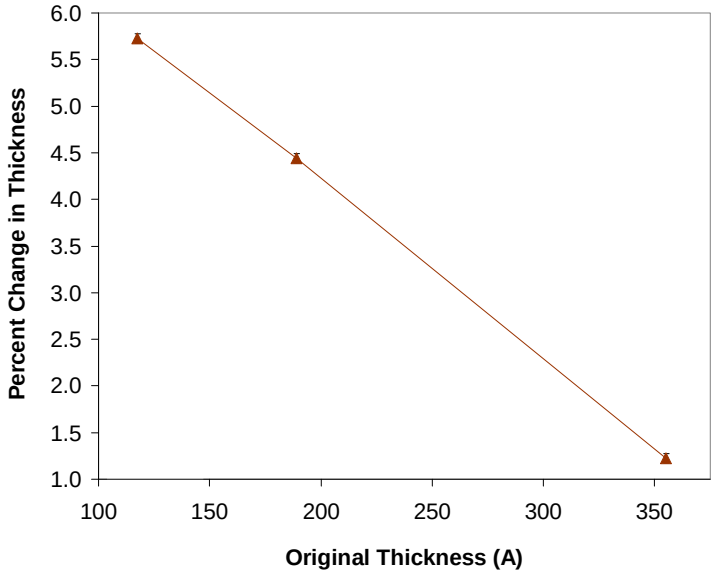

(a)

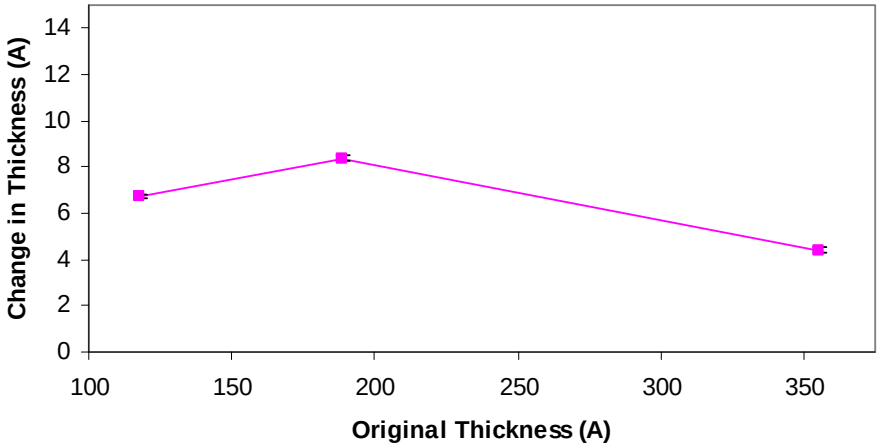

(b)

Figure 15. Change in thickness as a function of original film thickness, shown in terms of percent change (a) and absolute change (b). Thinner films show the largest change in thickness. (Note that the error bars are about the size of the data point symbol.)

In Situ Measurements of Film Thickness during Desorption

To further confirm and investigate the swelling response of the polythiophene films, experiments were performed to analyze desorption of the analyte from the film which resulted in a decrease in film thickness. Here, films were pre-exposed to acetone vapor and the film thickness was monitored as the acetone, a highly volatile compound, desorbed from the film. The

short scans in Figure 16 show the fringes shifting to the right, as a result of the thickness decrease. The fringe intensity drops with each scan suggesting beam damage, which may have been exacerbated by the presence of acetone in the chamber. Figure 17 shows a longer scan where the positions of the fringes clearly shift to the right. The original film thickness of the saturated film has a thickness of 187.1 Å. The accumulated beam damage makes it difficult to extract a reliable film thickness of the desorbed film, but the qualitative film thickness decrease is apparent.

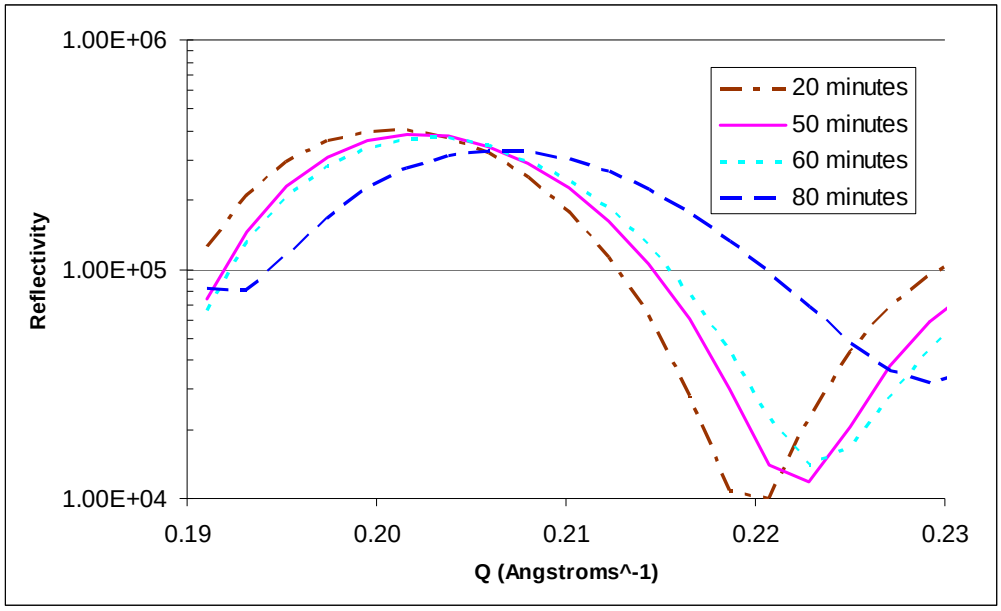

Figure 16. Partial scans showing the shifting fringes of a polybutylthiophene film as acetone desorbs from the film. Note that the fringes are shifting rightward indicating the film thickness is decreasing. The saturated film was placed in the chamber at 0 minutes and scanned every 10 minutes.

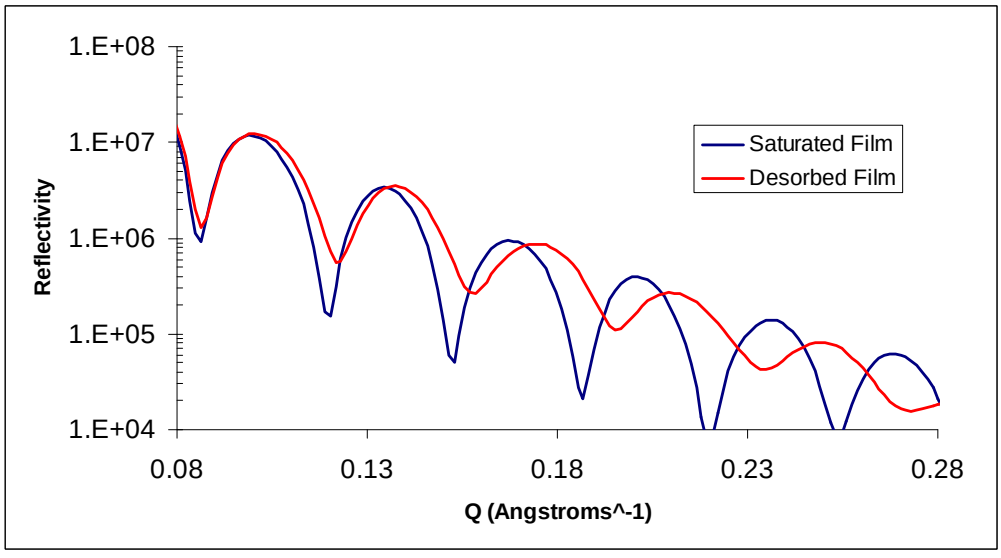

Figure 17. Full scan of a polybutylthiophene film confirming the de-swelling response of the film as acetone desorbs from the film.

All of the XRR data clearly shows that there is a physical interaction between the gaseous analyte species and the polythiophene films. It has been previously suggested that the analyte diffuses through the grain boundaries of the polythiophene film; this has been reinforced by ellipsometry measurements on polyalkoxythiophene films made by Torsi *et al*. They concluded that there is no swelling during the analyte exposure [1]. However, the ellipsometric response depends on both the film thickness and optical constant and these may be coupled in such a way to make thickness determination ambiguous. In contrast to this, the XRR measurements have unambiguously observed that the thickness increases in the polythiophene films due to swelling. At present, gas sensing with organic TFTs is only characterized as an electrical phenomenon with little understanding or evidence of the underlying physical mechanism. From these data, the electrical response has been correlated to physical swelling in the film.

The discrepancy between the magnitudes of the physical swelling response and the electrical response is interesting. It seems to indicate that the swelling response cannot completely account for the electrical change and that the two responses are arising from different mechanisms. As shown in Fig. 15(b), the film swelling is 4-6 Å, independent of film thickness. This is suggestive (although not definitive) of an interface effect, where the analyte is concentrated at or near the dielectric substrate-semiconductor interface. This interpretation is appealing because conductivity in organic TFTs takes place at a two-dimensional layer near the dielectric-semiconductor interface. This suggests that the transistor response arises from analytes that diffuse to the interface and interact with the mobile carriers, reducing the drain current at a given gate voltage. As shown in Fig. 15 and discussed above, the sensor response dependence on analyte concentration shows a smaller threshold than the film swelling. While it is possible that the film thickness change is below our detection limit at very low concentrations, these results suggest that the swelling (and interface analyte accumulation) cannot completely account for the electrical change. Other mechanisms like charge trapping or scattering are likely operative.

Furthermore, the data show that the swelling response saturates out at relatively low concentration for these thin films. In contrast, the field effect of the gate voltage provides ample carriers to interact with the analytes and, for sufficiently high gate voltages, the sensor response can respond to a much larger range of concentrations without saturating the response. This data seem to strengthen the argument that TFT as sensor elements have advantages over a bulk conductivity sensor because the former seem to be much more sensitive than the latter.

In conclusion, the in situ XRR scans show a physical interaction of polymer films with a gaseous species. These results help to elucidate the interactions between gas sensors derived from polymer films and the analyte species. The XRR data indicates that the films are absorbing the analyte which results in an increase in film thickness. Furthermore desorption has also been shown where the XRR fringes shift in the opposite direction. The most important factor that determines the swelling response is original film thickness.

Quartz Crystal Microbalance (QCM) Measurements

As a follow-up to the XRR measurements, quartz crystal microbalance (QCM) measurements were also performed to measure the mass uptake of the films in the presence of the analyte. While, the XRR measurements strongly indicate a physical interaction between the analyte and the sensor films, the QCM measurements are useful for several reasons. Measuring the mass

uptake of the polythiophene films cements the evidence of the physical interaction between the two and provides corroboration for the XRR data. Not only so, but the swelling response can only indirectly indicate the amount of analyte which diffuses into the film, while mass uptake measurements reveal how much analyte is absorbed by the polythiophene. Finally, this section also presents in situ electrical characterization performed during the mass uptake measurements. Therefore the mass uptake data helps to complete the tie between the physical and electrical responses.

As already mentioned, mass uptake is measured using a QCM. A quartz crystal is a piezoelectric that can detect small changes in mass down to the femtogram range by detecting changes in the resonant frequency of the quartz crystal. The resonant frequency, which is dependent upon the mass of the crystal, will increase as mass is adsorbed onto the crystal. The premier advantage of using a QCM is sensitivity since it is able to detect mass changes of femtograms under proper operating conditions. This kind of sensitivity makes it possible to detect the uptake of the analyte by the film since it is possible that only a small amount of analyte is absorbed by the film. Unfortunately, the sensitivity is also a double-edged sword because the measurement can easily pick up noise from vibrations, temperature fluctuations, or unwanted environmental contamination. However, this can be addressed through the use of proper calibration. For this reason, the theory and means for calibration will first be discussed.

Theory and Calibration of the QCM

Sauerbrey equation describes the resonant frequency of a QCM for a thin, rigid film as a function of changes in mass.

$$\Delta f = -C_f \cdot \Delta m \qquad \text{Equation 5.2}$$

where Δf is the observed frequency change in Hz,
Δm is the change in mass per unit area (g/cm^{-2})
C_f is the sensitivity factor for the crystal; 56.6 Hz μg^{-1}cm^2 for a 5 Mhz AT-cut crystal at room temperature

The sensitivity factor, C_f, is a fundamental property of the crystal,

$$C_f = \frac{2nf_0^{\,2}}{\left(\rho_q \mu_q\right)^{1/2}} \qquad \text{Equation 5.3}$$

n = number of the harmonic at which the crystal is driven
f_0 = the resonant frequency of the fundamental mode of the crystal in Hz
ρ_q = density of quartz = 2.648 g cm^{-3}
μ_q = shear modulus of quartz = 2.947 x 10^{11} g cm^{-1}s^{-2}

The Sauerbrey equation relies on C_f which is a fundamental property of the QCM crystal. Since it only accounts for the acousto-elastic properties of the QCM and not those of those of the film, this relationship is applicable only to thin-film, rigid, uniform deposits. Thus in theory the quartz crystal does not require calibration but in practice when soft films are used, calibration is necessary. To do this, the elasticity of the film can be modeled as an internal capacitance which be cancelled out with the appropriate circuit techniques.

Figure 18 shows the Butterworth-van Dyke (BVD) model, which is the electrical model for the quartz crystal near its series resonance. The quartz crystal is being driven by an automatic gain control (AGC) amplifier and is terminated by a load resistance, R_L. The components of the model represent as the following quantities:

> R_m corresponds to the dissipation of the oscillation energy from mounting structures in contact with the crystal and from air around the crystal (i.e. viscous loss).
> C_m corresponds to the stored energy in the quartz crystal comes from the elasticity of the quartz crystal and the surrounding air
> L_m corresponds to the inertial component of the oscillation and is related to the mass displaced during vibration
> C_o corresponds to the parasitic capacitance from the crystal electrodes, holder, and connectors. It acts as a shunt to the RLC network of the crystal itself.

Typical values for the crystals used here (1" diameter, 5 MHz) are: C_m = 33 fF, L_m = 30 mH, R_m = 10 ohms. For the experimental setup in this work, C_0 is about 20 pF.

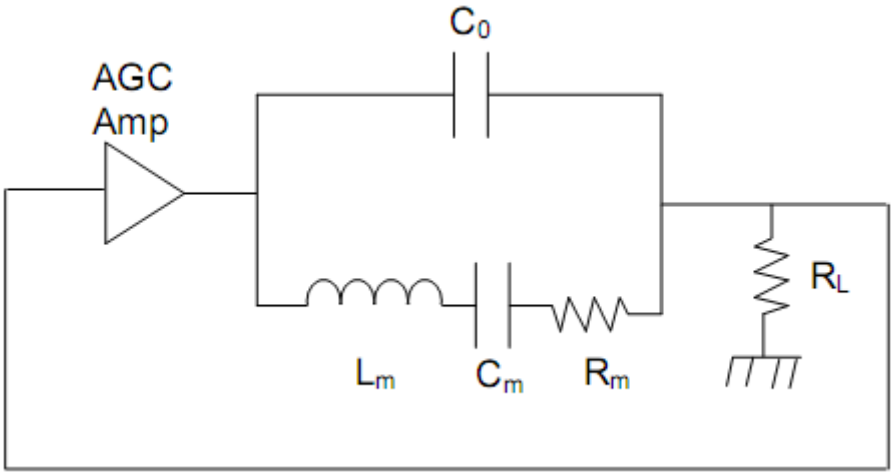

Figure 18. The Butterworth-van Dyke (BVD) model, which is the electrical model for the quartz crystal near its series resonance. The quartz crystal is being driven by an automatic gain control (AGC) amplifier and is terminated by a load resistance, R_L. A description of the components is in the text.

Under normal operation, C_0 cannot be ignored because it injects a leading current into the load, which introduces a phase error. Therefore, a varacter, C_v, is used to null out C_0 and cancel the injected current. The varacter is driven by the AGC amp along with the quartz crystal by means of a transformer with two secondary windings (Fig. 19). In this work, C_v was chosen to be

around 18 pF providing effective cancellation of the parasitic capacitances and compensating for a softer polymer film on the quartz crystal.

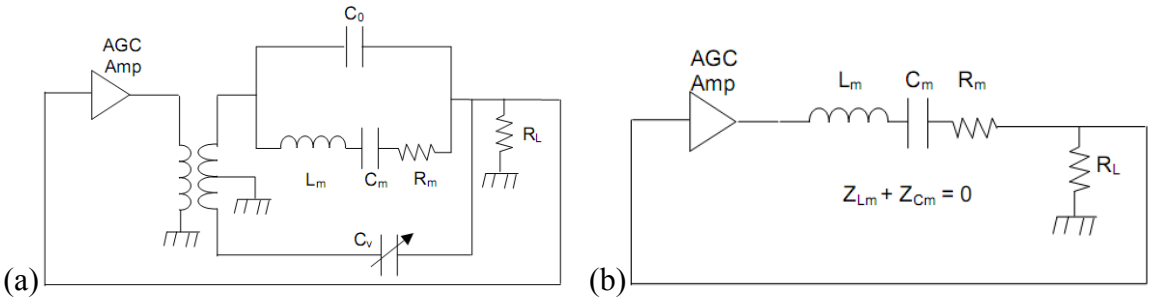

Figure 19. The method for canceling the parasitic capacitances, C_0. (a) A varacter, C_v, can be used to cancel the leading current injected by C_0. (b) The equivalent electrical model when C_0 is properly cancelled.

Another issue of calibration involves temperature fluctuations because the resonant frequency of the QCM varies with temperature. As temperature increases, the inertial and viscous losses cause a decrease in the QCM frequency. In practice, this temperature dependence limits the resolution of the QCM measurement because a slow temperature rise or fall will introduce a baseline drift in the QCM frequency. This baseline drift sets the lowest limit for which a frequency change can be ascribed to mass uptake. Implementing strict temperature control of the system can minimize this drift.

In order to calibrate for temperature, it is necessary to first characterize the degree of drift related to ambient temperature changes for the given experimental setup. For this measurement, the QCM setup was placed inside an enclosure that acted a temperature buffer and was run in continuous operation over a period of 24 hours. All experimental factors were identical to what be used in subsequent measurements. The film was fabricated using the same procedure as described in previous chapters, the only difference being the substrate. Polythiophene was dissolved in chloroform at the appropriate weight percent, filtered, and spun onto the quartz crystal instead of a silicon substrate. The quartz crystals were purchased from Stanford Research Systems and were used as received without an RCA clean. Like the silicon substrates, the quartz crystals were baked at 120 °C before and after spinning to remove moisture.

The quartz crystal with the film was placed inside a measurement apparatus that connects to an instrument called the QCM 200, which records the frequency and resistance of the quartz crystal. Both the apparatus and the machine were purchased from Stanford Research Systems. The apparatus was placed inside a custom sample chamber similar to the ones used for characterization of gas sensors, but modified to accommodate the holding apparatus and the necessary feedthrough to the QCM200. As shown in Figure 20, the sensor chamber is horizontal to fit the entire length of the apparatus, which is supported by a suspended ring.

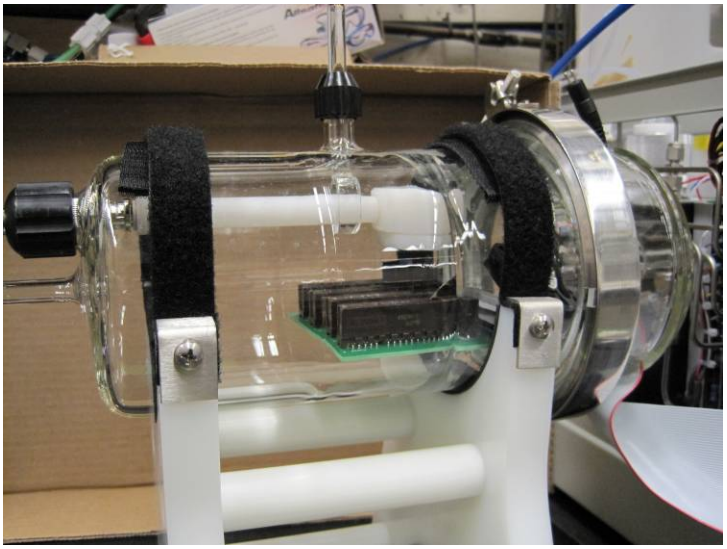

Figure 20. The custom test chamber used for QCM measurements. The chamber can accommodate the white QCM apparatus by a suspended ring as well as the TCard for measuring TFTs.

Figure 21 shows the resulting calibration curve over the 24-hour period. The quartz crystal exhibits a slow drift corresponding to changes in temperature that match the daytime and evening periods. The QCM oscillations are quite stable with the oscillation frequency returning close to its previous value after 24 hours. Zooming in on a shorter time period shows that for a 10 minute experimental period, the QCM exhibits a 2 to 3 Hertz drift, which translates into a detection limit of about 17.9 to 26.9 micrograms.

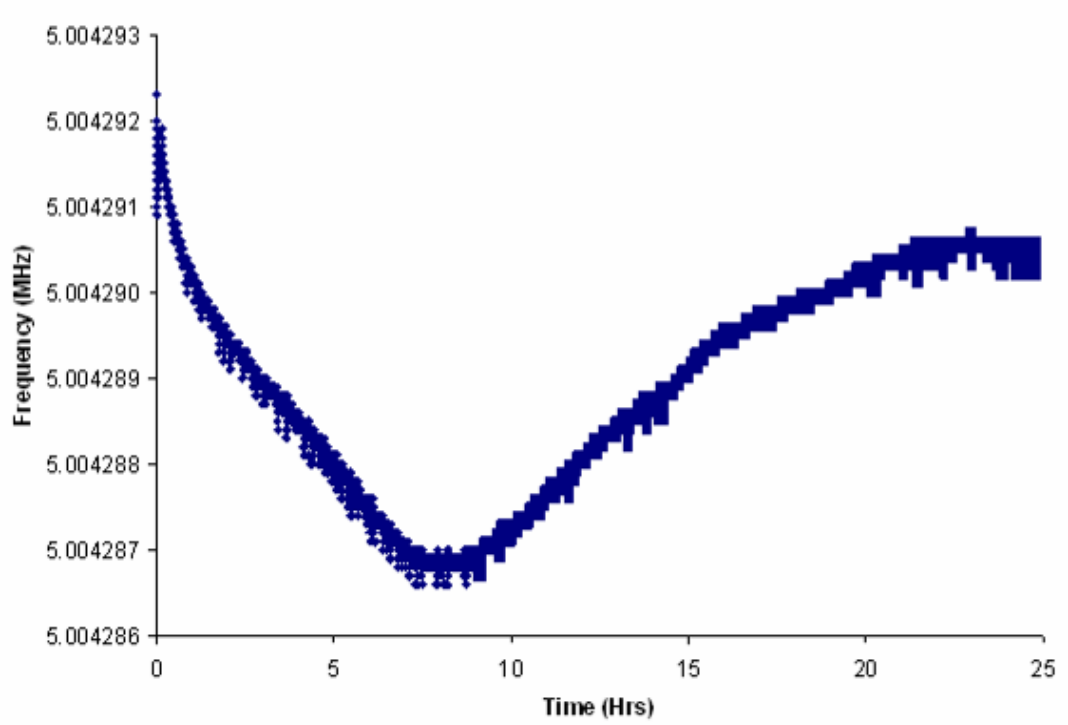

(a)

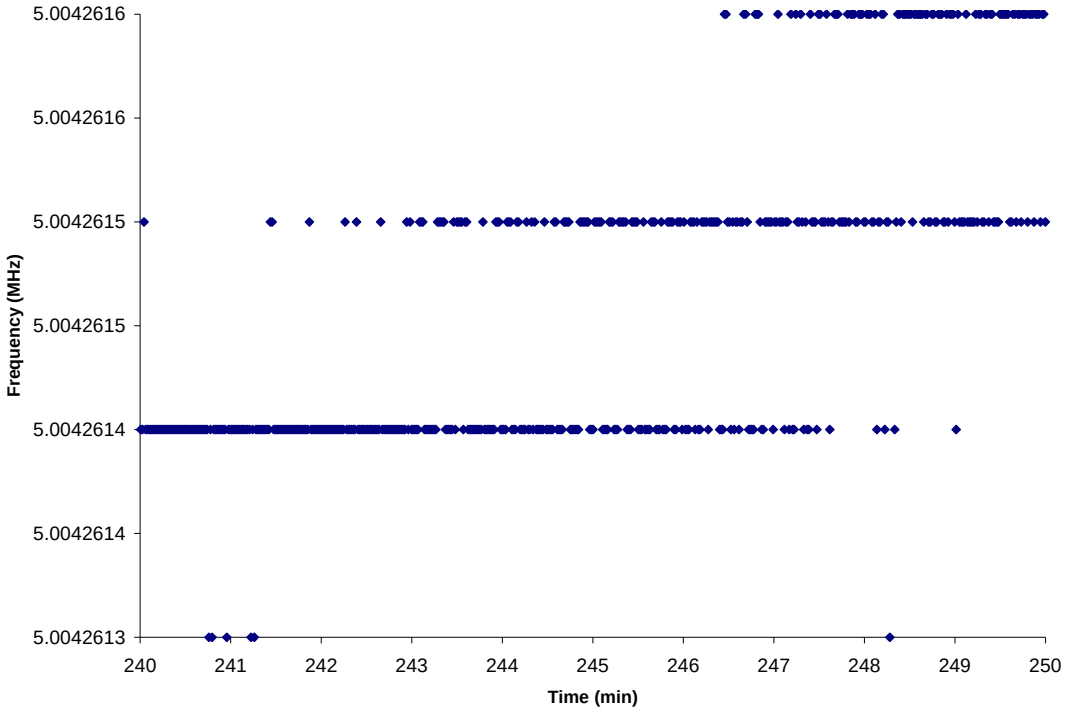

(b)

Figure 21. The calibration curve for QCM with a spun-cast polythiophene film. To characterize frequency fluctuations due to temperature, the frequency was monitored over (a) a 24 hour period and (b) a ten-minute period.

Mass Uptake Measurements of Polythiophene Films

Using this information to calibrate for the temperature drift, mass uptake measurements were performed for thin films of polybutylthiophene. All samples were prepared as just described. The frequency of the quartz crystal was monitored and after an initial warm-up period, 510 ppm of butylamine vapor was introduced using the syringe method from Chapter Five (Fig. 22).

The figure depicts the QCM response in terms of its frequency as a function of time. It is clear the introduction of the butylamine vapor results in a punctuated decrease in frequency, corresponding to an increase in mass, unlike that of the baseline drift. According to the Saurbrey equation, this frequency change of 6.2 Hz corresponds to a mass uptake of 55.5 micrograms.

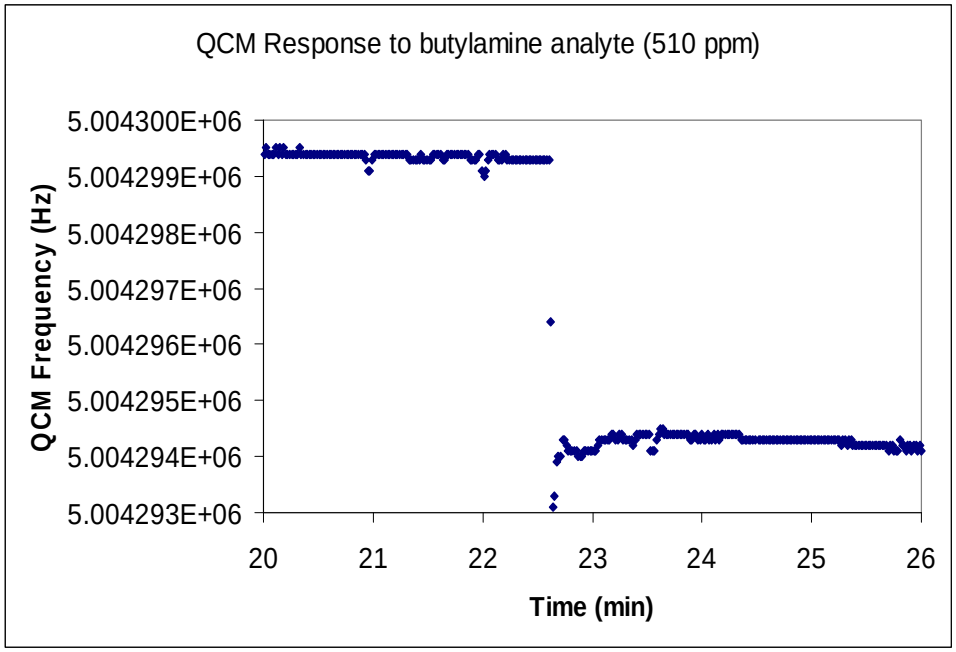

Figure 22. Response of QCM with polybutylthiophene film to 510 ppm of butylamine analyte. The introduction of the analyte causes an immediate decrease of 6.2 Hz which corresponds to a mass uptake of 55.5 μg.

The Sauerbrey equation predicts that mass uptake is linearly related to frequency change, a relationship that can be confirmed by measuring the response to additional concentrations of analyte. In Figure 23a, each data point corresponds to a fresh polythiophene sample that was exposed to a specific concentration of butylamine analyte. The data fit well to a linear relationship and the intercept is close to zero, which is physically reasonable. Figure 23b shows a similar plot illustrating mass uptake versus the concentration of analyte. The cut-off for detection using the QCM technique, with the current calibration, for which no frequency change is detected, is 200 ppm. The reason the relationship is non-linear may be due to the chemical affinity, μ, of the butylamine to the polybutylthiophene which can vary as the partial pressure of the butylamine increases.

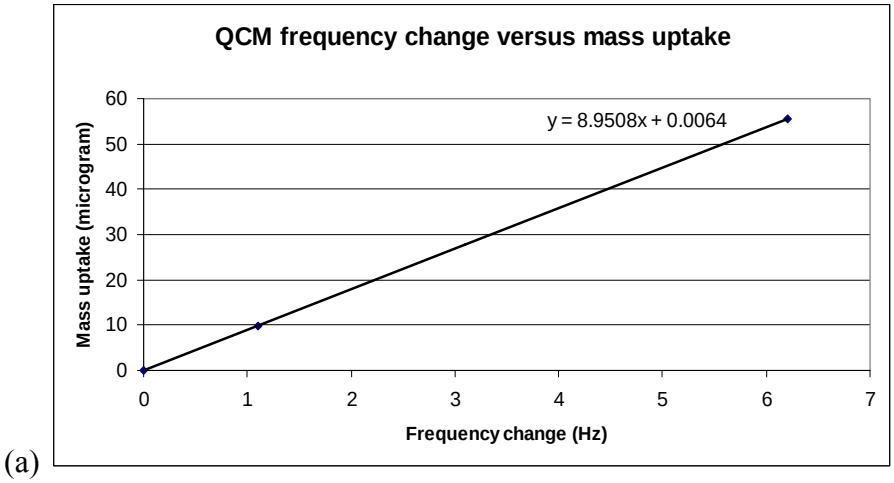

(a)

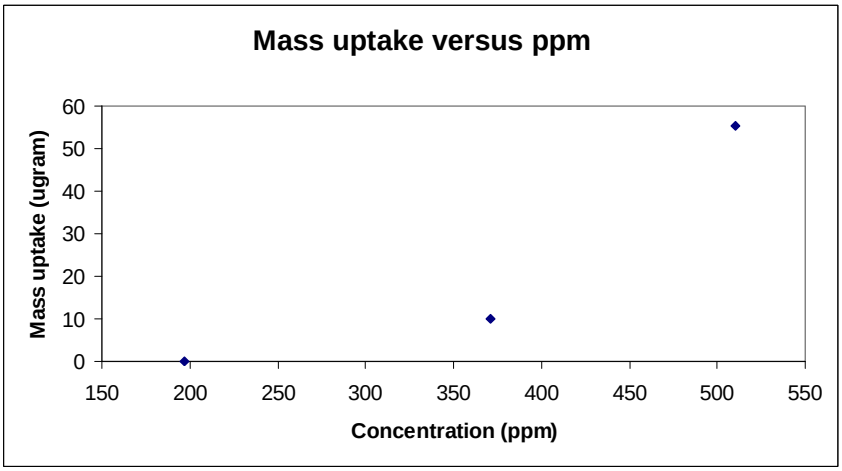

(b)

Figure 23. Mass uptake of the QCM as a function of (a) the change in frequency and (b) concentration. These figures show that the limit of detection for the QCM technique, with the current calibration, is 200 ppm.

In order to corroborate these QCM results with the electrical response of the sensor, in situ electrical characterization was performed along with the QCM measurements. The in situ measurement was performed by spin casting a thin film of polythiophene onto a silicon substrate with gold contacts under identical deposition conditions as the thin film of the quartz crystal. This analogous film was placed in the modified sample chamber together with the QCM apparatus and simultaneously interrogated as both devices were exposed to butylamine amine vapor. The electrical response and the QCM measurement of the in-situ experiment are shown in Figure 24. Exposure to 370 ppm of butylamine analyte resulted in a mass uptake of 9.85 micrograms with a corresponding 95.6% decrease in the drain current of the polythiophene TFT.

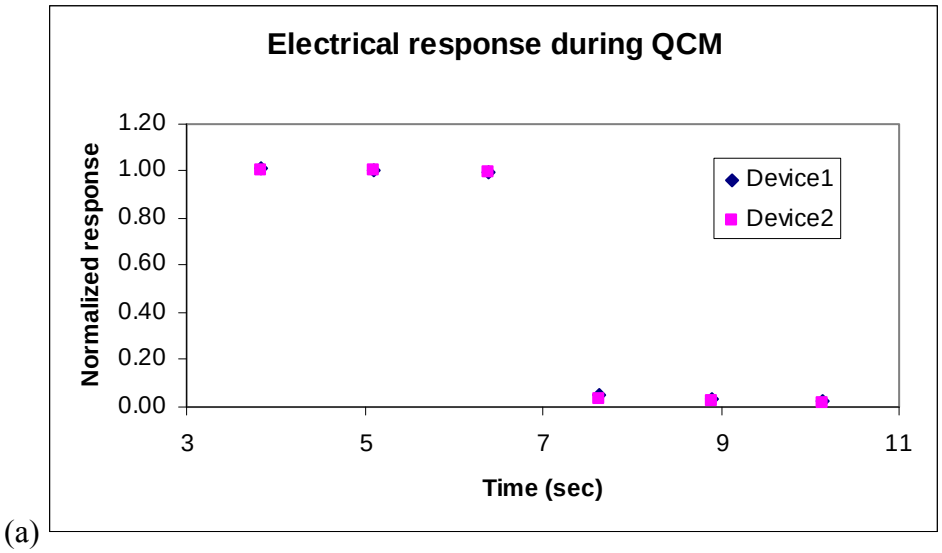

(a)

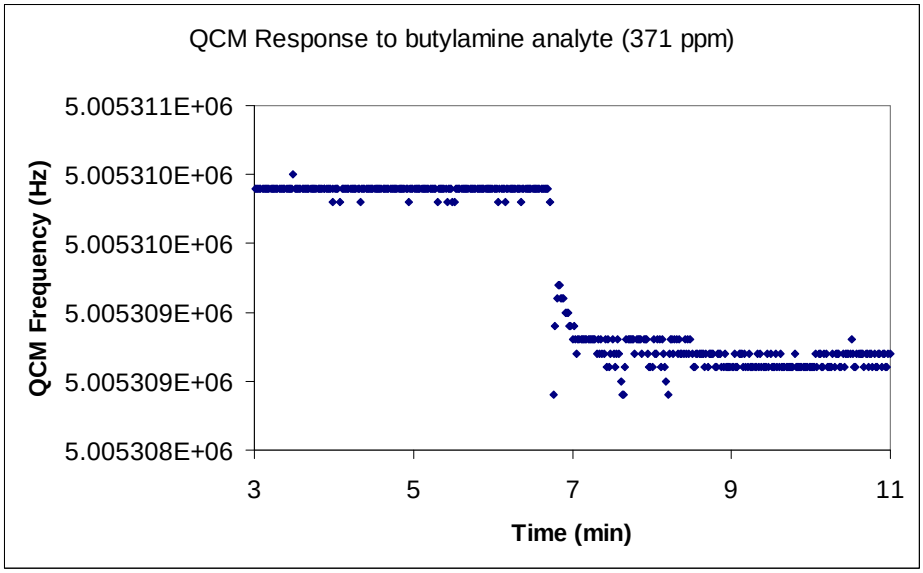

(b)

Figure 24. Shows the in situ electrical characterization performed with the QCM measurement. Both films were simultaneously exposed to the butylamine analyte giving rise to the (a) electrical response of the TFT and (b) the frequency response of the QCM.

The data indicate that for a relatively small change in mass, there are large changes in the drain current. While it is certainly possible to lower the detection limit of the frequency change through better temperature control in order to measure small mass changes, it is likely that the electrical response will still be much larger than the mass uptake. This is a similar phenomenon to the XRR data, where only small swelling changes were observed despite large changes in the electrical behavior. This suggests that physical uptake of the analyte cannot completely account for the electrical change as consistent with the XRR results.

Discussion

Taken as a whole, these experimental findings shed some light on the nature of the sensor-analyte interaction. To start, the measurements confirm that the analyte is physically interacting with the sensor films. In fact, it is reasonable to conclude that the analyte is being incorporated into the film as confirmed by the swelling response measured by XRR and the mass uptake measurements with the QCM.

The physical changes measured through XRR and QCM seem to be much smaller in magnitude than the electrical response at the same exposure concentration. For instance, as shown in the previous section, exposure to 10 ppm of butylamine to a polydecylthiophene film results in a thickness change of about 2% while the electrical change is around 40% (Fig. 14). Also, both XRR and QCM data show a lower threshold for measurement than the electrical response. QCM has the highest threshold at about 200 ppm of analyte, whereas XRR has a threshold of about 50 ppm; meanwhile the electrical response is clearly visible at single ppm levels.

This dynamic may indicate that electrical response is arising from a different mechanism than the physical swelling or uptake responses. Since electrical conduction is related to the charge carriers at the accumulation layer, it seems plausible that the uptake of the analyte by the film and the interaction of the analyte with the charge carriers can be viewed as separate events. This may explain why a relatively small uptake causes large changes in electrical behavior.

These observations are incorporated into the following model, which describes the sensor-analyte interaction. According to this model, the analyte interaction with the polythiophene film is broken down into the following steps (Fig. 25):

1. The analyte sorbs onto the polythiophene film. The surface concentration is a function of temperature, pressure and the partition coefficient, κ.
2. The analyte diffuses from the surface of the film to the semiconductor-oxide interface.
3. The analyte reaches the boundary of the electric potential profile. The presence of the analyte, which can be treated as a dopant or impurity, perturbs the potential profile and induces a shift in the threshold voltage.
4. The analyte reaches the conduction layer at the interface. This causes a trapping of the mobile carriers and scattering events at the interface, causing a decrease in mobility.

Steps 3 and 4 may be iterative in nature: the trapping of carriers or introduction of traps by the analyte, causes more band bending, which then affects the carrier concentration.

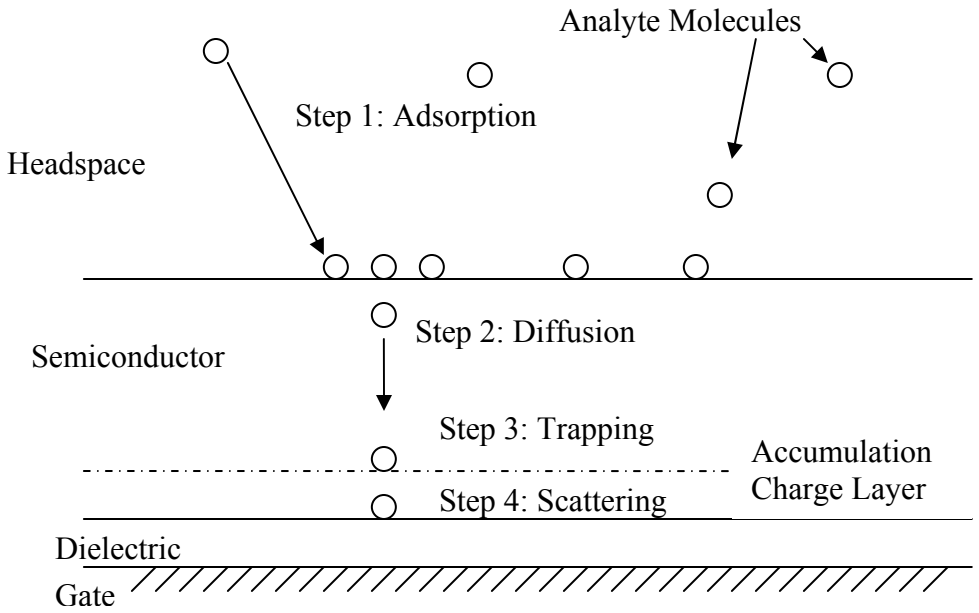

Figure 25. This picture outlines the steps of analyte interaction with the sensor film. Note that it is for conceptual purposes and is not to scale.

This model is consistent with the foregoing experimental observations. It distinguishes between the absorption of the analyte into the film, which gives rise to the physical swelling response and mass increase, and the interaction of the analyte with the charge carriers at the semiconductor-dielectric interface, which gives rise to the electrical response. This model will be revisited and further developed in the next chapter when discussing how the parameters of the film are varied to engineer its sensing behavior.

Conclusion

Based on both of these investigations it is reasonable to conclude that there is a physical interaction between the analyte and the film but that this interaction alone cannot account for the entire sensor response. The in situ swelling response and the mass uptake measurements indicate that the polythiophene film most likely absorbs the analyte. This is important because previously gas sensing by organic TFTs has been a completely electrical phenomenon, whereas these results indicate a physical basis for the sensing behavior.

Furthermore, the discrepancy between the electrical response and the swelling response indicate that physical changes along cannot account for the electrical response. Most likely, the two arise from different mechanisms where the physical changes are a result of analyte being absorbed by the film and are volumetric in nature, but the electrical changes are due to the analyte interacting with the charge conduction layer at the semiconductor-oxide interface, which is two-dimensional to first order. This reasoning is consistent with the greater sensitivity observed in electrical responses and is plausible when one considers that in inorganic transistors

the introduction of impurities at relatively low concentrations can induce large changes in its electrical properties. This dynamic highlights the advantage of using TFTs as gas sensors since the electrical effect amplifies the physical interaction. At the same time, physical changes are in fact present in these sensor films and should not be ignored in any mechanistic model of the sensor response.

In summary, this chapter presents novel work on characterizing physical changes in polythiophene thin films in response to gas vapors. Moreover, these changes are corroborated with the electrical behavior of polythiophene TFTs. The results show that these devices are highly sensitive as gas sensors since physical changes in the film can result in large, unequivocal changes in electrical behavior.

XRR and QCM data show that during exposure to the gaseous analyte, there are swelling changes in and mass uptake by the film, respectively. Meanwhile, GIXD data show that changes in the film properties can lead to changes in the film morphology. The following chapter will talk more about how these changes can be leveraged to differentiate sensor response among the polythiophene devices and used to create useful arrays of gas sensors.

Chapter 6 Engineering the Sensor Array

For an electronic nose, what is required is not simply a single sensor element but an array of sensor elements that work in tandem to produce recognition to a variety of analytes. The previous chapters have introduced polythiophene as good sensor materials that can implemented as an organic TFT. However, for polythiophene to be a truly viable electronic nose material, it must be differentiable such that an array of polythiophene sensors can be incorporated with each polythiophene TFT having a different sensor response.

This chapter will explore the engineering of polythiophene sensor arrays capable of discriminating between analytes. In previous chapters, it has been suggested that polythiophene chemistry is amenable to differentiation via functionalization of the thiophene side chain. As already discussed, the side chain is an ideal site for functionalization for the purposes of the changing the sensor behavior. Chang *et al* have previously demonstrated end functionalizing polythiophene can change the sensor behavior of polythiophene [1]; if adding a single functional group at the end of the polymer chain can affect the sensor response, modifying the side chains that are present on every thiophene unit along the chain should provide greater control over the sensor behavior. Moreover, modifying the side chain circumvents exotic synthetic routes with low yields; in fact, some polythiophene varieties with different side chains are already commercially available.

Most importantly and unlike nearly all the prior art, this work on engineering side chains will be based on the physical interactions that have been investigated and presented in the previous chapters. In these chapters, measurements have not only shown the physical interaction that is occurring between the sensor and the analyte, but how the morphology of the film affects this interaction. This chapter will leverage these interactions and explore the how the material parameters, fabrication process, and chemistry that can tune the behavior of these polythiophene sensors. By adjusting some of these knobs, one can begin engineering simple yet powerful sensor arrays.

Discrimination of Analyte Vapors

There are several key considerations when confronting a sensor array. The most important is discrimination followed by sensitivity and linearity. Discrimination is the ability to define one analyte from another with a degree of certainty. Sensitivity is the threshold of the sensor response to an analyte or analytes of interest. It may be a relative metric depending on the needs of the application. Linearity is character of the sensor response to the analyte concentration. It is needed for proper calibration and quantitative responses.

The paramount consideration for any viable gas sensor is discrimination. A sensor must be able to identify the analyte of interest with an appreciable specificity interval and a relatively low false positive rate. Oftentimes, research efforts focus on distinguishing between classes of molecules, yet in many attractive applications, such as environmental monitoring or product spoilage detection, it is important to discriminate within each class of molecule.

Food spoilage detection, discussed at length in Chapter Two, is one such application. As mentioned in that chapter, detection of spoilage or decay can be accomplished by monitoring the presence of certain markers, many of which are volatile biogenic amines that are the byproduct of microbial degradation [2-5]. Putrescine and cadaverine, both responsible for the odor of rotting flesh, are extremely reliable markers [6,7], while trimethylamine, a volatile molecule possessing three branches, is an accurate predictor of fish spoilage (Fig. 1) [8,9]. However, while these biogenic amines are reliable markers of decay processes, other biogenic amines occur in varying concentrations during the spoilage process, for some amines their concentrations may decrease during spoilage [10]. Generally, more complex and larger molecules become prevalent as the decay progresses; nonetheless, this type of overlap is a challenge with using markers for proper spoilage detection. Even laboratory techniques like mass spectroscopy, which are suited for identifying the elemental composition of a sample, will have trouble discriminating between these molecules. This shows that it is not sufficient to identify the presence of amines generally, or to monitor a specific amine molecule, but the relative concentrations of many amines.

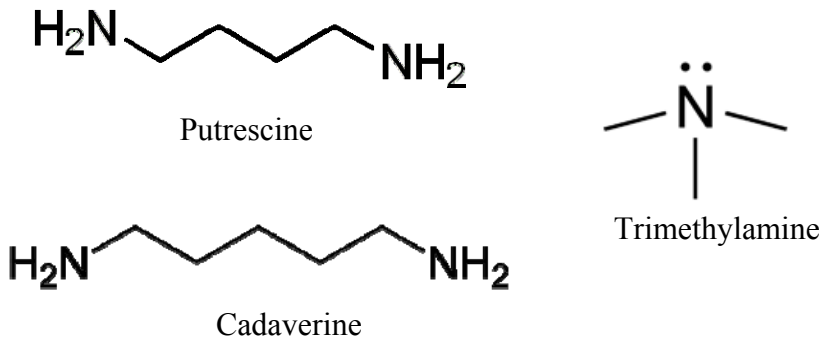

Figure 1. Important markers, or byproducts, produced during meat spoilage process

This illustrates that discrimination needs to encompass the entire makeup of the molecule including its chemical substituents as well the arrangement of these substitutents. Chemical discrimination, i.e. discrimination based on the chemical groups in the analyte, is not always sufficient to achieve adequate detection. In addition to differentiating between classes of molecules, e.g. amines, alcohols, thiols, etc., physical, or size, discrimination must be used to distinguish between analytes of different sizes or of different molecular arrangements.

Consistent with this discussion, discrimination is classified into types: physical and chemical. Physical discrimination is characterized as distinguishing between analytes based on their size and steric properties, while the latter is recognition based on the chemical identity and constituents (e.g. functional groups) of the analyte. Those with a chemistry background will recognize this distinction as “sterics versus electronics”, an archetypal classification in the field of organic chemistry which describes basic chemical interactions and the consequences thereof.

Pathways for Physical Discrimination of Vapors

Regarding physical discrimination, a comprehensive study by Bissell *et al* [11] found that different classes of analytes, including alcohols, esters, alkanes, and aromatics, elicited responses of different strengths from polypyrrole and polythiophene based sensors, but that, within each class of analytes, the sensor response was linearly related to saturated vapor concentration, regardless of the specific size or shape of the analyte molecule. Therefore, if sensors are to be able to discriminate within analyte classes, it will require more than simply changing the functional group of the active material.

Effect of Side Chains on Device Performance

As mentioned in previous chapters, the side chains of each thiophene unit in the polythiophene molecule present interesting and attractive sites of modification. Before it is possible to engineer a better sensor, there must be an adequate understanding of how the sensor behavior is affected by the side chain. The two basic modifications to the side chain include changing its length as well as functionalizing the side chain. Previous work with GIXD has shown that the side chain affects the film morphology. Besides the morphology, it is important to determine how the electrical behavior is also affected, especially since these sensors are based on TFTs.

In order to determine the effect of the side chain on the electrical performance, the mobility, threshold voltage, and I_{DSAT}, of 36 polythiophene TFTs of varying side lengths were measured and analyzed using ANOVA. All devices were fabricated according to the procedure outlined in Chapter Three. The results show that the basic semiconducting behavior is still preserved (Fig. 2), and that the side chain length affects the mobility of the device, while leaving the threshold voltage unchanged (Fig. 3). This change in mobility results in differences in I_{DSAT} between polythiophenes of differing side chain lengths (Fig. 4). Devices possessing side chain lengths of four and six show higher mobility values which leads to higher drive currents with statistical significance at the 5% confidence level with a p-value <.0001. These results are consistent with what has been reported with the literature [12-14], where polydecylthiophene shows a noticeable drop off in performance and shorter side chains give rise to higher currents. As expected, polyhexylthiophene shows the highest drain current, a result which has been demonstrated by other groups who attribute the high current to ideal film morphology [14,15].

A possible explanation may be the change in pi-stacking orientation observed in the GIXD measurements in the preceding chapter. The direction of the pi-stacking orientation corresponds to the highest conductive path. In OTFTs, where the charge transport direction is in the plane of the film from source to drain, the shorter side chain films have a pi stacking direction that is also orientated in the plane of the film. However with longer side chain films, the pi stacking direction is orthogonal to the charge transport plane, which could be the reason for lower carrier mobilities.

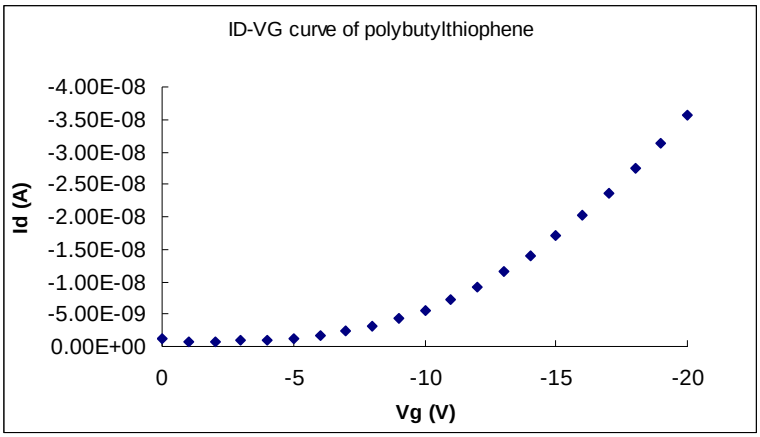

Figure 2. I_D-V_G curves of a polybutylthiophene device (18 nm thickness) showing that the basic transistor behavior is preserved despite a different side chain length. I_D-V_G sweeps of polyoctylthiophene devices (not shown) also produced similar characteristics.

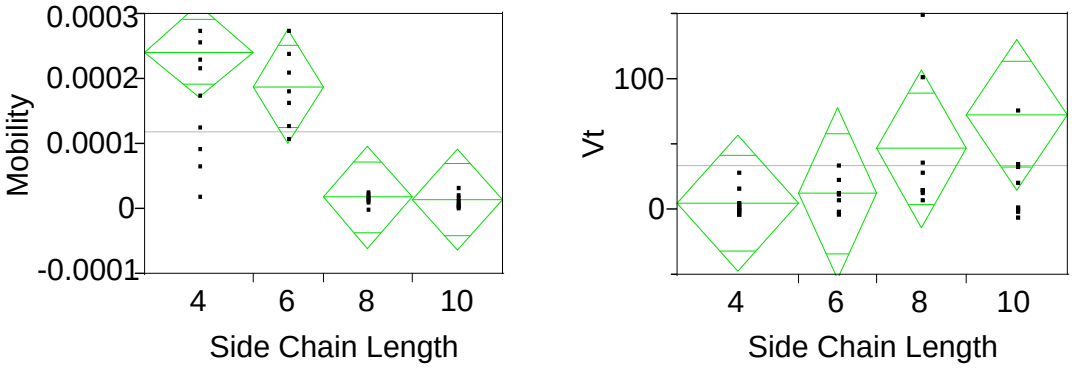

Figure 3. (a) ANOVA of mobility, μ, versus side chain length and (b) ANOVA of threshold voltage, V_T, versus side chain length. A total of 36 devices were tested; the p-values for mobility and V_T are <0.0001 and 0.3013, respectively at the 5% confidence level.

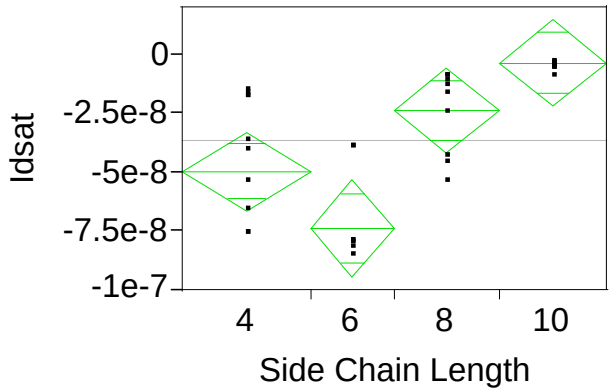

Figure 4. ANOVA of saturation drain current, I_{DSAT}, versus side chain length. A total of 36 devices were tested; the p-value is <.0001 at the 5% confidence level

Tuning the Sensor Behavior

Having determined the electrical effect of the side chain, the crucial question concerns how the sensing behavior is impacted. Besides the side chain, there are other processing parameters which possibly affect the sensor response. This includes the weight percent of the spin solution (which determines film thickness), the anneal time and temperature, and the presence of a hexamethyldisilazane (HMDS) interlayer between the interface of the polythiophene semiconductor and the dielectric.

In terms of film morphology, both the weight percent and anneal time were discussed and examined in the previous chapter on mechanistic investigations. It was shown that weight percent clearly determines the film thickness as is expected with spun-cast polymer films. In the case of anneal time, it was shown that lengthening the anneal time did not produce any major changes to the morphology of the film except to reduce the intensity of its diffraction pattern. The HMDS interlayer has been shown quite definitively to improve mobility in polythiophene TFTs [16]. The most plausible explanation is that the interlayer, deposited on the dielectric prior to the deposition of the active layer, improves the ordering of the polythiophene film at the interface. Since charge conduction occurs at this interface, the improved ordering results in increased field-effect mobility.

To determine if any of the aforementioned factors have any effect on the sensor response, a series of screening experiments were conducted which revealed that the anneal time, the anneal temperature, and the presence of an HMDS interlayer, bear no statistical significance on the gas sensing response. The results in the previous chapter showed that the anneal time and temperature do not impact the film morphology, and the results here show that they do not affect the gas sensing response. While the presence of an HMDS interlayer has been known to improve the mobility in an organic TFT, it does not affect the sensing behavior. This may indicate that the sensing behavior is a relative effect, where the drain current is proportionally reduced in the presence of the gaseous species. While the improvement in ordering does increase the amount of current, the absolute value of the drain current does not affect the normalized sensor response. Employing an HMDS interlayer may still be of value, since it does increase the signal to noise ratio by elevating the current levels of the TFT sensor. However in this work, the HMDS interlayer was not employed in devices presented in future discussions for the sake of experimental simplicity.

Meanwhile, the screening experiments verified the major supposition that the side chains play a role in the sensing behavior. Since the side chain is actually affecting the crystalline spacing, changing the film morphology appears to impact the interaction between the sensor film and the analyte. Film thickness also affects the film morphology and it is particularly interesting because it can be adjusted independently of the side chain length.

Factor	Bounds
Side Chain Length	4 Carbons to 10 Carbons
Film Thickness	18 nm to 140 nm
Analyte Length	4 Carbons, 7 Carbons

Table I. Factors and bounds for the multi-factorial sensor experiment. The measured response is the saturation drain current, I_{DSAT}.

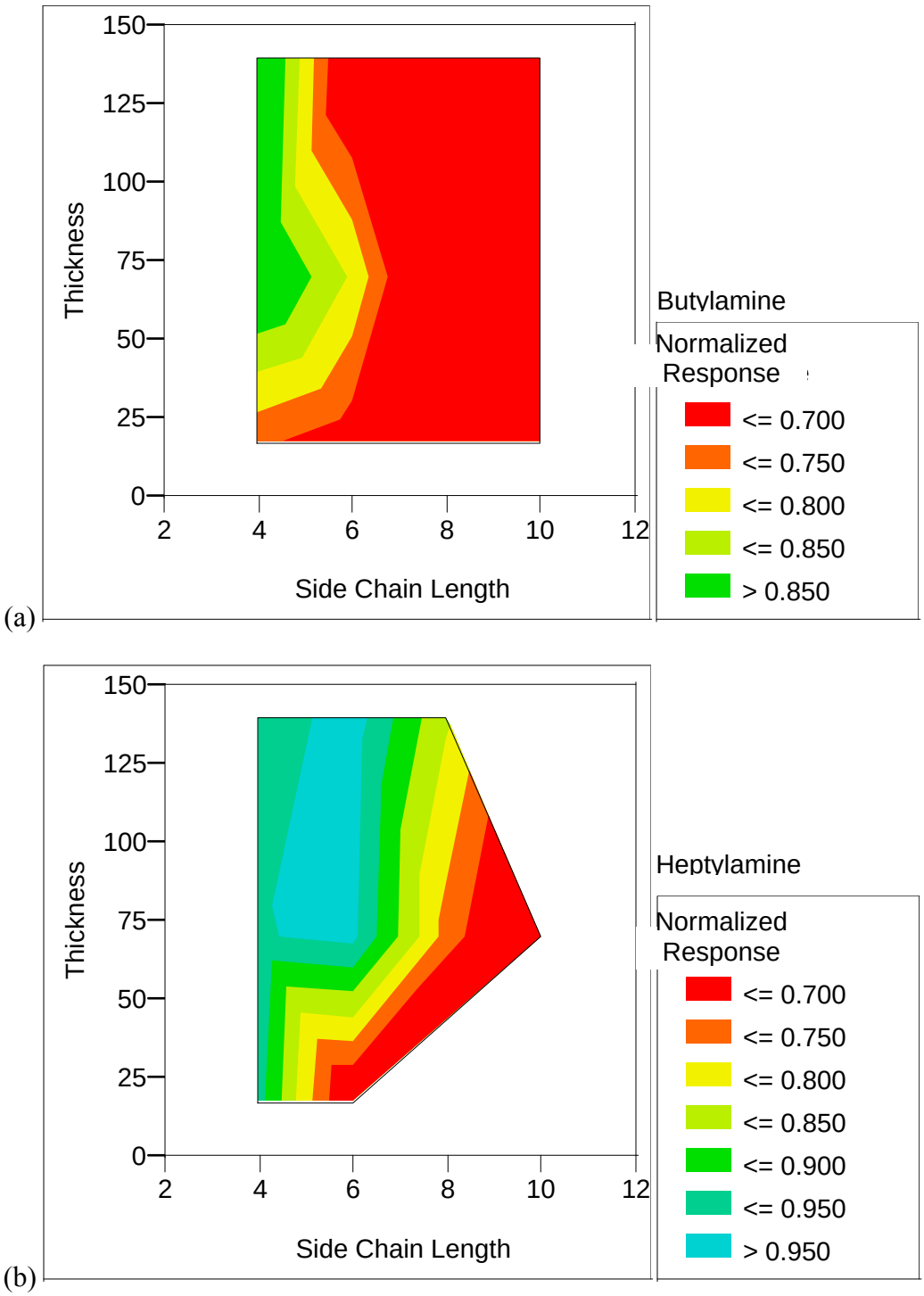

Figure 5a. Contour plot showing the sensor response to (a) butylamine analyte (10 ppm) and (b) octylamine analyte (10 ppm) as a function of side chain length and film thickness; the response is the saturation drain current normalized to its pre-exposure value

Therefore, the effect of film thickness along with the side chain length was further characterized through a set of full-factorial experiments. The devices were prepared according to the standard procedure and analytes were introduced via the direct injection method. Sensor characterization was performed with the custom setup. The measured response is the saturation drain current and the factors and bounds are listed in Table II. In each experiment, the sensors were operated for five minutes before being exposed to the analyte. A concentration of 10 ppm was used for both butylamine and heptylamine analyte, two molecules which are comparable to many biogenic amines. The results are summarized with contour plots in Figure 5.

Figure 5a shows the overall response of the polyalkylthiophene sensors to the butylamine analyte. The color corresponds to the normalized response of the saturation current, with a lower number indicating a larger change; hence red corresponds to the largest sensor response. At larger side chain lengths, there is no thickness dependence and the response is stronger since a shorter analyte can penetrate more easily into the film. As the side chain decreases, a thickness dependence begins to appear with the thinner films showing a stronger response. The cross-over at which this happens is around four or five carbons, which is when the length of the side chain becomes comparable to the size of the analyte.

This interaction is clearly seen if we look more closely at some of the constituent data shown in Figure 6, where response of sensor with a butyl side chain of 4 carbons is distinct from the other sensors with longer side chains. In this case, the short length of side chain excludes butylamine from interacting significantly with the sensor; meanwhile, longer side chains are unable to exclude the analyte and show a stronger decrease in current. Therefore, the similar size of the side chain and the analyte strongly mitigates the sensor response, demonstrating size exclusion as a possible mechanism to physical discrimination. This kind of exclusion highlights pathways for engineering size discrimination with a possible resolution of one to two carbons.

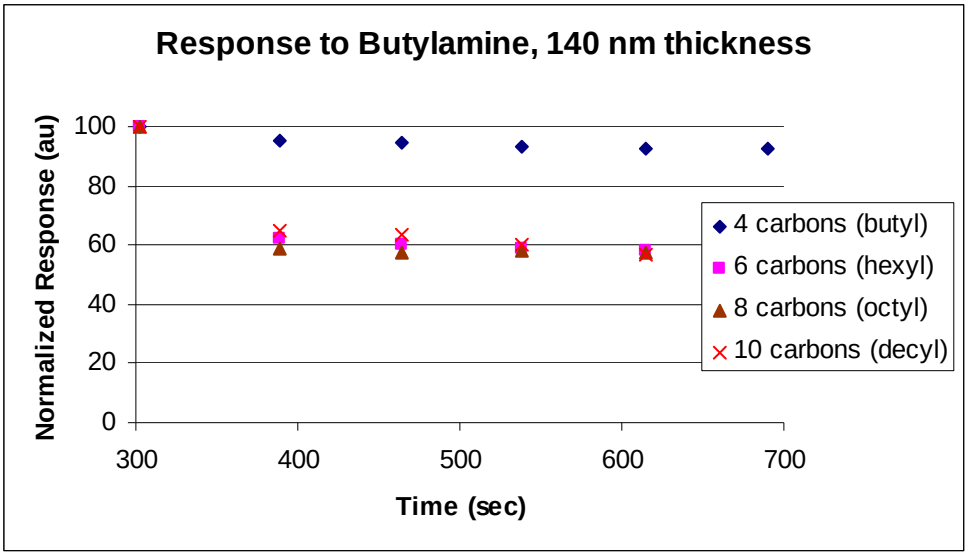

Figure 6. The sensor response of polythiophene of varying side chain lengths to a butylamine analyte

Figure 5b shows the results of the multi-factorial experiment for the octylamine analyte. Just as with the butylamine analyte response in Fig. 5a, the transition where thickness dependence becomes significant happens when the analyte size is comparable to the side chain length. With a heptylamine analyte, this occurs at a longer side chain length of about six to eight carbons, again demonstrating the viability of using varying side chains to detect size differences in the analyte. Overall, there is a much stronger thickness dependence, attributed to the larger size of the analyte, which enhances the importance of diffusion. The largest response comes from thinner films with long side chains while thick films show the smallest response. If done properly, varying both thickness and side chain length, analyte sizes can be elucidated.

This interaction can be highlighted by showing again some plots of the constituent data (Fig. 7). This figure shows the responses of two sets of sensors. The first set comprises sensors of four different side chain lengths with a film thickness of 140 nm; the second set spans similar lengths (although the decyl side chain of 10 carbons is not included) but with a thickness of 70 nm. As

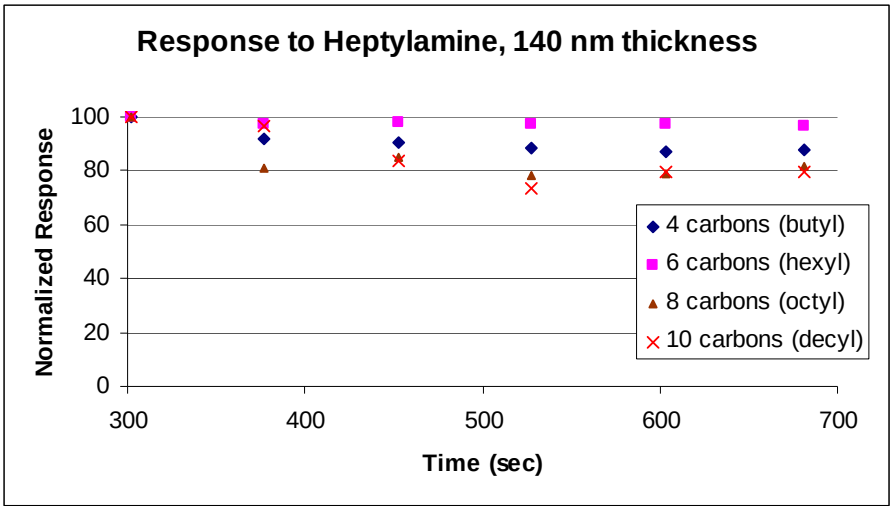

(a)

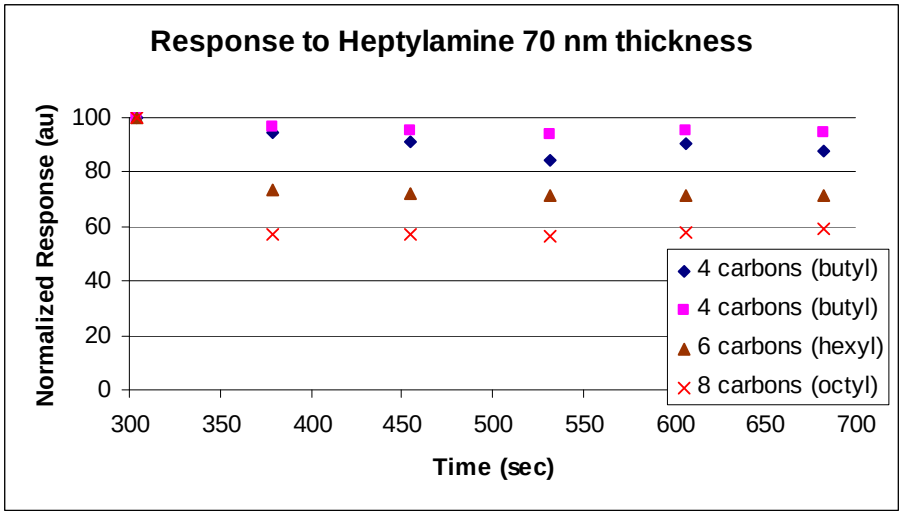

(b)

Figure 7. The sensor response of polythiophene sensors with varying side chain lengths to a heptylamine analyte. The sensors have a film thickness of 140 nm (a) and 70 nm (b).

expected, the thinner films as a whole show a stronger response than the thicker companies. Note that films of an intermediate thickness show a response that falls in between the thicker and thinner films. (The explicit plot for this is not shown but the data are present in the contour plot.)

The most interesting and striking feature is that the degree to which each response is enhanced as the film thins depends on the length of the side chain. For instance, with the short butyl side chain the response changes slightly as the film thickness decreases but with the longer octyl side chain, thinning the film results in a larger shift. As will be shown, this kind of interplay between film thickness and side chain length can be exploited to engineer arrays capable of discriminating for the analyte size.

In examining these interactions, the most plausible explanation for this behavior is that the relative ease with which the analyte penetrates into the film is being controlled, thereby adjusting the degree of interaction between the analyte and the charge carriers at the oxide interface. Whenever the side chain length is larger than the analyte, the analyte easily penetrates into film to interact with the carriers and film thickness is unimportant. Conversely, when the side chain length is much smaller than the analyte size, diffusion of the analyte becomes more important and the sensor response exhibits a stronger thickness dependence.

The ability to discriminate an analyte is most clearly depicted when examining a complete series of side chain lengths. This set of data shows how the response of gas sensors vary as the side chain is lengthened from four carbons to eight. In the first figure, sensors possessing a side chain length of four carbons (butyl) are exposed to butylamine analyte (Fig. 8). As consistent with the previous plots, when the analyte size is comparable to the side chain length, the thinner films show the stronger responses.

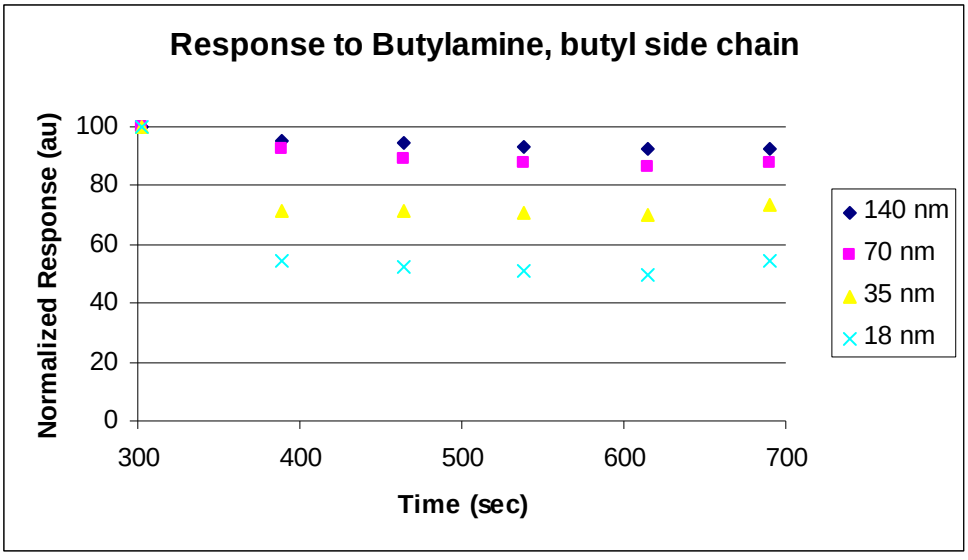

Figure 8. Gas sensors with a butyl side chain of varying thicknesses exposed to butylamine analyte.

When the side chain is lengthened by two carbons to become a hexyl group, a few effects begin to emerge (Fig. 9). First, the four responses become more closely grouped, showing that the thickness dependence decreases as the side chain length becomes larger than the analyte. Also, the four responses collectively become stronger being grouped within the 60% to 80% response range. (Note that the order of the responses, in terms of film thicknesses, from smallest to largest has changed from the situation with the butylamine analyte; the reason for this is unclear.)

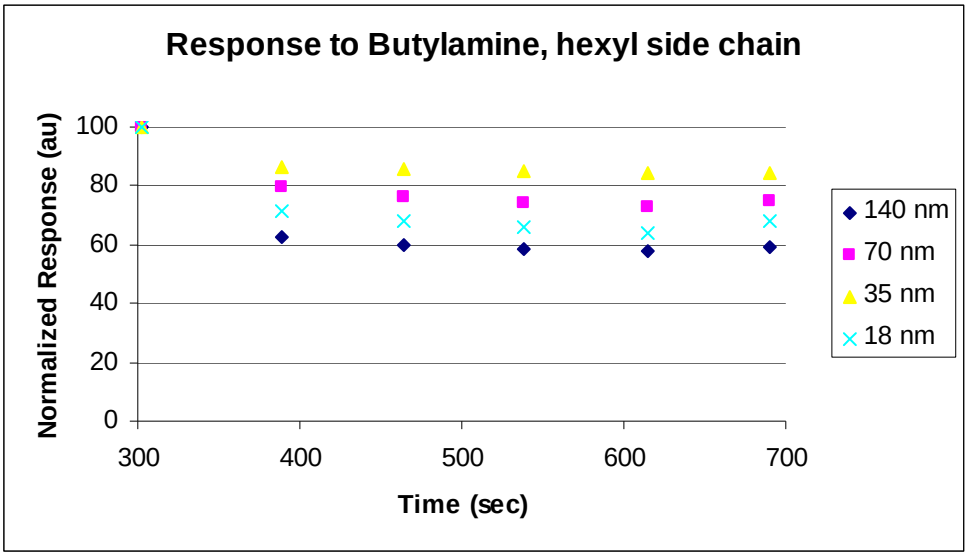

Figure 9. Gas sensors with a hexyl side chain of varying thicknesses exposed to butylamine analyte.

Finally, when the side chain is lengthened by another two carbons to an eight-carbon octyl side chain, the thickness dependence completely disappears (Fig. 10). Now the responses are entirely grouped together at around 60%. By examining this series, it seems that the resolution of the size discrimination is quite good and one can potentially discriminate analytes down to one or two carbons. The fact that the film thickness order breaks down at the intermediate side chain length of six carbons may imply that there are other interactions present when the analyte size and side chain length are close to each other.

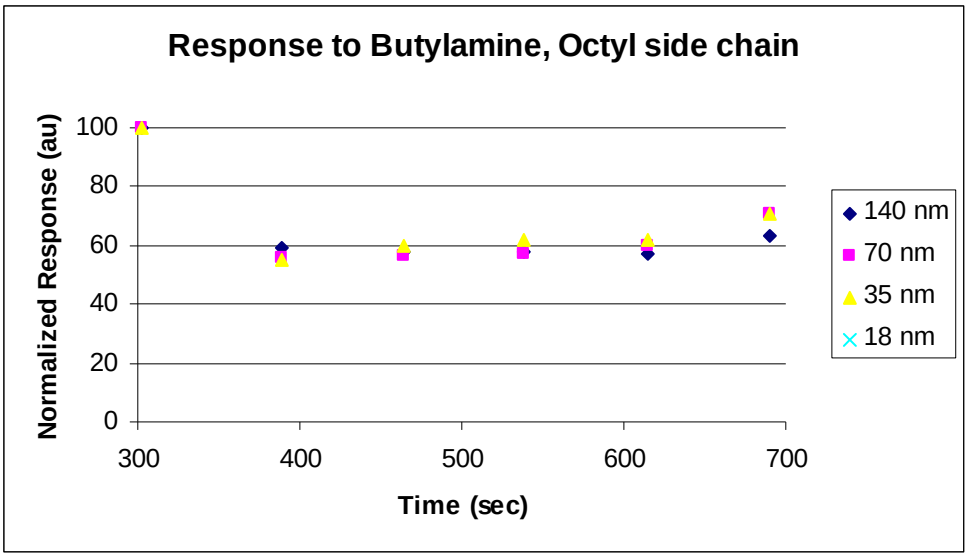

Figure 10. Gas sensors with an octyl side chain of varying thicknesses exposed to butylamine analyte.

Polythiophene Sensor Arrays Demonstrating Physical Discrimination

To demonstrate the ability to exploit size differences of analytes, sensor arrays were fabricated using polythiophenes of different side chain lengths and film thicknesses. Two small sensor arrays of four sensors each employed permutations between two different side chain lengths (four carbons and eight carbons) and two different film thicknesses (70 nm and 140 nm). One array was exposed to octylamine vapor at a concentration of 8.7 ppm and the other was exposed to butylamine vapor of the same concentration. The two arrays produced markedly different responses as shown in Figure 11. Note that the scale is different for the two plots. Although the sensor response is smaller for the octylamine exposure, the responses are consistent as verified with follow-up measurements.

The array that responded to the octylamine vapor showed four varied response among its constituent sensors. Between the two side chains, the longer side chain sensors gave a larger response as consistent with what was previously observed. Additionally, a thickness dependence is present between the sensors, with the thinner films showing a larger response as consistent with the other data. In contrast, the second array showed a very different aggregate response when exposed to butylamine vapor. In this array, the thickness dependence completely disappeared and the sensor response is determined predominantly by the side chain length.

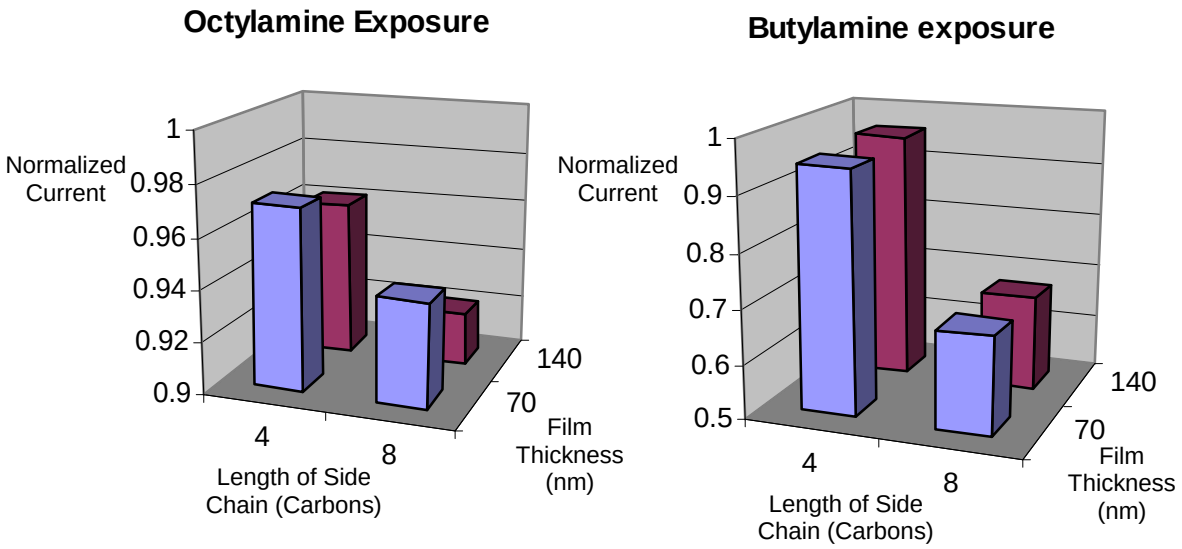

Figure 11. Sensor array responses to octylamine analyte and butylamine analyte at a concentration of 8.9 ppm. Note that the scale is different for the two plots.

These responses exploit many of the exclusion interactions from the previous data. The butylamine vapor interacts most strongly with the polyoctylthiophene since the analyte is much smaller than the d-spacing of the film and so it penetrates into the film with greater ease. When the side chain length decreases, so does the d-spacing, and the response is mitigated. In the situation with octylamine, the analyte is much larger compared to the d-spacing of the film so the same trend is still observed with the side chain length, but the thickness dependence becomes more important because penetration by the analyte is impeded by its large size.

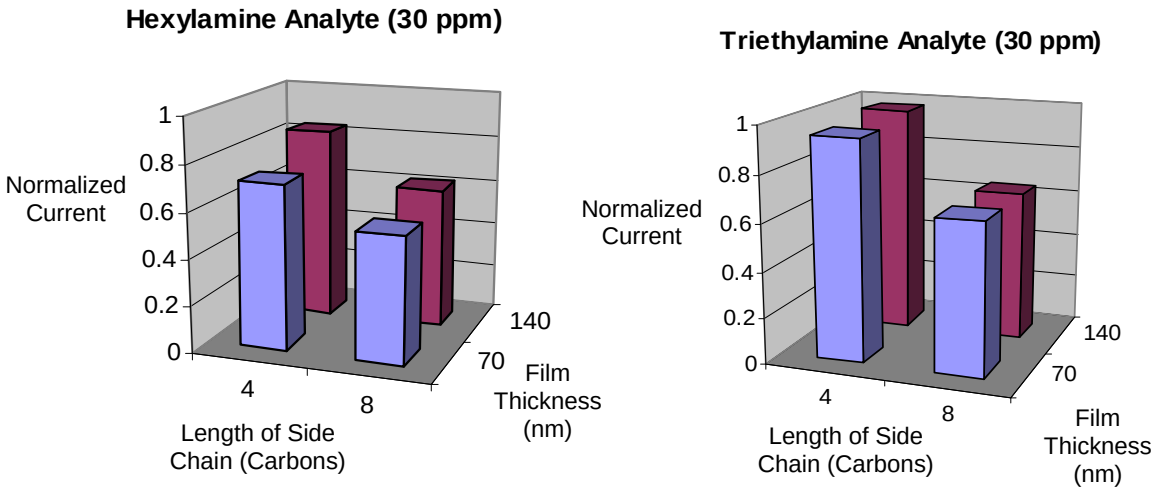

Figure 12. Sensor array responses to hexylamine analyte and triethylamine analyte at a concentration of 30 ppm.

By using this simple arrays, novel and important discrimination can be performed based on the size of the analyte. This kind of discrimination is useful and not possible with current sensing paradigms and even difficult with other analytical techniques like gas chromatography-mass spectroscopy (GC-MS).

This motif not only works with different sizes, but it can be extended to discriminate between analytes of different carbon arrangements as shown here between a linear analyte and a branched analyte. Here the same two arrays were fabricated and one was exposed to hexylamine vapor at 30 ppm and another to triethylamine vapor at same concentration of 30 ppm (Fig. 12).

The two sensor array responses show a similar dynamic as with the previous scenario. Due to its compact chemical structure, the triethylamine analyte is a smaller analyte than the linear hexylamine. Therefore the straight chain hexylamine analyte causes a sensor response that is dependent on side chain as well as film thickness; meanwhile, the branched triethylamine analyte, though it contains the same numbers of carbons, exhibits a thickness independent response because it is smaller and more compact than its linear analog.

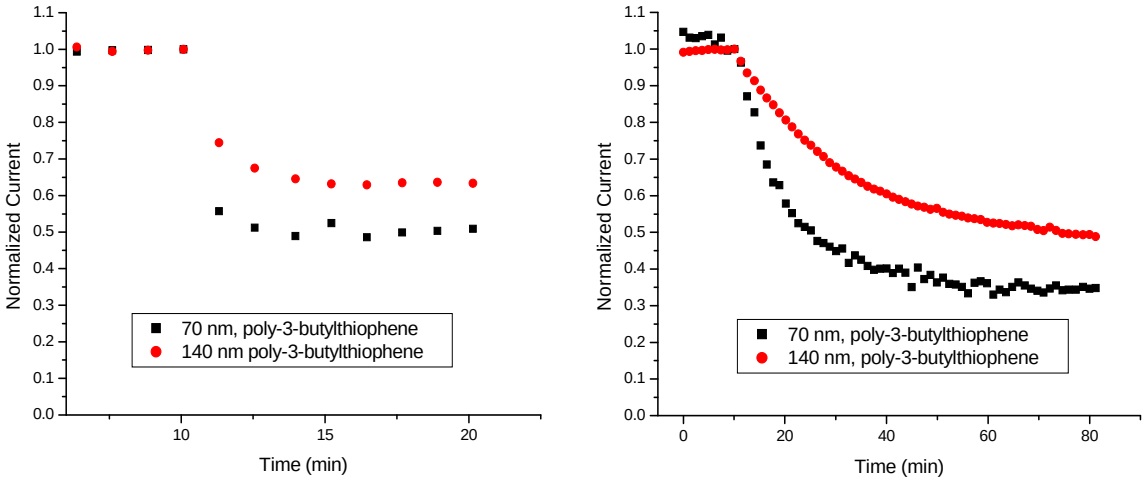

Figure 13. Response of polybutylthiophene devices from the sensor array to hexylamine analyte and triethylamine analyte as a function of time.

While the triethylamine analyte is similar to the butylamine analyte in size, it is unlike the butylamine because it has a branched structure which can impede diffusion into the film. In fact, if we examine the sensor response to triethylamine over time we can observe a transient character to the response. Figure 13 shows the sensor response of the two polybutylthiophene sensors as a function of time to each analyte.

The prolonged transient response of triethylamine analyte as seen in Figure 13 is attributed to the steric hindrance caused by its branched structure which the analyte encounters as it penetrates into the film. Characterizing this transient response, we see that the time to reach 36.8% percent of the final response is 32 minutes for the 140 nm thick film and 21 minutes for the 70 nm film which means a thinner film reaches its final value more quickly. Thus the transient character of

the sensor response provides another level of dimensionality which can be used to further discriminate the analyte size, in this case, the steric arrangement of the molecule.

Array Response to Gas Mixtures

To explore and demonstrate the robustness of this approach, these arrays are used to perform physical discrimination even in the presence of analyte mixtures. Sensor arrays composed of four sensors each with permutations of 70 nm and 140 nm film thicknesses and 4 carbon (butyl) and 6 carbon (hexyl) side chain lengths were fabricated and exposed to mixtures of triethylamine and hexylamine vapors at two different relative ratios. Figure 14 shows the response to the first ratio, a 1:2 mixture of triethylamine to hexylamine (10 ppm:20 ppm). For clarity, the sensor responses are shown on four different plots, though they were operated as one array. The response to the second mixture with a relative ratio of 2:1, i.e. triethylamine vapor at 20 ppm concentration mixed with hexylamine vapor at 10 ppm, is show n Figure 15.

This mixture response is quite interesting because the array response shows a combination of the step response associated with the hexylamine analyte and the gradual response associated with the triethylamine analyte, with the overall character of the response being determined by the more abundant analyte. This is evident with Sensor A (polybutylthiophene with a film thickness of 70 nm) where the response to each mixture bears characteristics of a step response to the hexylamine-rich mixture and has more transient character with the triethylamine-rich mixture. (This mixture response as a combination of the two responses will be formalized shortly.)

The effectiveness of the array is notable because the responses of the other sensors are different depending on their parameters. For instance Sensor B (polybutylthiophen, 140 nm), which has a larger film thickness than Sensor A, is more exclusive to the hexylamine analyte than Sensor A. While it shows differing responses to the mixtures, the transient character attributed to triethylamine is much stronger than with Sensor A. Notably, both of these sensors show a transient response in the triethylamine mixture but Sensor A still shows a step-like quality with a large shift immediately after the exposure whereas Sensor B shows a gradual response immediately after and throughout the exposure. By contrast, Sensor D (hexyl thick) is less sensitive to the branched triethylamine analyte and therefore shows a similar step-like response to both mixtures. In this case, Sensor D is acting like a threshold sensor whose response gives bounds to the relative sizes of the analytes that are present. By integrating these responses of the four elements in this simple array, we can see how discrimination is engineered to generate unique signatures based on differences in the analyte even in the presence of mixtures.

These sensor arrays can generate unique signatures to various analytes even in the presence of mixtures. The effectiveness of the array comes from the ability to distinguish between the absolute shift of each constituent sensor and the relative shifts among the sensors. The former is due to analyte concentration while the latter gives rise to the ‘shape’ of the entire array response, providing a way to ascribe unique signatures to various analytes, even in the presence of mixtures. The fact that these arrays work in the presence of mixtures shows the robustness of this pathway for physical discrimination.

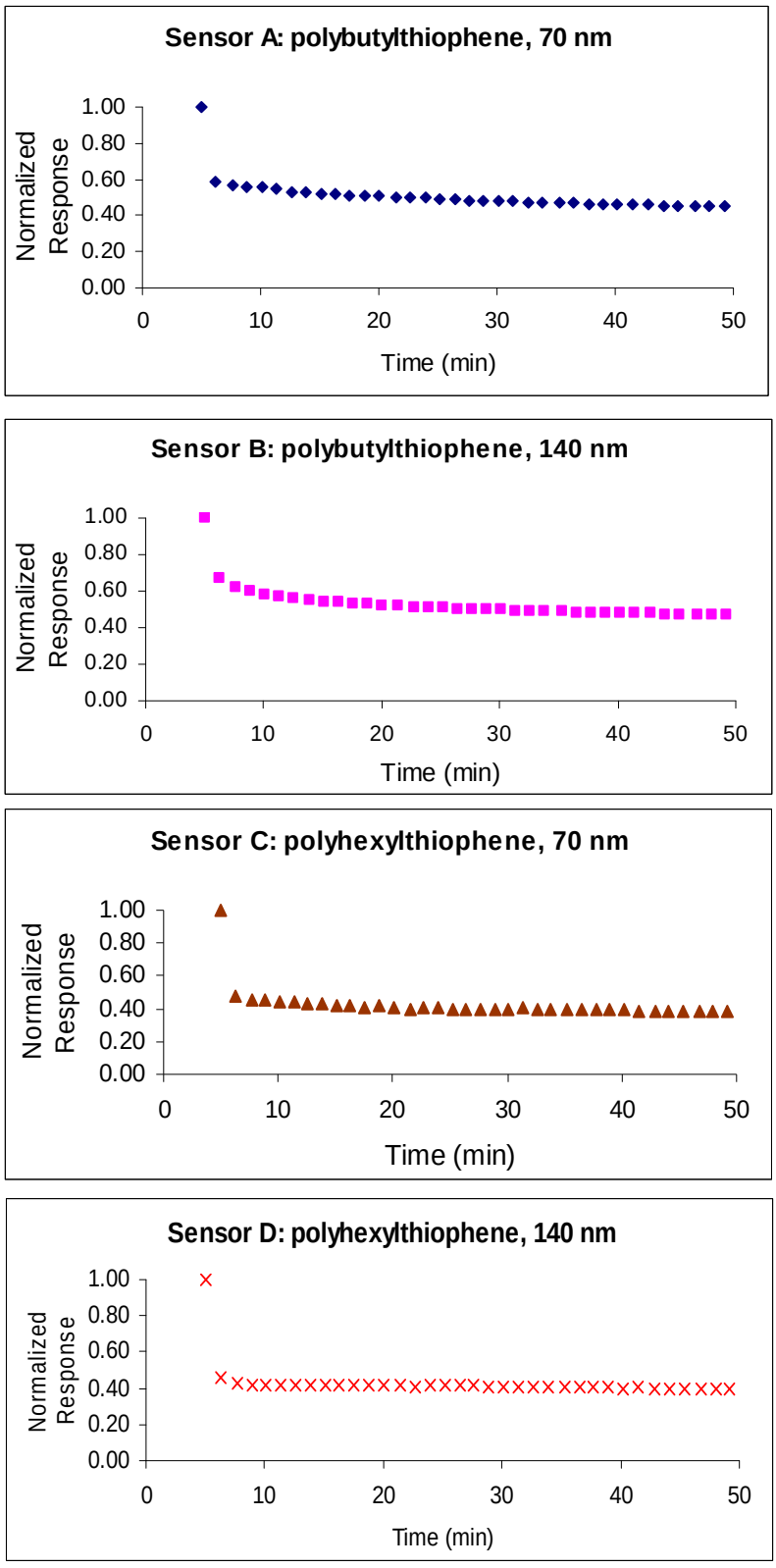

Figure 14. Response of a sensor array to gas mixture of triethylamine:hexylamine (10 ppm:20 ppm). For clarity, the sensor responses are shown separately.

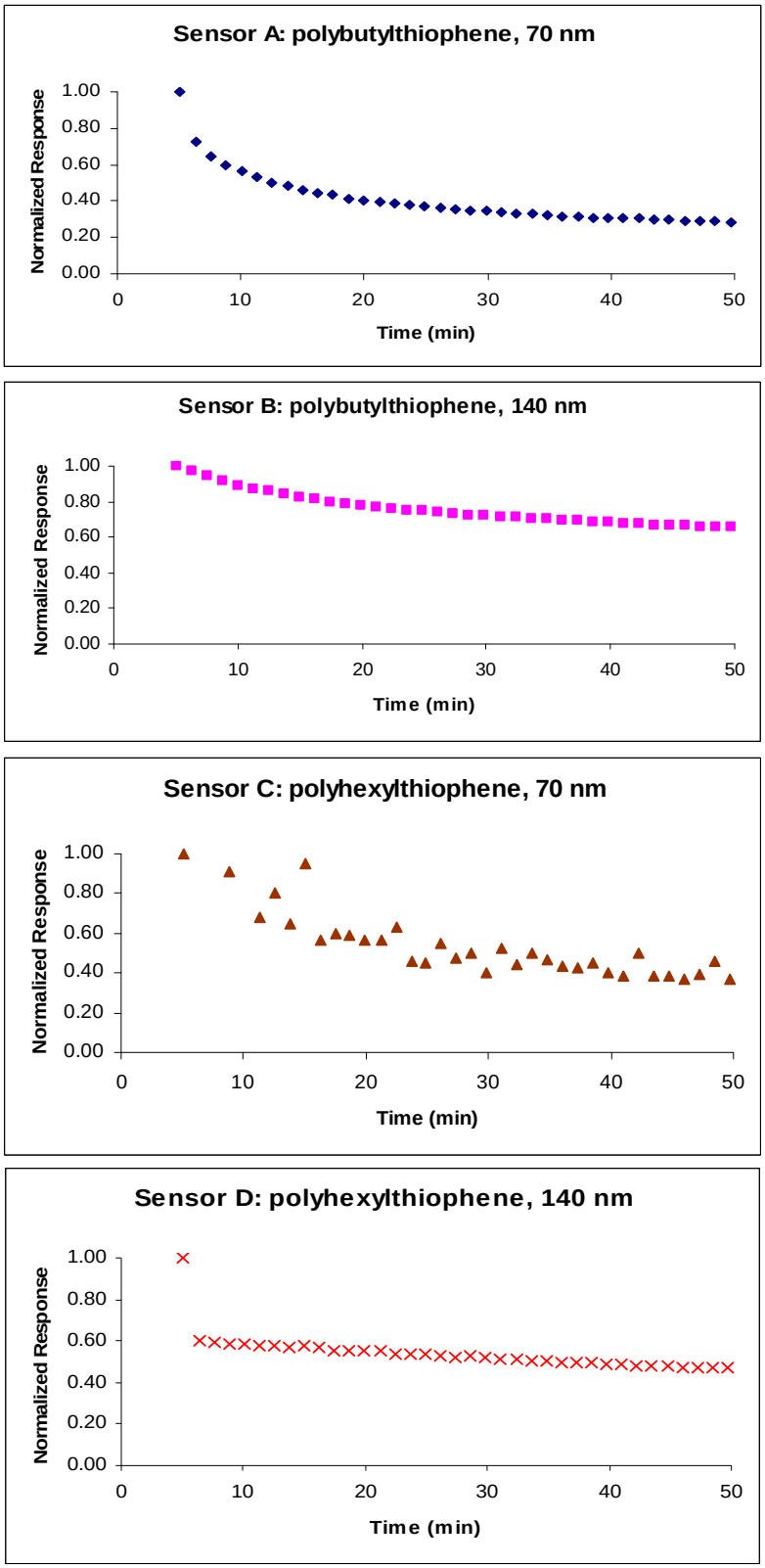

Figure 15. Response of sensor array to a gas mixture of triethylamine:hexylamine (20 ppm:10 ppm). For clarity, the sensor responses are shown separately.

As mentioned earlier, the mixture response is in fact a linear combination of two component responses and can be characterized as such. This characterization will be demonstrated for Sensor A exposed to a 20 ppm hexylamine:10 ppm triethylamine mixture (though the same procedure can be repeated for the other sensors as well). First, the sensor responses to the component analytes must be formalized. Figure 16 shows the response of Sensor A to 20 ppm of hexylamine.

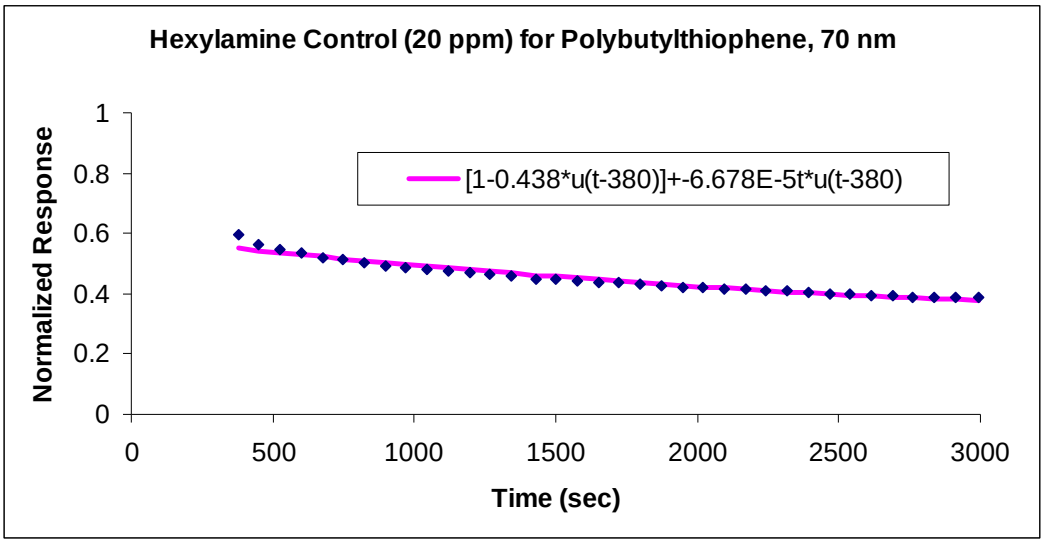

Figure 16. Sensor response to the component analyte 20 ppm of hexylamine vapor. This component response will be used to characterize the mixture response to hexylamine:triethylamine (20 ppm:10 ppm) vapor.

To characterize this sensor response as a function of time, $\boldsymbol{R}(t)$, it is described as a linear combination of two functions, S(t) and $T(t)$, where $S(t)$ is used to describe the step response character of the sensor response and $T(t)$ describes the transient behavior of the response. In the case of the step response, $S(t)$ will always have the form of $1 - A \cdot u(t)$, where A scales the degree of the step response and $u(t)$ is given as

$$u(t) = \begin{cases} 0, & \text{for } t < 0 \\ 1, & \text{for } t \geq 0 \end{cases}$$

The unit step response, u(t), also appears in the transient response because the sensor does not respond until the analyte is introduced

Therefore, the sensor response to the hexylamine analyte with $\boldsymbol{R}_{HA}(t)$ can be fitted with,

$$\boldsymbol{R}_{HA}(t) = [1 - \alpha\, u(t-T_0)] + \beta \cdot t(t) \qquad \text{Equation 6.1}$$

where α and β are the weighting factors between the two response and T_0 represents the time at the which the analyte is introduced. In this case, the sensor basically shows a step response with a 56% decrease in current but since there is a small slope to the response $\boldsymbol{R_{HA}}(t)$ is fully characterized as

$$\boldsymbol{R_{HA}}(t) = 0.44 \cdot \left[1 - u(t - T_0)\right] - 6.68 \times 10^{-5} t \cdot u(t - T_0)$$

where $\alpha = 0.44$, $\beta = 6.68$E-5, and $T_0 = 380$ seconds.

In the case of the triethylamine analyte, the sensor response is completely transient so $S(t) = 0$. Therefore, $\boldsymbol{R_{TEA}}(t)$, the response function to triethylamine vapor is given by

$$\boldsymbol{R_{TEA}}(t) = 15.7 t^{-0.49} \cdot u(t - T_0) \qquad \text{Equation 6.2}$$

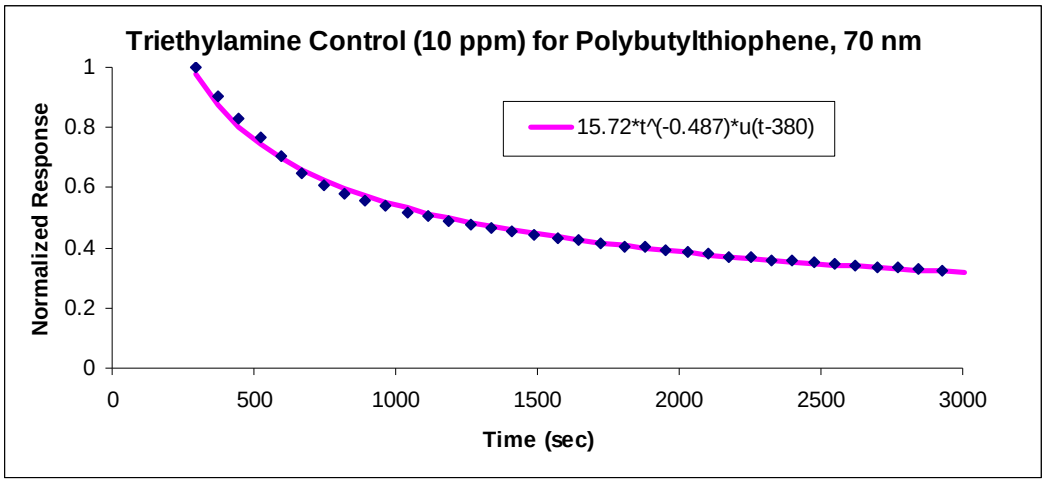

Figure 17. Sensor response to the component analyte 10 ppm of triethylamine vapor. This component response will be used to characterize the mixture response to hexylamine:triethylamine (20 ppm:10 ppm) vapor.

The response to the mixture, $\boldsymbol{R_{HA\text{-}TEA}}(t)$ can now be described as a linear combination of these two sensor functions in response to the control vapors. If the weighting factor of $\boldsymbol{R_{HA}}(t)$ is chosen to be twice that of $\boldsymbol{R_{HEA}}(t)$, as consistent with the relative concentration of the two analytes, then the total response is

$$\begin{aligned}\boldsymbol{R_{HA-TEA}}(t) &= 0.25\,\boldsymbol{R_{HA}}(t) + 0.125\,\boldsymbol{R_{TEA}}(t) \\ &= 0.25\left(0.44 \cdot \left(1 - u(t - T_0)\right) - 6.68 \times 10^{-5} t \cdot u(t - T_0)\right) + 0.125\left(15.7 t^{-0.49} \cdot u(t - T_0)\right)\end{aligned}$$

In this case, the chosen weighting factors do not sum to one. This may be because the weighting factors also determine the magnitude of the total response, which is affected by the total concentration of the analyte mixture (e.g. 30 ppm for this example). In other words, the response to 20 ppm of hexylamine is perturbed by the presence of 10 ppm of triethylamine. To support this possibility, it is noted that if 0.66 and 0.33 are chosen as the weighting factors, the fit is less ideal but still matches the overall sensor response. The possibility of exploring cross-interactions between analytes will be discussed later as a possible avenue for future work.

The final response function $\boldsymbol{R}_{HA\text{-}TEA}(t)$ is shown, along with the experimental response in Figure 18. The fit matches very well with the experimental response, confirming that it is possible to consider and characterize the mixture response in terms of the constituent responses.

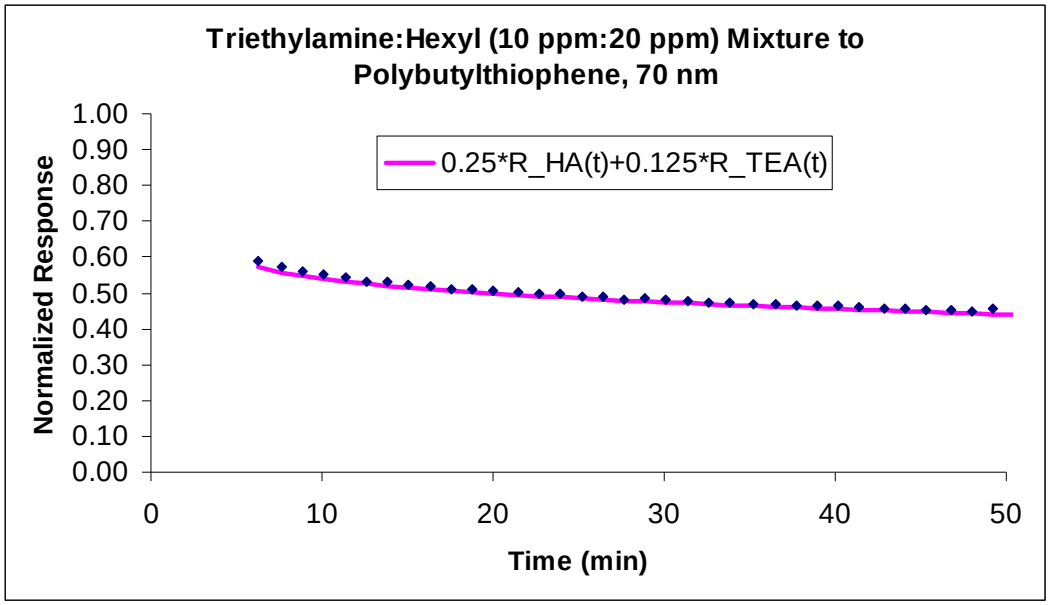

Figure 18. Sensor response to the hexylamine:triethylamine (20 ppm:10 ppm) vapor mixture and the corresponding fit as a linear combination of the component responses. The fit matches well with the experimental data.

Proposed Model of Sensor-Analyte Interaction

Based on the experimental data as well as the physical analysis thus far, the model proposed in the previous chapter is developed in order to conceptualize how discrimination of the analyte can be achieved by varying the side chain length and the film thickness.

For reference, the steps present in Chapter Five are briefly repeated here with the accompanying figure: (Fig. 19):

1. The analyte sorbs onto the polythiophene film.
2. The analyte diffuses from the surface of the film to the semiconductor-oxide interface.
3. The analyte reaches the boundary of the electric potential profile.
4. The analyte reaches the conduction layer at the interface.

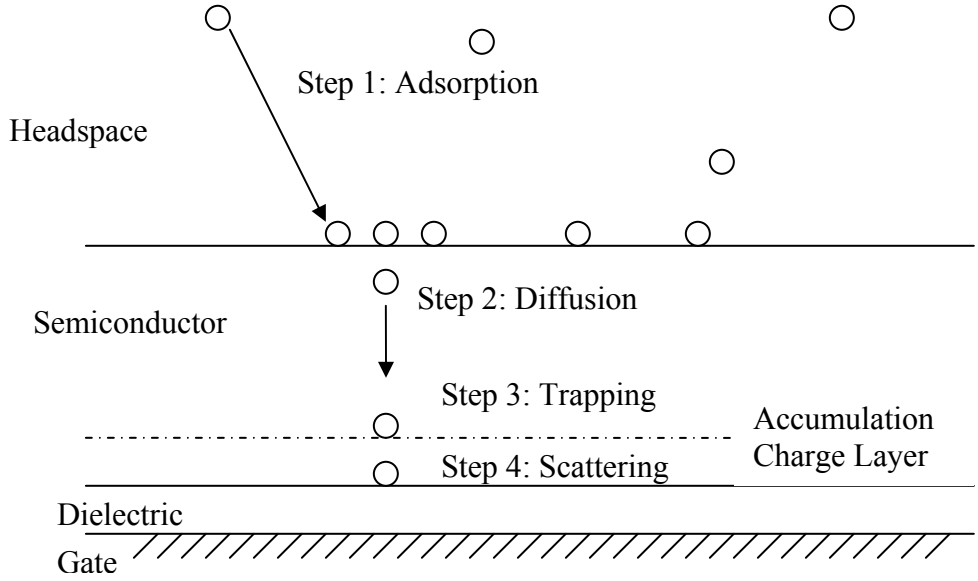

Figure 19. This picture outlines the steps of analyte interaction with the sensor film. Note that it is for conceptual purposes and is not to scale.

Continuing with this framework, Figure 20 further depicts the analyte-sensor interaction, beginning with the analyte from the ambient adsorbing onto the surface of the film. The surface concentration of the analyte denoted by $C_A(0)$ is a function of the partition coefficient of the sensor film, κ_{PT}, as well as the ambient temperature, T, and pressure, P. The analyte then diffuses into the film, of thickness T, until it reaches the conducting layer at the oxide interface. It is the concentration of analyte at this interface, $C_A(x=T)$ that gives rise to the electrical response of the sensor. This concentration is dependent on the film thickness, T, and the diffusion coefficient, D_A, of the analyte. This diffusion coefficient D_A encapsulates the effect of d-spacing since it is a function of the analyte size relative to the length of the side chain. Therefore by tuning both D_A and film thickness, T, we have two complementary knobs can be independently adjusted to engineer physical discrimination.

Figure 20 also shows the potential profile in the film arising from the gate voltage. As with most organic materials, the extent of the band bending into the film may be quite significant [17]. This corresponds with step 3 of the framework, showing that analytes some distance away from the interface can also attribute to the sensor's electrical response acting as dopants or impurities which perturb the band bending in the film.

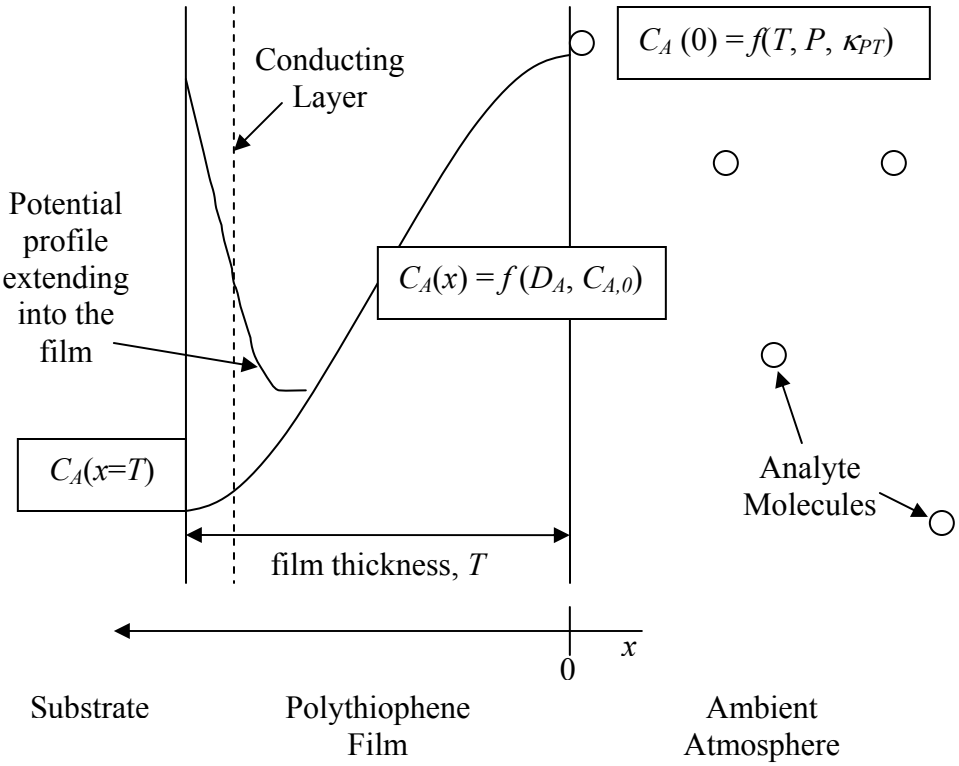

Figure 20. Conceptual framework for physical discrimination

This model accounts for several empirical observations:

- The physical interaction with and uptake of the analyte by the sensor as confirmed with swelling changes via XRR and the mass uptake measurements with the QCM.
- The diffusion behavior of the analyte is consistent through the thickness dependence and the GIXD data showing the variations of d-spacing as set by the side chain length.
- The shift in both field effect mobility, μ, and threshold voltage, V_T, that causes an effective decrease in the saturation drain current, I_{DSAT}. Also the V_T shift is usually punctuated and then slowly changes over time, this may be the result of the perturbation in the potential profile caused by the analyte.
- Accounts for the interplay between physical and electrical interactions. The physical interaction is the absorption and diffusion of the analyte into the material which depends on thickness and d-spacing; while the electrical interaction depends on the interaction of the analyte with conducting carriers at the semiconductor-dielectric interface. This implies that the underlying mechanism for the swelling response differs from that of the electrical response.

More importantly, this model provides a framework that provides pathways for engineering discrimination in sensor arrays. In order to properly engineer discrimination, there must be at least two orthogonal knobs that can each be turned separately. This is often ignored in most

schemes, where only chemical affinity (or the partition coefficient in the case of the above discussion) is considered for discrimination. This includes chemiresistors, where the affinity is tuned by mixing additives into a conducting polymer, or OTFTs, where the affinity is changed through specialized functional groups. Because this route only relies on one parameter, the degree of discrimination is limited—especially since there are only a small number of chemical interactions that can be exploited. For these approaches that rely on partitioning of the analyte within the film, Zellers *et al*. have indicated that the discrimination power of the array levels off at around five or six sensors [18].

Thus, in order to properly engineer discrimination, one can simultaneously adjust the film thickness and d-spacing of the films. In the framework that has been described, adjusting the d-spacing modifies the diffusion of the analyte through the film. The benefit of using these two knobs is that they come from existing parameters without introducing custom or exotic materials work. Most importantly, these two knobs are orthogonal because film thickness can be changed independent of the side chain and vice versa. According to the discussion above, it is imperative that these two knobs be orthogonal in order to achieve any reasonable physical discrimination.

In the case of mixtures of analyte vapors, it has been shown that mixture response is a combination of the component responses. When this is true, the mixture response can be easily encapsulated by this framework. However, it is conceivable that the mixture response may not be a simple, linear combination of the individual responses; for instance, this might happen if there is an additional interaction between the constituent vapors or if the surface concentration of an analyte will affect the chemical affinity of another analyte. For the sake of completeness, it is briefly noted how the framework should be adjusted. In such cases, the partition coefficient of analyte A is no longer a function of only C_A (the concentration of analyte A in the sorbent phase) and $C_{A,V}$ (the concentration of analyte A in the vapor phase), but also depends on C_B (the concentration of analyte B in the sorbent phase) and $C_{B,V}$ (the concentration of analyte B in the vapor phase). Also, while it is generally safe to assume to that the diffusion coefficient will remain unchanged, it is possible the coefficient will change if both species are chemically similar or have charged functional groups. Either way, the diffusion gradient of each species in a vapor mixture may be impacted, by a change in the surface, or starting, concentration as well as change in the diffusion coefficient.

Routes for Chemical Discrimination of Vapors

For the sake of completeness this section will present some of the work showing chemical discrimination by changing the functional group on the side chain. Most sensor research falls in this category, so chemical discrimination has already been demonstrated for many different motifs and strategies [19], including acid-base interactions [20], and hydrogen bonding [21], and dipole moments [22]. Therefore, the goal of this work is to demonstrate that this type of discrimination is feasible within the scheme of varying polythiophene side chains.

Polythiophenes with ester-based side chains will be examined and compared to the polythiophenes that have been used thus far. These polythiophenes, shown in Figure 21, possess side chains where the terminal hydrogen of the chain has been replaced with a carboxylic acid ester that has an ethyl group as the aryl substituent, thus constituting a side chain with an ester group.

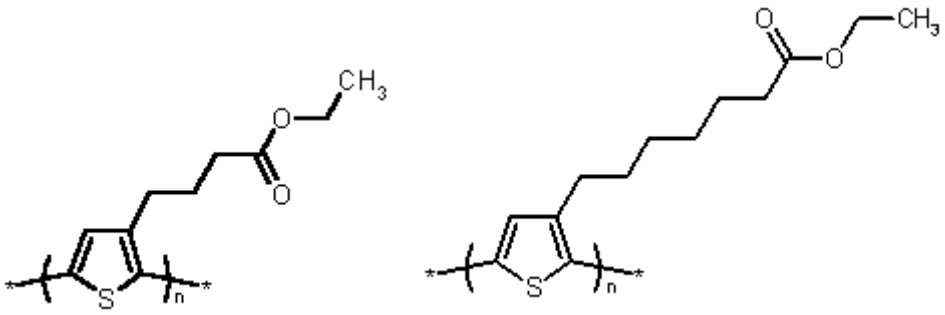

Figure 21. Polythiophene with ester based side chains with (a) four carbon segment, poly[3-(ethyl-4-butanoate)thiophene-2,5-diyl], and (b) seven carbon segment, poly[3-(ethyl-7-heptanoate)thiophene2,5-diyl].

GIXD data from the previous chapter has shown that the presence of the ester group chains do not impact the in-plane and out-of-plane spacing, both of which are still set by the length of side chain despite differences in the molecular arrangement. It is also important to confirm the electrical behavior of a polythiophene TFT with ester side chains. Polythiophene with ester side chains were purchased Rieke Metals and were used to fabricate TFTs using exactly the same procedure as with polythiophene with alkyl side chains. The TFTs were interrogated with the same voltages as before. While the polythiophene still shows electrical behavior, the semiconducting character is severely mitigated. There is also a large amount of leakage current at low gate voltages; this current, usually attributed as leakage current between the drain and the gate, can be addressed through better electrical isolation of the TFT. Usually this leakage is negligible, and the severity here is attributed to the presence of the ester group in the side chain although the mechanism is unclear. Nevertheless, TFTs made from the polythiophene containing the ester functional groups still show gate modulation of the drain current as shown in the I_D-V_G curve (Fig. 22).

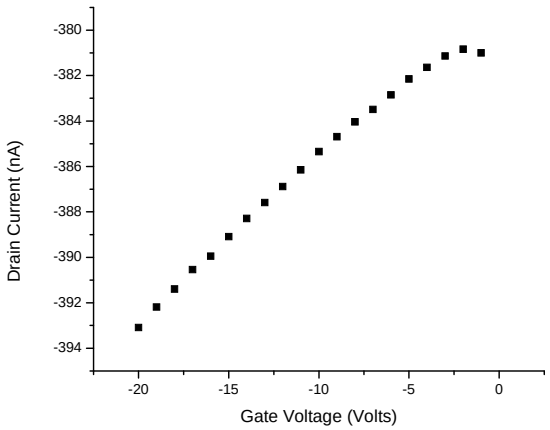

Figure 22. The I_D-V_G curve of a poly-(3-ethyl-4-butanoate)thiophene TFT. The device conducts appreciable amounts of current, though the transconductance is greatly reduced.

As sensors, the polythiophene with ester side chains behave like their alkyl counterparts. Although the transconductance is lower, the devices show the same marked decrease in response to an analyte. Figures 23 show the response of polyheptanoatethiophene to two amine analytes, butylamine vapor and octylamine vapor. The side chains of polyheptanoatethiophene contain a seven carbon segment along with an ester group. In each exposure, the analogous polyoctylthiphene derived sensor, which contains an eight carbon long side chain, was also exposed alongside the polyheptanoatethiophene sensor. In both case the sensors with ester based side chains respond less strongly to the amine vapors than to their alkyl counterparts.

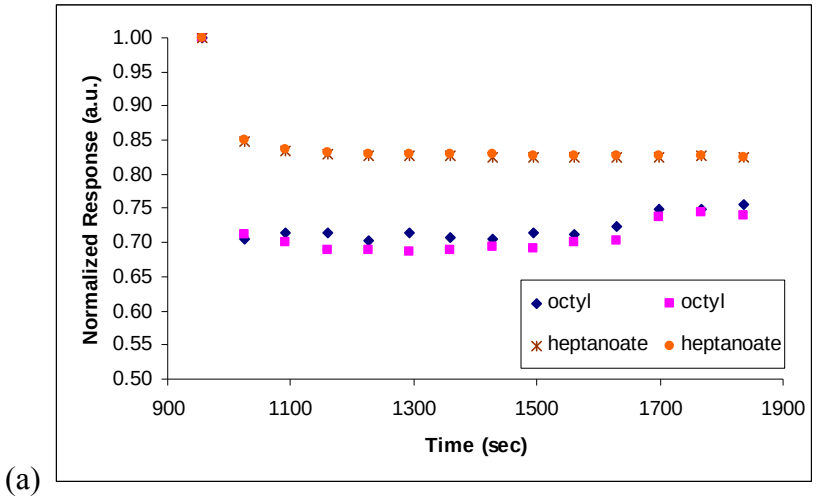

(a)

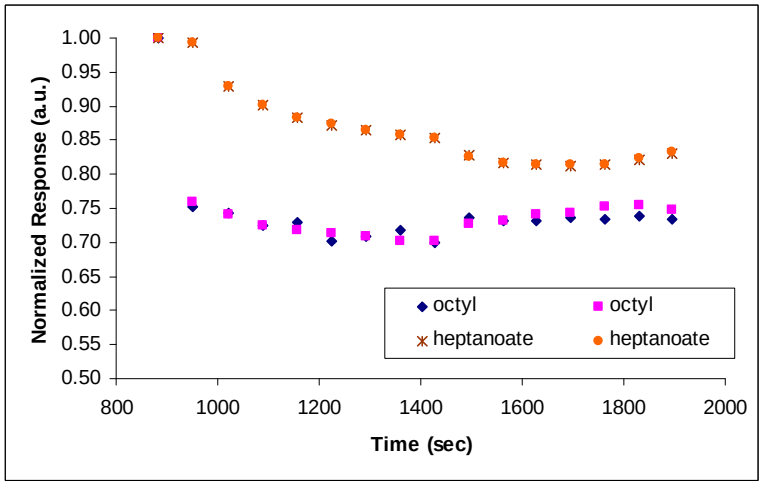

(b)

Figure 23. Response of polythiophene TFT with ester side chain containing seven carbons (heptanoate) to (a) 9 ppm of octylamine vapor and to (b) 9 ppm of butylamine vapor; polythiophenes with an alkyl side chain containing eight carbons (octyl) were also simultaneously exposed as a comparison. The reason for the transient character in (b) is unknown.

Since it is postulated that changing the side chain will affect the sensing response, the amine response is compared to the response to alcohols, a different class of analytes where the terminal amine is replaced by a hydroxy moiety. In contrast to amine analytes, the response to alcohol

vapors is different, being barely discernible. Upon introduction of butanol vapor, the polyheptanoatethiophene sensor shows a punctuated drop that is difficult to perceive with the naked eye. As Figure 24 demonstrates, monitoring the current difference makes it obvious that there is a response to the vapor. Furthermore, removal of the vapor with purging causes another change in the sensor response as a further confirmation that the butanol vapor did interact with the sensor material. The exacerbated bias stress effect may be due to an insufficient warm-up period prior to sensor exposure.

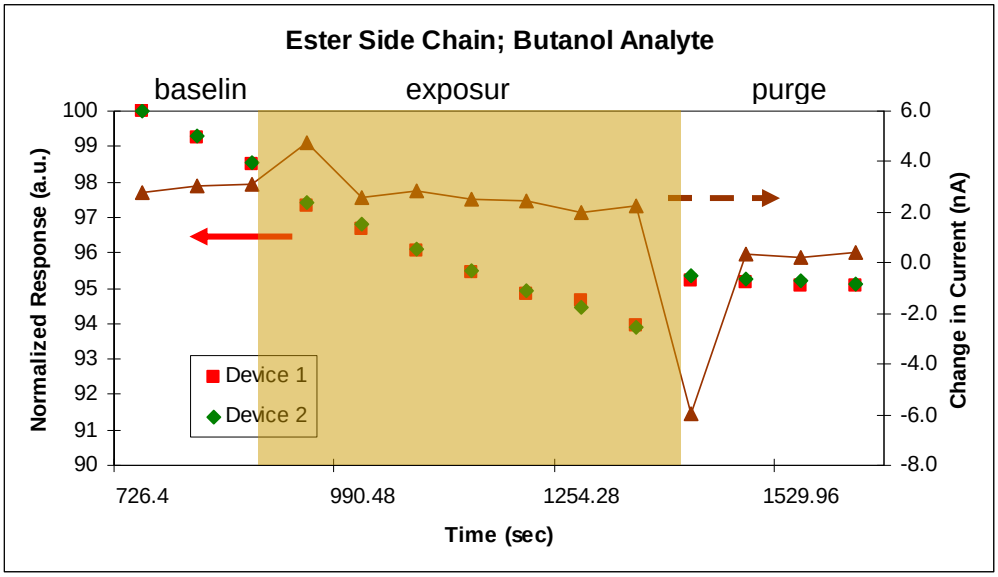

Figure 24. Polythiophene sensor with ester side chains exposed to 79 ppm of butanol analyte.

The particularly muted, yet present, response to alcohols is potentially advantageous. Successful discrimination requires that the individual responses are varied among the constituent sensors and a punctuated difference such this can be easily exploited. For instance in this scenario, if both alcohols and amines are included as potential analytes, then the ester containing polythiophene sensors can help discriminate between amines and alcohols since the alkyl containing polythiophene sensors respond to both. This example demonstrates the advantages of an array because, on its own, the ester containing polythiophene transistor would be a poor alcohol sensor, but in coordination with the alkyl based sensor, the sensor responses of both are leveraged.

Thus, in addition to tuning the length of the side chain, the chemical substituents of the side chain may also be changed. For ester-based side chains this still preserves the semiconducting properties as well as the sensor behavior, yet affects the degree of the sensor response. A major advantage of changing the chemical functional group is that it is orthogonal to side chain length since the two can be modified independently. Therefore it is possible to use these knobs to create a discrimination motif similar to what was done with physical discrimination when thickness and side chain length were modified simultaneously.

Revised Model of Sensor-Analyte Interaction

The framework presented in the previous section can be adjusted to incorporate chemical interactions between the functional groups of the side chain and those of the analyte. This can be done by modifying the surface concentration and the diffusion coefficient. In particular, the partition coefficient is varied because the functional group changes the chemical environment for the analyte which will affect the surface concentration. By virtue of the same argument, i.e. the change in chemical environment within the film, the diffusion coefficient of the analyte may also change. Therefore, diffusion is no longer adjusted the solely by tuning the d-spacing of the film, since electronic effects are now present within the material.

It may be possible that second order effects can further improve discrimination since diffusion is also a function of the side group. For instance, smaller d-spacing can impede diffusion but so can certain electronic effects like the polarity of the functional group. For instance, without functionalization, a nonpolar and polar analyte of similar size would diffuse similarly through the film. However, the addition of a polar side chain would affect the diffusion coefficients, retarding the diffusion of the polar analyte using the same principle as column chromatography. This has been proven to be successful method in chromatography and could be employed to add another dimension of discrimination.

Linearity and Sensitivity of Polythiophene Gas Sensors

Thus far the matter of discrimination has been addressed. Experimental data show the penultimate issues of linearity and sensitivity are also strongly determined by the side chain. This makes intuitive sense and underscores the importance of choosing the appropriate material parameters and properly engineering the side chains in sensor arrays.

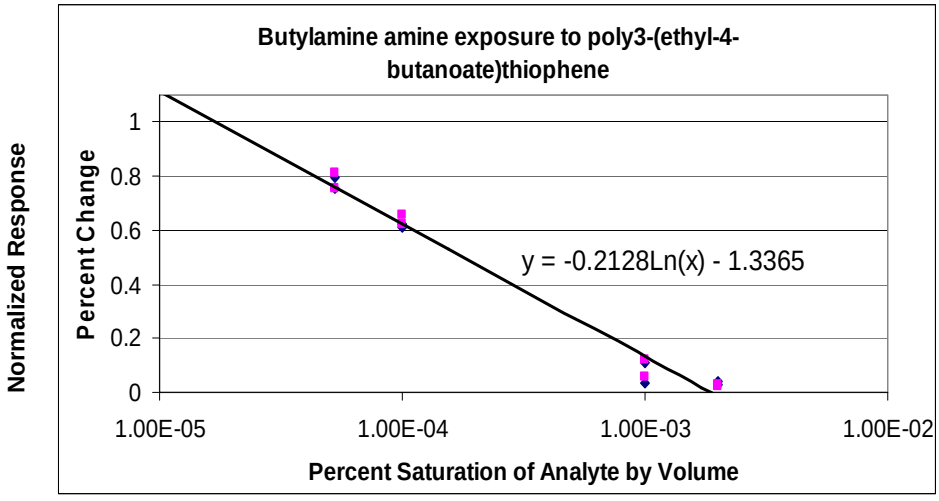

Figure 25. Plot for characterizing sensitivity and linearity of a polythiophene gas sensor.

Among current sensor research, there is no standard procedure for determining these two metrics. In most sensor work, sensitivity and linearity are not considered or are loosely characterized, perhaps with a single number that indicates the lowest analyte concentration that the sensor can detect. In this section, these two parameters are more thoroughly characterized by exposing a sensor to multiple concentrations of a single analyte and measuring the sensor response at each concentration. The data are compiled into a single plot as depicted in Figure 26. From this plot, sensitivity and linearity are characterized by fitting the data and performing a few simple extractions.

The plot in Figure 25 represents a polybutanoatethiophene sensor exposed to multiple concentrations of butylamine analyte. Here, the sensor response shows a logarithmic dependence on the analyte concentration and can be fitted to a straight line on a semi-log plot. Using this line, the sensitivity can be characterized by two metrics: the slope of the straight line fit and the y-intercept when the normalized sensor response is equal to one. The former is a measure of sensitivity in terms of responsiveness since the slope tells the change in sensor response to a change in analyte concentration. The latter is a threshold measurement since the concentration at which the sensor response is one is equivalent to the lowest measurable concentration. Of course, in practice, sensitivity may be limited by the noise floor of the overall circuit; however, this methodology provides an ultimate limit to the sensing floor. For this polybutanoatethiophene sensor the slope is determined to be -0.213 and the sensitivity limit is 1.70E-5, which corresponds to 1.4 ppm. These exposures and extractions are repeated for other polythiophenes and other analytes and the results are tabulated in Table II. In most cases, the polythiophene sensor showed a logarithmic dependence on analyte concentration, though in some cases the response was linear. The data indicate that the sensor response is well-defined over a range of analyte concentrations, so while the sensor behavior is not strictly linear, it seems linearity can be addressed through proper calibration.

In examining the table, it can be seen that the identity of the analyte plays a large role in determining the response. A quick glance shows that the slope and limit values are different between butylamine and octylamine. However, when looking at the response within each analyte, the length of the side chain determines the response more strongly than the chemical group. For instance, when looking at octylamine, the butyl and butanoate side chains have similar responses as well as the octyl and heptanoate responses. In other words, tuning linearity and sensitivity is also determined b the side chains. Therefore when engineering these sensor arrays the proper choice of side chain has a profound effect on several aspects of its performance.

Polythiophene Side Chain	**Butylamine Analyte**		**Octylamine Analyte**	
	Slope	**'Limit'**	**Slope**	**'Limit'**
Butyl	-0.19	1.78E-5 (1.6 ppm)	-0.020*	0.43* (566 ppm)
Butanoate	-0.21	1.70E-5 (1.5 ppm)	-0.028*	-4.54*
Octyl	-0.18	1.58E-5 (1.4 ppm)	-0.070	3.16E-4 (0.42 ppm)
Heptanoate	-0.18	1.34E-5 (1.2 ppm)	-0.070	5.4E-4 (0.711 ppm)

Table II. Sensitivity of different polythiophenes with various side chain s to butylamine and octylamine analytes. (*) indicates that sensor response was linear with respect to concentration

Conclusion

In summary, this chapter presents seminal work on engineering sensor arrays. Important parameters have been elucidated in determining and controlling the sensor response, including modifying the side chain and functional group. Most importantly, by tuning some of these parameters very powerful discrimination motifs has been shown, which hold even in the presence of analyte mixtures. All this has been accomplished without using exotic synthetic routes but instead employing easily accessibly parameters and leveraging robust interactions that have been verified with analytical methods. Despite the simplicity of this approach, a new and valuable discrimination based on structural differences has been shown, which cannot be accomplished with current e-nose technologies or even by traditional analytical approaches like mass spectroscopy. In addition, a consistent framework has been presented which can also be used to develop future pathways for discrimination.

Chapter 7 Future Work and Summary

A great number of advances have been made since organic transistors were first demonstrated as gas sensors and many are presented in this work here. But there is still much work if polythiophene TFTs are to become enabling technologies for widespread and innovative electronic nose applications. This chapter will discuss future work for polythiophene based gas sensors and summarize what has been accomplished here.

For polythiophene gas sensors to become truly viable, the issue of mixtures requires more study especially since the sensors will always be dealing with mixtures of analytes in real world usage. It was demonstrated in Chapter Six that the mixture response is a linear combination of the component responses. However, this may not always be the case; for example, it is conceivable that the presence of one analyte interacting with the sensor film would affect the surface concentration of another analyte species or that there will be cross-interactions between chemically dissimilar analytes. Thus it is important to comprehensively characterize the mixture response to determine if the presence of one analyte species will mitigate or enhance the response to another species. In situ XRR measurements have shown considerable promise for monitoring sensor-analyte interactions and would be equally useful for monitoring these with analyte mixtures. The following presents a brief sketch of how these interactions could be determined based on the methodologies from Chapter Six.

Understanding other cross-interactions between analytes would begin with in situ x-ray reflectivity (XRR) studies along with in situ electrical characterization. By using the custom setup to introduce vapor mixtures, the sensor films would be exposed to a mixture where the relative concentrations of the analytes could be continuously varied. Several pairs of analytes could be evaluated: two analytes of similar and dissimilar sizes, a branched analyte with a linear analyte of similar size. Initially, only amines would be evaluated; although, most likely, cross-interactions would be found with pairs of chemically dissimilar analytes. Future studies would incorporate such pairs of analytes to investigate polar, nonpolar, charge-based, and acid-base, interactions. Another study could include moisture, or water vapor. As mentioned in previous chapters, moisture is always an issue with gas sensors and while this can be addressed using a differential sensing architecture, it would still be beneficial to characterize the effect of moisture in any analyte gas.

Such investigations would indicate if the presence of a second analyte affects the physical interaction between an analyte and the polythiophene film. The experiments will show if thickness changes due to one analyte are the same regardless of the presence of another species. If the changes are different, then monitoring the thickness change of the film as the concentration of another analyte varies can show how the surface concentration changes of one analyte in the presence of another analyte.

Since the custom setup is capable of simultaneous characterization in situ with the XRR measurement, both the physical interactions and the electrical response can be monitored together and the latter can be used to corroborate the physical measurements. If any cross-interactions are detected by the XRR technique, then it is worthwhile to see if the sensor response shows any deviation from being a linear combination of the component responses.

Sensor Array Engineering

The sensor array is the heart of the electronic nose because the functionality and usefulness of an electronic nose is ultimate governed by the capabilities of its array. Unfortunately, designing powerful sensor arrays is not as straightforward as adding more sensor elements. A major contribution of this work is to demonstrate the possibility and effectiveness of employing certain strategies to engineer useful arrays. In fact, the approach, adopted by many, of simply adding as many sensors as possible has even led to the belief that sensor arrays require numerous elements with each new sensor adding minimal value. In contrast, this work has shown that with as little as four elements, very useful arrays can be produced if the parameters are chosen correctly.

The strategies that have been presented thus far can be been built upon and expanded to fabricate even more effective and complex arrays. The use of chemical discrimination in tandem with physical discrimination methods is an obvious area for future exploration. This would include looking at more functional groups and characterizing the behavior of the sensor in response to various analytes of different chemical constituencies. Besides alkyl and ester-derived side chains, polythiophene molecules possessing carboxylate and carboxylic acid terminated side chains are also commercially available and can be explored immediately as possible sensors (Fig. 1). It is also possible to synthesis custom materials using novel synthetic techniques. In doing so, it is important to preserve the semiconducting property as well as the solubility properties. The latter is important because side chains play a large role in the solubility of the polythiophene, an important consideration for ink-jet printing.

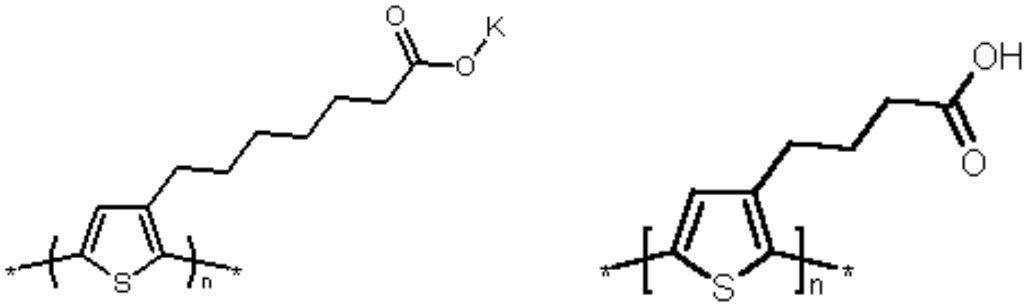

(a) (b)

Figure 1. Polythiophene derivatives possessing (a) carboxylate and (b) carboxylic acid terminated side chains.

Ideally, the analyte-sensor interaction could be elucidated in chemical terms along with this characterization work. This way, it would be possible to use specific chemical moieties to target certain classes of analytes. This understanding of the chemical interactions between the functional group of the side chain and of the analyte can also include how these interactions affects the charge transport behavior of the polythiophene. This will require analytical techniques besides XRR. One candidate is x-ray photoelectron spectroscopy (XPS), though XPS will only show covalent bonds which are unlikely in these cases. It has been noted that FTIR has been

employed with limited success, though further efforts could prove fruitful. The benefits of an analytical technique for monitoring the sensor-analyte interaction should encourage discovery of a suitable technique.

Once a basic understanding is obtained, it would be very interesting to find discrimination motifs such as those presented in Chapter Seven where different parameters can be independently and simultaneously adjusted. These strategies would engineer even more powerful discrimination by tuning both physical parameters and chemical parameters.

Novel Device Structures

Besides exploring more interactions and characterizing what has been previously discovered, more sophisticated engineering methods can also be explored. One potentially attractive sensor structure would employ bilayer films, where a second, additional layer is deposited on top of the polythiophene film. This layer would possess physical properties suitable for the sensor application. In the simplest case, it acts as a buffer providing additional control for the types of discrimination presented in this chapter. However there may be more creative routes; for instance, the layer can enhance discrimination by excluding certain type of analytes or as a way to create extreme selectivity, it could react with the analyte and create a byproduct that is detected by the underlying layer. Since the underlying polythiophene film is the charge conduction layer, there is greater freedom is selecting the material for this top layer.

This approach was recently and successfully demonstrated by Huang et al [1]. In this case, the top layer was similar to the bottom layer except for the presence of terminal hydroxy groups which was believed to increase sensitivity to the analyte. A structure of their device is shown in Figure 2.

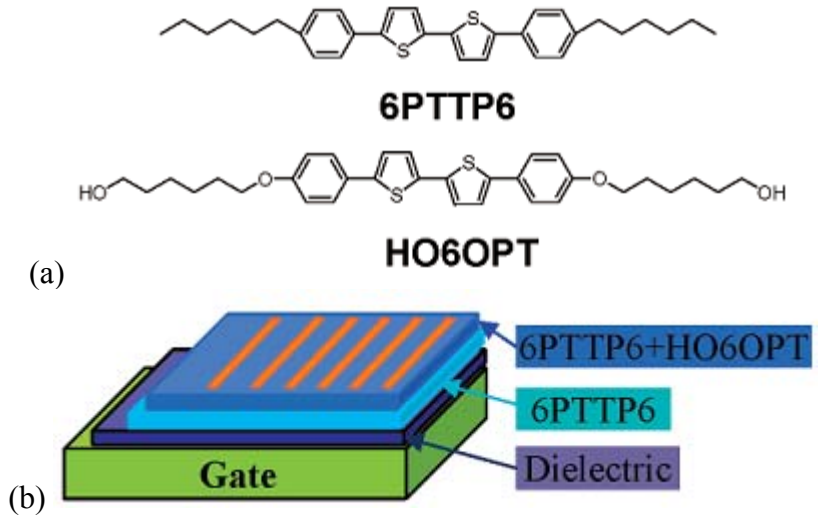

Figure 2. OTFT gas sensor employing a bilayer morphology demonstrated by Huang *et al* [1].

A more extreme version of this idea would be to employ blends of active materials, rather than a homogeneous film as the sensor. This may be a suitable approach for functionalized materials like polythiophene because if certain functional groups modify the sensor response to particular analytes, then a blended composition of differently functionalized materials may provide intermediate responses. For instance, Chang *et al* demonstrated the use of acidic and basic functional groups to modify the sensor response based on acidity [2]. It may be possible to extend this motif by using a blend to discriminate between vapors of varying and intermediate acidity. The use of such blends may improve the performance of a sensor array by providing a more continuous spectrum of responses. If blends are to be seriously pursued, they will require appropriate materials characterization. As in the case with most heterogeneous media, different phases exist for different compositions and even processing conditions. The phase behavior of a blend would need to first be adequately characterized. However, once the phase diagram is characterized, it is possibly that there may be many phases that can be exploited for sensing applications.

Summary

In summary, the research presented here has demonstrated the viability of polythiophene as basic gas sensors. A new understanding of the physical interactions and dependencies thereof has been attained through original characterization work utilizing in situ techniques. For the first time, the electrical sensing behavior of organic TFTs has been corroborated and measured in physical terms with multiple measurements. This understanding has been exploited and leveraged to engineer useful arrays of polythiophene TFTs. The experimental results from these arrays showcase several robust discrimination motifs which are suitable with vapor mixtures, providing seminal capabilities to enable exciting applications like spoilage detection.

Many of these results have been submitted and published in peer reviewed journals [3-5] and presented at conferences [6-8] and they represent an important contribution to gas sensor research and organic electronics. As a body, they provide compelling evidence that polythiophene TFTs are ideal candidates for sensor arrays. With continued research, a low-cost fully-printed electronic nose may be realized.

References

Chapter One

[1] J.W. Gardner and P.N. Bartlett, "A brief history of electronic noses," *Sensors and Actuators B: Chemical*, vol. 18, Mar. 1994, pp. 210-211.

[2] J. Gardner and P. Bartlett, *Electronic Noses Principles and Applications*, New York, NY: Oxford University Press, 1999.

[3] J. Chang, "Functionalized Polythiophene Thin-Film Transistors for Low-Cost Gas Sensor Arrays," University of California, Berkeley, 2006.

[4] H. Sirringhaus, T. Kawase, R.H. Friend, T. Shimoda, M. Inbasekaran, W. Wu, and E.P. Woo, "High-Resolution Inkjet Printing of All-Polymer Transistor Circuits," *Science*, vol. 290, Dec. 2000, pp. 2123-2126.

[5] S. Molesa, A. de la Fuente Vornbrock, P. Chang, and V. Subramanian, "Low-Voltage Inkjetted Organic Transistors for Printed RFID and Display Applications," *IEEE Internationl Electron Device Meeting Technical Digest*, 2005, pp. 5.4.1-5.4.4.

[6] W. Clemens, W. Fix, J. Ficker, A. Knobloch, and A. Ullmann, "From polymer transistors toward printed electronics," *Journal of Materials Research*, vol. 19, Jul. 2004, pp. 1963-1973.

[7] D. Gamota, P. Brazis, K. Kalyanasundaram, and J. Zhang, *Printed organic and molecular electronics*, Springer, 2004.

[8] A.C. Arias, S.E. Ready, R. Lujan, W.S. Wong, K.E. Paul, A. Salleo, M.L. Chabinyc, R. Apte, R.A. Street, Y. Wu, P. Liu, and B. Ong, "All jet-printed polymer thin-film transistor active-matrix backplanes," *Applied Physics Letters*, vol. 85, Oct. 2004, pp. 3304-3306.

[9] M.C. Tanese, D. Fine, A. Dodabalapur, and L. Torsi, "Interface and gate bias dependence responses of sensing organic thin-film transistors," *Biosensors and Bioelectronics*, vol. 21, Nov. 2005, pp. 782-788.

[10] L. Torsi, A. Dodabalapur, L. Sabbatini, and P.G. Zambonin, "Multi-parameter gas sensors based on organic thin-film-transistors," *Sensors and Actuators B: Chemical*, vol. 67, Sep. 2000, pp. 312-316.

[11] F. Liao, C. Chen, and V. Subramanian, "Organic TFTs as gas sensors for electronic nose applications," *Sensors and Actuators B: Chemical*, vol. 107, Jun. 2005, pp. 849-855.

[12] B. Crone, A. Dodabalapur, A. Gelperin, L. Torsi, H.E. Katz, A.J. Lovinger, and Z. Bao, "Electronic sensing of vapors with organic transistors," *Applied Physics Letters*, vol. 78, Apr. 2001, pp. 2229-2231.

Chapter Two

[1] J.W. Gardner and P.N. Bartlett, *Sensors and sensory systems for an electronic nose*, Springer, 1992.

[2] *Sniffing out terrorism : the use of dogs in homeland security : hearing*, DIANE Publishing, .

[3] J. Gardner and P. Bartlett, *Electronic Noses Principles and Applications*, New York, NY: Oxford University Press, 1999.

[4] T.C. Pearce, S.S. Schiffman, H.T. Nagle, and J.W. Gardner, *Handbook of machine olfaction: electronic nose technology*, Wiley-Vch, 2006.

[5] J.H.J. Huis in't Veld, "Microbial and biochemical spoilage of foods: an overview," *International Journal of Food Microbiology*, vol. 33, Nov. 1996, pp. 1-18.

[6] "WHO | Food technologies and public health, 1995."

[7] S. Roller, "Physiology of food spoilage organisms," *International Journal of Food Microbiology*, vol. 50, Sep. 1999, pp. 151-153.

[8] P.S. Mead, L. Slutsker, V. Dietz, L.F. McCaig, J.S. Bresee, C. Shapiro, P.M. Griffin, and R.V. Tauxe, "Food-Related Illness and Death in the United States," *Emerging Infection Disease*, vol. 5, Oct. 1999, p. 607 to 625.

[9] C. Blackburn, *Food spoilage microorganisms*, Boca Raton: CRC Press LLC, 2006.

[10] J. Jay, *Modern Food Microbiology*, New York: Chapman & Hall, 1996.

[11] G.E. Nychas and C.C. Tassou, "Spoilage Processes and Proteolysis in Chicken as Detected by HPLC," *Journal of the Science of Food and Agriculture*, vol. 74, 1997, pp. 199-208.

[12] E. Kress-Rogers and C. Brimelow, *Instrumentation and Sensors for the Food Industry*, Cambridge: Woodhead Publishing, 2001.

[13] K.B. Mullis and F.A. Faloona, "Specific synthesis of DNA in vitro via a polymerase-catalyzed chain reaction," *Methods in Enzymology*, vol. 155, 1987, pp. 335-350.

[14] Gutierrez, Garcia, Gonzalez, Sanz, Hernandez, and Martin, "Quantitative detection of meat spoilage bacteria by using the polymerase chain reaction (PCR) and an enzyme linked immunosorbent assay (ELISA)," *Letters in Applied Microbiology*, vol. 26, 1998, pp. 372-376.

[15] C.[. Yost and F.[. Nattress, "The use of multiplex PCR reactions to characterize populations of lactic acid bacteria associated with meat spoilage," *Letters in Applied Microbiology*, vol. 31, Aug. 2000, pp. 129-133.

[16] Scheu P.M., Berghof K., and Stahl U., "Detection of pathogenic and spoilage micro-organisms in food with the polymerase chain reaction," *Food Microbiology*, vol. 15, Feb. 1998, pp. 13-31.

[17] R. Dainty, R. Edwards, and C. Hibbard, "Time course of volatile compound formation during refrigerated storage of naturally contaminated beef in air," *Journal of Applied Microbiology*, vol. 59, 1985, pp. 303-309.

[18] B. Perez de Castro, M.A. Asensio, B. Sanz, and J.A. Ordonez, "A method to assess the bacterial content of refrigerated meat.," *Appl. Environ. Microbiol.*, vol. 54, Jun. 1988, pp. 1462-1465.

[19] E. Drosinos and R. Board, "Metabolic activities of pseudomonads in batch cultures in extract of minced lamb," *Journal of Applied Microbiology*, vol. 77, 1994, pp. 613-620.

[20] A. Kakouri and G. Nychas, "Storage of poultry meat under modified atmospheres or vacuum packs: possible role of microbial metabolites as indicator of spoilage," *Journal of Applied Microbiology*, vol. 76, 1994, pp. 163-172.

[21] H. Alomirah, I. Alli, B. Gibbs, and Y. Konishi, "Identification of Proteolytic Products as Indicators of Quality in Ground and Whole Meat," *Journal of Food Quality*, vol. 21, 1998, pp. 299-316.

[22] Braun P., Fehlhaber K., Klug C., and Kopp K., "Investigations into the activity of enzymes produced by spoilage-causing bacteria: a possible basis for improved shelf-life estimation," *Food Microbiology*, vol. 16, Oct. 1999, pp. 531-540.
[23] M.H.S. Santos, "Biogenic amines: their importance in foods," *International Journal of Food Microbiology*, vol. 29, Apr. 1996, pp. 213-231.
[24] R.H. Dainty, R.A. Edwards, C.M. Hibbard, and S.V. Ramantanis, "Bacterial sources of putrescine and cadaverine in chill stored vacuum-packaged beef," *Journal of Applied Microbiology*, vol. 61, 1986, pp. 117-123.
[25] R. Edwards, R. Dainty, and C. Hibbard, "Putrescine and cadaverine formation in vacuum packed beef," *Journal of Applied Microbiology*, vol. 58, 1985, pp. 13-19.
[26] C.O. Gill and K.G. Newton, "Spoilage of vacuum-packaged dark, firm, dry meat at chill temperatures.," *Appl. Environ. Microbiol.*, vol. 37, Mar. 1979, pp. 362-364.
[27] G. Molin and A. Ternstrom, "Numerical Taxonomy of Psychrotrophic Pseudomonads," *J Gen Microbiol*, vol. 128, Jun. 1982, pp. 1249-1264.
[28] I.J. Seymour, M.B. Cole, and P.J. Coote, "A substrate-mediated assay of bacterial proton efflux/influx to predict the degree of spoilage of beef mince stored at chill temperatures," *The Journal of Applied Bacteriology*, vol. 76, Jun. 1994, pp. 608-615.
[29] J. Jay, "Microorganisms in fresh ground meats: the relative safety of products with low versus high numbers," *Meat Science*, vol. 43, 1996, pp. 59-66.
[30] C.O. GILL, "Substrate Limitation of Bacterial Growth at Meat Surfaces," *Journal of Applied Microbiology*, vol. 41, 1976, pp. 401-410.
[31] G.J. Nychas, V.M. Dillon, and R.G. Board, "Glucose, the key substrate in the microbiological changes occurring in meat and certain meat products.," vol. 10, 1988, pp. 203-231.
[32] L.R. Freeman, G.J. Silverman, P. Angelini, C. Merritt, and W.B. Esselen, "Volatiles produced by microorganisms isolated from refrigerated chicken at spoilage.," *Appl. Environ. Microbiol.*, vol. 32, Aug. 1976, pp. 222-231.
[33] R. Dainty, R. Edwards, C. Hibbard, and J. Marnewick, "Volatile compounds associated with microbial growth on normal and high pH beef stored at chill temperatures," *Journal of Applied Microbiology*, vol. 66, 1989, pp. 281-289.
[34] R.A. Edwards, R.H. Dainty, and C.M. Hibbard, "Volatile compounds produced by meat pseudomonads and related reference strains during growth on beef stored in air at chill temperatures," *Journal of Applied Microbiology*, vol. 62, 1987, pp. 403-412.
[35] T. Jackson, G. Acuff, and J. Dickson, *In Food Microbiology: Fundamentals and Frontiers*, Washington, DC: ASM Press, 1997.
[36] L. Stanbridge and A. Davies, *In The Microbiology of Meat and Poultry*, London: Blackie Academic & Professional, 1998.
[37] J. Hartman, "A Possible Objective Method for the Rapid Estimation of Flavors in Vegetables," *Proceedings of the American Society for Horticulture Science*, vol. 64, 1954, pp. 335-342.
[38] J.W. Gardner and P.N. Bartlett, "A brief history of electronic noses," *Sensors and Actuators B: Chemical*, vol. 18, Mar. 1994, pp. 210-211.
[39] K. Persaud and G. Dodd, "Analysis of discrimination mechanisms in the mammalian olfactory system using a model nose," *Nature*, vol. 299, print. 1982, pp. 352-355.
[40] J. Gardner, H. Shurmer, and T. Tan, "Application of an electronic nose to the discrimination of coffees," *Sensors and Actuators B: Chemical*, vol. 6, Jan. 1992, pp. 71-

75.
[41] C. Di Natale, F.A.M. Davide, A. D'Amico, G. Sberveglieri, P. Nelli, G. Faglia, and C. Perego, "Complex chemical pattern recognition with sensor array: the discrimination of vintage years of wine," *Sensors and Actuators B: Chemical*, vol. 25, Apr. 1995, pp. 801-804.
[42] J. Chang, "Functionalized Polythiophene Thin-Film Transistors for Low-Cost Gas Sensor Arrays," University of California, Berkeley, 2006.
[43] F. Udrea, S. Santra, P.K. Guha, S.Z. Ali, J.A. Covington, W.I. Milne, J.W. Gardner, and S. Maeng, "Nanotubes and Nanorods on CMOS Substrates for Gas Sensing," 2009, pp. 19-26.
[44] E. Comini, G. Faglia, M. Ferroni, A. Ponzoni, and G. Sberveglieri, "Metal Oxide Nanowires As Promising Materials For Miniaturised Electronic Noses," 2009, pp. 12-14.
[45] A. Vasiliev, R. Pavelko, S. Gogish-Klushin, D. Kharitonov, O. Gogish-Klushina, A. Pisliakov, A. Sokolov, N. Samotaev, V. Guarnieri, M. Zen, and L. Lorenzelli, "Sensors Based on Technology "Nano-on-Micro" for Wireless Instruments Preventing Ecological and Industrial Catastrophes," *Sensors for Environment, Health and Security*, 2009, pp. 205-227.
[46] J.A. Covington and J.W. Gardner, "Carbon Nanomaterial Polymer Composite ChemFET and Chemoresistors For Vapour Sensing," 2009, pp. 38-41.
[47] H. Shurmer, J. Gardner, and H. Chan, "The application of discrimination technique to alcohols and tobaccos using tin-oxide sensors," *Sensors and Actuators*, vol. 18, Jul. 1989, pp. 361-371.
[48] H. Abe, T. Yoshimura, S. Kanaya, Y. Takahashi, Y. Miyashita, and S. Sasaki, "Automated odor-sensing system based on plural semiconductor gas sensors and computerized pattern recognition techniques," *Analytica Chimica Acta*, vol. 194, 1987, pp. 1-9.
[49] P. Corcoran, H.V. Shurmer, and J.W. Gardner, "Integrated tin oxide sensors of low power consumption for use in gas and odour sensing," *Sensors and Actuators B: Chemical*, vol. 15, Aug. 1993, pp. 32-37.
[50] J. Gardner and P. Bartlett, *Electronic Noses Principles and Applications*, New York, NY: Oxford University Press, 1999.
[51] A. Dall' Olio, G. Dascola, V. Varacca, and C. Bocchi, "Electron paramagnetic resonance and conductivity of an electrolyte oxypyrrole [(pyrrole polymer)] black," vol. 267, 1968, pp. 433–435.
[52] D. Blackwood and M. Josowicz, "Work function and spectroscopic studies of interactions between conducting polymers and organic vapors," *The Journal of Physical Chemistry*, vol. 95, Jan. 1991, pp. 493-502.
[53] P. Topart and M. Josowicz, "Characterization of the interaction between poly(pyrrole) films and methanol vapor," *The Journal of Physical Chemistry*, vol. 96, 1992, pp. 7824-7830.
[54] J. Janata and M. Josowicz, "Conducting polymers in electronic chemical sensors," *Nat Mater*, vol. 2, Jan. 2003, pp. 19-24.
[55] J.W. Gardner, T.C. Pearce, S. Friel, P.N. Bartlett, and N. Blair, "A multisensor system for beer flavour monitoring using an array of conducting polymers and predictive classifiers," *Sensors and Actuators B: Chemical*, vol. 18, Mar. 1994, pp. 240-243.
[56] B. Polk, "ChemFET arrays for chemical sensing microsystems," *Sensors, 2002. Proceedings of IEEE*, 2002, pp. 732-735 vol.1.
[57] A. Barbaro, C. Colapicchioni, E. Davini, G. Mazzamurro, A. Piotto, and F. Porcelli, "CHEMFET Devices for biomedical and environmental applications," *Advanced Materials*,

vol. 4, 1992, pp. 402-408.
[58] K. Pearson and Pearson, K., "On Lines and Planes of Closest Fit to Systems of Points in Space," *Philosophical Magazine*, vol. 2, 1901, pp. 559–572.
[59] J.W. Gardner, E.L. Hines, and M. Wilkinson, "Application of artificial neural networks to an electronic olfactory system," *Measurement Science and Technology*, vol. 1, 1990, pp. 446-451.
[60] T. Aishima, "Discrimination of liquor aromas by pattern recognition analysis of responses from a gas sensor array," *Anal. Chim. Acta*, vol. 243, 1991, pp. 293–300.
[61] J.W. Gardner and J. Yinon, *Electronic noses & sensors for the detection of explosives*, Springer, 2004.
[62] K.J. Albert, N.S. Lewis, C.L. Schauer, G.A. Sotzing, S.E. Stitzel, T.P. Vaid, and D.R. Walt, "Cross-Reactive Chemical Sensor Arrays," *Chemical Reviews*, vol. 100, Jul. 2000, pp. 2595-2626.
[63] N.A. Rakow and K.S. Suslick, "A colorimetric sensor array for odour visualization," *Nature*, vol. 406, 2000, pp. 710-713.
[64] J. Park, W.A. Groves, and E.T. Zellers, "Vapor Recognition with Small Arrays of Polymer-Coated Microsensors. A Comprehensive Analysis," *Analytical Chemistry*, vol. 71, 1999, pp. 3877-3886.

Chapter Three

[1] W. Brütting, *Physics of organic semiconductors*, Vch Verlagsgesellschaft Mbh, 2005.
[2] J. Chang, "Functionalized Polythiophene Thin-Film Transistors for Low-Cost Gas Sensor Arrays," University of California, Berkeley, 2006.
[3] G. Horowitz, "Organic thin film transistors: From theory to real devices," *J. Mater. Res*, vol. 19, 2004, pp. 1946–1962.
[4] M.H. Yoon, C. Kim, A. Facchetti, and T.J. Marks, "Gate dielectric chemical structure-organic field-effect transistor performance correlations for electron, hole, and ambipolar organic semiconductors.," *Journal of the American Chemical Society*, vol. 128, 2006, p. 12851.
[5] J. Zaumseil and H. Sirringhaus, "Electron and ambipolar transport in organic field-effect transistors," *Chem. Rev*, vol. 107, 2007, pp. 1296–1323.
[6] L. Chua, J. Zaumseil, J. Chang, E.C. Ou, P.K. Ho, H. Sirringhaus, and R.H. Friend, "General observation of n-type field-effect behaviour in organic semiconductors," *Nature*, vol. 434, Mar. 2005, pp. 194-199.
[7] T. Lindner, G. Paasch, and S. Scheinert, "Influence of distributed trap states on the characteristics of top and bottom contact organic field-effect transistors," vol. 19, 2004, pp. 2014-2027.
[8] H. Katz and J. Huang, "Thin-Film Organic Electronic Devices," *ANNUAL REVIEW OF MATERIALS RESEARCH*, vol. 39, 2009, pp. 71-92.
[9] C. Huang, J.E. West, and H.E. Katz, "Organic field-effect transistors and unipolar logic gates on charged electrets from spin-on organosilsesquioxane resins," *Advanced functional materials*, vol. 17, 2007, p. 142.
[10] E. Menard, V. Podzorov, S. Hur, A. Gaur, M. Gershenson, and J. Rogers, "High-

Performance n- and p-Type Single-Crystal Organic Transistors with Free-Space Gate Dielectrics," *Advanced Materials*, vol. 16, 2004, pp. 2097-2101.

[11] H.E. Katz, J. Johnson, A.J. Lovinger, and W. Li, "Naphthalenetetracarboxylic Diimide-Based n-Channel Transistor Semiconductors: Structural Variation and Thiol-Enhanced Gold Contacts," *Journal of the American Chemical Society*, vol. 122, 2000, pp. 7787-7792.

[12] H.E. Katz, A.J. Lovinger, J. Johnson, C. Kloc, T. Siegrist, W. Li, Y. Lin, and A. Dodabalapur, "A soluble and air-stable organic semiconductor with high electron mobility," *Nature*, vol. 404, Mar. 2000, pp. 478-481.

[13] C.D. Dimitrakopoulos, S. Purushothaman, J. Kymissis, A. Callegari, and J.M. Shaw, "Low-Voltage Organic Transistors on Plastic Comprising High-Dielectric Constant Gate Insulators," *Science*, vol. 283, Feb. 1999, pp. 822-824.

[14] Z. Bao and J.J. Locklin, *Organic field-effect transistors*, CRC Press, 2007.

[15] N.F. Mott and E.A. Davis, *Electronic processes in non-crystalline materials*, Oxford Clarendon, 1979.

[16] V. Ambegaokar, B.I. Halperin, and J.S. Langer, "Hopping conductivity in disordered systems," *Physical Review B*, vol. 4, 1971, pp. 2612–2620.

[17] N. Tessler, Y. Preezant, N. Rappaport, and Y. Roichman, "Charge Transport in Disordered Organic Materials and Its Relevance to Thin-Film Devices: A Tutorial Review," *Advanced Materials*, vol. 21, 2009, pp. 2741-2761.

[18] A. Salleo, T.W. Chen, A.R. V\ölkel, Y. Wu, P. Liu, B.S. Ong, and R.A. Street, "Intrinsic hole mobility and trapping in a regioregular poly (thiophene)," *Physical Review B*, vol. 70, 2004, p. 115311.

[19] T. Sekitani, S. Iba, Y. Kato, Y. Noguchi, T. Someya, and T. Sakurai, "Suppression of DC bias stress-induced degradation of organic field-effect transistors using postannealing effects," *Applied Physics Letters*, vol. 87, 2005, p. 073505.

[20] J. Lee, M. Heeney, S. Tierney, I. McCulloch, A. Murphy, J. Liu, J.M.J. Frechet, and V. Subramanian, ""Stability in OTFT gas sensors," Organic Thin-Film Electronics, edited by A.C. Arias, N. Tessler, L. Burgi, and J.A. Emerson," *Mater. Res. Soc. Symp. Proc.*, vol. 871E, Warrendale, PA, 2005, p. I1.5.

[21] M. Matters, D.M. De Leeuw, P.T. Herwig, and A.R. Brown, "Bias-stress induced instability of organic thin film transistors," *Synthetic Metals*, vol. 102, 1999, pp. 998–999.

[22] R.A. Street, A. Salleo, and M.L. Chabinyc, "Bipolaron mechanism for bias-stress effects in polymer transistors," *Physical Review B*, vol. 68, 2003, p. 85316.

[23] A. Salleo and R.A. Street, "Light-induced bias stress reversal in polyfluorene thin-film transistors," *Journal of Applied Physics*, vol. 94, 2003, p. 471.

[24] J.B. Chang and V. Subramanian, "Effect of active layer thickness on bias stress effect in pentacene thin-film transistors," *Applied Physics Letters*, vol. 88, 2006, p. 233513.

[25] J.M. Charlesworth, A.C. Partridge, and N. Garrard, "Mechanistic studies on the interactions between poly(pyrrole) and organic vapors," *The Journal of Physical Chemistry*, vol. 97, May. 1993, pp. 5418-5423.

[26] T. Li, J.W. Balk, P.P. Ruden, I.H. Campbell, and D.L. Smith, "Channel formation in organic field-effect transistors," *Journal of Applied Physics*, vol. 91, Apr. 2002, pp. 4312-4318.

[27] S.J. Zilker, C. Detcheverry, E. Cantatore, and D.M. De Leeuw, "Bias stress in organic thin-film transistors and logic gates," *Applied Physics Letters*, vol. 79, 2001, p. 1124.

[28] H.L. Gomes, P. Stallinga, F. Dinelli, M. Murgia, F. Biscarini, D.M. De Leeuw, T. Muck, J.

Geurts, L.W. Molenkamp, and V. Wagner, "Bias-induced threshold voltages shifts in thin-film organic transistors," *Applied Physics Letters*, vol. 84, 2004, p. 3184.
[29] D.B.A. Rep, A.F. Morpurgo, W.G. Sloof, and T.M. Klapwijk, "Mobile ionic impurities in organic semiconductors," *Journal of Applied Physics*, vol. 93, 2003, p. 2082.
[30] T. McLean, "Barriers to the implementation of plastic electronics," 2004.
[31] R.D. Yang, J. Park, C.N. Colesniuc, I.K. Schuller, W.C. Trogler, and A.C. Kummel, "Ultralow drift in organic thin-film transistor chemical sensors by pulsed gating," *Journal of Applied Physics*, vol. 102, 2007, pp. 034515-7.
[32] V. Subramanian, J. Lee, V. Liu, and S. Molesa, "Printed Electronic Nose Vapor Sensors for Consumer Product Monitoring," *IEEE International Solid State Circuits Conference*, vol. Paper 15.3, Feb. 2006.
[33] S.K. Park, D.A. Mourey, S. Subramanian, J.E. Anthony, and T.N. Jackson, "High-mobility spin-cast organic thin film transistors," *Applied Physics Letters*, vol. 93, Jul. 2008, pp. 043301-3.
[34] C.E. Mauldin, K. Puntambekar, A.R. Murphy, F. Liao, V. Subramanian, J.M.J. Fréchet, D.M. DeLongchamp, D.A. Fischer, and M.F. Toney, "Solution-Processable α,ω-Distyryl Oligothiophene Semiconductors with Enhanced Environmental Stability," *Chemistry of Materials*, vol. 21, May. 2009, pp. 1927-1938.
[35] O.D. Jurchescu, S. Subramanian, R.J. Kline, S.D. Hudson, J.E. Anthony, T.N. Jackson, and D.J. Gundlach, "Organic Single-Crystal Field-Effect Transistors of a Soluble Anthradithiophene," *Chemistry of Materials*, vol. 20, Nov. 2008, pp. 6733-6737.

Chapter Four

[1] A.C. Arias, S.E. Ready, R. Lujan, W.S. Wong, K.E. Paul, A. Salleo, M.L. Chabinyc, R. Apte, R.A. Street, Y. Wu, P. Liu, and B. Ong, "All jet-printed polymer thin-film transistor active-matrix backplanes," *Applied Physics Letters*, vol. 85, Oct. 2004, pp. 3304-3306.
[2] W. Clemens, W. Fix, J. Ficker, A. Knobloch, and A. Ullmann, "From polymer transistors toward printed electronics," *Journal of Materials Research*, vol. 19, Jul. 2004, pp. 1963-1973.
[3] S. Molesa, A. de la Fuente Vornbrock, P. Chang, and V. Subramanian, "Low-Voltage Inkjetted Organic Transistors for Printed RFID and Display Applications," *IEEE Internationl Electron Device Meeting Technical Digest*, 2005, pp. 5.4.1-5.4.4.
[4] H. Sirringhaus, T. Kawase, R.H. Friend, T. Shimoda, M. Inbasekaran, W. Wu, and E.P. Woo, "High-Resolution Inkjet Printing of All-Polymer Transistor Circuits," *Science*, vol. 290, Dec. 2000, pp. 2123-2126.
[5] V. Subramanian, J. Lee, V. Liu, and S. Molesa, "Printed Electronic Nose Vapor Sensors for Consumer Product Monitoring," *IEEE International Solid State Circuits Conference*, vol. Paper 15.3, Feb. 2006.
[6] J.B. Chang, V. Liu, V. Subramanian, K. Sivula, C. Luscombe, A. Murphy, J. Liu, and J.M.J. Frechet, "Printable polythiophene gas sensor array for low-cost electronic noses," *Journal of Applied Physics*, vol. 100, Jul. 2006, pp. 014506-7.

[7] M.C. Tanese, D. Fine, A. Dodabalapur, and L. Torsi, "Interface and gate bias dependence responses of sensing organic thin-film transistors," *Biosensors and Bioelectronics*, vol. 21, Nov. 2005, pp. 782-788.
[8] B. Crone, A. Dodabalapur, A. Gelperin, L. Torsi, H.E. Katz, A.J. Lovinger, and Z. Bao, "Electronic sensing of vapors with organic transistors," *Applied Physics Letters*, vol. 78, Apr. 2001, pp. 2229-2231.
[9] J. Huang, J. Miragliotta, A. Becknell, and H.E. Katz, "Hydroxy-Terminated Organic Semiconductor-Based Field-Effect Transistors for Phosphonate Vapor Detection," *Journal of the American Chemical Society*, vol. 129, 2007, pp. 9366-9376.
[10] L. Torsi, M.C. Tanese, N. Cioffi, M.C. Gallazzi, L. Sabbatini, P.G. Zambonin, G. Raos, S.V. Meille, and M.M. Giangregorio, "Side-chain role in chemically sensing conducting polymer field-effect transistors," *J. Phys. Chem. B*, vol. 107, 2003, pp. 7589–7594.
[11] F. Liao, C. Chen, and V. Subramanian, "Organic TFTs as gas sensors for electronic nose applications," *Sensors and Actuators B: Chemical*, vol. 107, Jun. 2005, pp. 849-855.
[12] L. Torsi, A. Dodabalapur, L. Sabbatini, and P.G. Zambonin, "Multi-parameter gas sensors based on organic thin-film-transistors," *Sensors and Actuators B: Chemical*, vol. 67, Sep. 2000, pp. 312-316.
[13] J.M. Charlesworth, A.C. Partridge, and N. Garrard, "Mechanistic studies on the interactions between poly(pyrrole) and organic vapors," *The Journal of Physical Chemistry*, vol. 97, May. 1993, pp. 5418-5423.
[14] L. Torsi, M.C. Tanese, N. Cioffi, M.C. Gallazzi, L. Sabbatini, and P.G. Zambonin, "Alkoxy-substituted polyterthiophene thin-film-transistors as alcohol sensors," *Sensors and Actuators B: Chemical*, vol. 98, Mar. 2004, pp. 204-207.
[15] H. Katz and J. Huang, "Thin-Film Organic Electronic Devices," *ANNUAL REVIEW OF MATERIALS RESEARCH*, vol. 39, 2009, pp. 71-92.
[16] L. Torsi, A.J. Lovinger, B. Crone, T. Someya, A. Dodabalapur, H.E. Katz, and A. Gelperin, "Correlation between Oligothiophene Thin Film Transistor Morphology and Vapor Responses," *The Journal of Physical Chemistry B*, vol. 106, Dec. 2002, pp. 12563-12568.
[17] J. Janata and M. Josowicz, "Conducting polymers in electronic chemical sensors," *Nat Mater*, vol. 2, Jan. 2003, pp. 19-24.
[18] P. Topart and M. Josowicz, "Transient effects in the interaction between polypyrrole and methanol vapor," *The Journal of Physical Chemistry*, vol. 96, Oct. 1992, pp. 8662-8666.
[19] B. Adhikari and S. Majumdar, "Polymers in sensor applications," *Progress in Polymer Science*, vol. 29, Jul. 2004, pp. 699-766.
[20] J. Lee, M. Heeney, S. Tierney, I. McCulloch, A. Murphy, J. Liu, J.M.J. Frechet, and V. Subramanian, ""Stability in OTFT gas sensors," Organic Thin-Film Electronics, edited by A.C. Arias, N. Tessler, L. Burgi, and J.A. Emerson," *Mater. Res. Soc. Symp. Proc.*, vol. 871E, Warrendale, PA, 2005, p. I1.5.
[21] R.H. Dainty, R.A. Edwards, C.M. Hibbard, and S.V. Ramantanis, "Bacterial sources of putrescine and cadaverine in chill stored vacuum-packaged beef," *Journal of Applied Microbiology*, vol. 61, 1986, pp. 117-123.
[22] R. EDWARDS, R. DAINTY, and C. HIBBARD, "Putrescine and cadaverine formation in vacuum packed beef," *Journal of Applied Microbiology*, vol. 58, 1985, pp. 13-19.

Chapter Five

[1] L. Torsi, M.C. Tanese, N. Cioffi, M.C. Gallazzi, L. Sabbatini, and P.G. Zambonin, "Alkoxy-substituted polyterthiophene thin-film-transistors as alcohol sensors," *Sensors and Actuators B: Chemical*, vol. 98, Mar. 2004, pp. 204-207.

[2] P. Dutta, "Grazing incidence X-ray diffraction," *Current Science*, vol. 78, Jun. 2000, pp. 1478-1483.

[3] S. Fritz, "Structure and Transport in Organic Semiconductor Thin Films," University of Minnesota, 2006.

[4] T.J. Prosa, M.J. Winokur, J. Moulton, P. Smith, and A.J. Heeger, "X-ray-diffraction studies of the three-dimensional structure within iodine-intercalated poly(3-octylthiophene)," *Physical Review B*, vol. 51, Jan. 1995, p. 159.

[5] T.J. Prosa, M.J. Winokur, J. Moulton, P. Smith, and A.J. Heeger, "X-ray structural studies of poly(3-alkylthiophenes): an example of an inverse comb," *Macromolecules*, vol. 25, 1992, pp. 4364-4372.

[6] H. Yang, T.J. Shin, Z. Bao, and C.Y. Ryu, "Structural transitions of nanocrystalline domains in regioregular poly(3-hexyl thiophene) thin films," *Journal of Polymer Science Part B: Polymer Physics*, vol. 45, 2007, pp. 1303-1312.

[7] B. Adhikari and S. Majumdar, "Polymers in sensor applications," *Progress in Polymer Science*, vol. 29, Jul. 2004, pp. 699-766.

[8] P. Bertrand, A. Jonas, A. Laschewsky, and R. Legras, "Ultrathin polymer coatings by complexation of polyelectrolytes at interfaces: suitable materials, structure and properties," *Macromolecular Rapid Communications*, vol. 21, 2000, pp. 319-348.

[9] K. Kago, H. Endo, H. Matsuoka, H. Yamaoka, N. Hamaya, M. Tanaka, and T. Mori, "Characterization of thin polymer films by X-ray reflectometry with synchrotron radiation," *JOURNAL OF SYNCHROTRON RADIATION*, vol. 5, Sep. 1998, pp. 1304-1308.

[10] M.F. Toney, C.M. Mate, K.A. Leach, and D. Pocker, "Thickness Measurements of Thin Perfluoropolyether Polymer Films on Silicon and Amorphous-Hydrogenated Carbon with X-Ray Reflectivity, ESCA and Optical Ellipsometry," *Journal of Colloid and Interface Science*, vol. 225, May. 2000, pp. 219-226.

[11] J. Schmitt, T. Gruenewald, G. Decher, P.S. Pershan, K. Kjaer, and M. Loesche, "Internal structure of layer-by-layer adsorbed polyelectrolyte films: a neutron and x-ray reflectivity study," *Macromolecules*, vol. 26, Dec. 1993, pp. 7058-7063.

[12] J. Schmitt, G. Decher, W.J. Dressick, S.L. Brandow, R.E. Geer, R. Shashidhar, and J.M. Calvert, "Metal nanoparticle/polymer superlattice films: Fabrication and control of layer structure," *Advanced Materials*, vol. 9, 1997, pp. 61-65.

[13] K. Tashiro, M. Kobayashi, T. Kawai, and K. Yoshino, "Crystal structural change in poly(3-alkyl thiophene)s induced by iodine doping as studied by an organized combination of X-ray diffraction, infrared/Raman spectroscopy and computer simulation techniques," *POLYMER*, vol. 38, Jun. 1997, pp. 2867-2879.

[14] J. Lu, E. Lee, and R. Thomas, "The analysis and interpretation of neutron and X-ray specular reflection," *ACTA CRYSTALLOGRAPHICA SECTION A*, vol. 52, Jan. 1996, pp. 11-41.

[15] M. Tolan, *X-Ray Scattering from Soft-Matter Thin Films: Materials Science and Basic Research*, Springer-Verlag Telos, 1999.

[16] L.G. Parratt, "Surface Studies of Solids by Total Reflection of X-Rays," *Physical Review*, vol. 95, Jul. 1954, p. 359.
[17] M. Tolan, *X-Ray Scattering from Soft-Matter Thin Films: Materials Science and Basic Research*, Berlin; New York: Springer-Verlag Telos, 1999.
[18] J. Daillant and A. Gibaud, *X-ray and Neutron Reflectivity Principles and Applications*, New York: Springer, 1999.

Chapter Six

[1] J.B. Chang, V. Liu, V. Subramanian, K. Sivula, C. Luscombe, A. Murphy, J. Liu, and J.M.J. Frechet, "Printable polythiophene gas sensor array for low-cost electronic noses," *Journal of Applied Physics*, vol. 100, Jul. 2006, pp. 014506-7.
[2] R. Dainty, R. Edwards, and C. Hibbard, "Time course of volatile compound formation during refrigerated storage of naturally contaminated beef in air," *Journal of Applied Microbiology*, vol. 59, 1985, pp. 303-309.
[3] Braun P., Fehlhaber K., Klug C., and Kopp K., "Investigations into the activity of enzymes produced by spoilage-causing bacteria: a possible basis for improved shelf-life estimation," *Food Microbiology*, vol. 16, Oct. 1999, pp. 531-540.
[4] H. Alomirah, I. Alli, B. Gibbs, and Y. Konishi, "Identification of Proteolytic Products as Indicators of Quality in Ground and Whole Meat," *Journal of Food Quality*, vol. 21, 1998, pp. 299-316.
[5] A. Kakouri and G. Nychas, "Storage of poultry meat under modified atmospheres or vacuum packs: possible role of microbial metabolites as indicator of spoilage," *Journal of Applied Microbiology*, vol. 76, 1994, pp. 163-172.
[6] R.H. Dainty, R.A. Edwards, C.M. Hibbard, and S.V. Ramantanis, "Bacterial sources of putrescine and cadaverine in chill stored vacuum-packaged beef," *Journal of Applied Microbiology*, vol. 61, 1986, pp. 117-123.
[7] R. Edward, R. Dainty, and C. Hibbard, "Putrescine and cadaverine formation in vacuum packed beef," *Journal of Applied Microbiology*, vol. 58, 1985, pp. 13-19.
[8] L. Gram and H.H. Huss, "Microbiological spoilage of fish and fish products," *International Journal of Food Microbiology*, vol. 33, Nov. 1996, pp. 121-137.
[9] A. Pacquit, K.T. Lau, H. McLaughlin, J. Frisby, B. Quilty, and D. Diamond, "Development of a volatile amine sensor for the monitoring of fish spoilage," *Talanta*, vol. 69, Apr. 2006, pp. 515-520.
[10] M.H.S. Santos, "Biogenic amines: their importance in foods," *International Journal of Food Microbiology*, vol. 29, Apr. 1996, pp. 213-231.
[11] R.A. Bissell, K.C. Persaud, and P. Travers, "The influence of non-specific molecular partitioning of analytes on the electrical responses of conducting organic polymer gas sensors," *Physical Chemistry Chemical Physics*, vol. 4, 2002, pp. 3482-3490.
[12] Z. Bao, J.A. Rogers, and H.E. Katz, "Printable organic and polymeric semiconducting materials and devices," *Journal of Materials Chemistry*, vol. 9, 1999, pp. 1895-1904.
[13] H.E. Katz and Z. Bao, "The Physical Chemistry of Organic Field-Effect Transistors," *The Journal of Physical Chemistry B*, vol. 104, Feb. 2000, pp. 671-678.

[14] Z. Bao and A.J. Lovinger, "Soluble Regioregular Polythiophene Derivatives as Semiconducting Materials for Field-Effect Transistors," *Chemistry of Materials*, vol. 11, 1999, pp. 2607-2612.
[15] H. Sirringhaus, N. Tessler, and R.H. Friend, "Integrated Optoelectronic Devices Based on Conjugated Polymers," *Science*, vol. 280, Jun. 1998, pp. 1741-1744.
[16] M. Surin, P. Leclere, R. Lazzaroni, J. Yuen, G. Wang, D. Moses, A. Heeger, S. Cho, and K. Lee, "Relationship between the microscopic morphology and the charge transport properties in poly(3-hexylthiophene) field-effect transistors," *JOURNAL OF APPLIED PHYSICS*, vol. 100, Aug. 2006.
[17] J.M. Charlesworth, A.C. Partridge, and N. Garrard, "Mechanistic studies on the interactions between poly(pyrrole) and organic vapors," *The Journal of Physical Chemistry*, vol. 97, May. 1993, pp. 5418-5423.
[18] J. Park, W.A. Groves, and E.T. Zellers, "Vapor Recognition with Small Arrays of Polymer-Coated Microsensors. A Comprehensive Analysis," *Analytical Chemistry*, vol. 71, 1999, pp. 3877-3886.
[19] H.E. Katz, "Chemically Sensitive Field-Effect Transistors and Chemiresistors: New Materials and Device Structures," *Electroanalysis*, vol. 16, 2004, pp. 1837-1842.
[20] R.A. McGill, T.E. Mlsna, R. Chung, V.K. Nguyen, and J. Stepnowski, "The design of functionalized silicone polymers for chemical sensor detection of nitroaromatic compounds," *Sensors and Actuators B: Chemical*, vol. 65, Jun. 2000, pp. 5-9.
[21] E.J. Houser, T.E. Mlsna, V.K. Nguyen, R. Chung, R.L. Mowery, and R. Andrew McGill, "Rational materials design of sorbent coatings for explosives: applications with chemical sensors," *Talanta*, vol. 54, May. 2001, pp. 469-485.
[22] J. Huang, J. Miragliotta, A. Becknell, and H.E. Katz, "Hydroxy-Terminated Organic Semiconductor-Based Field-Effect Transistors for Phosphonate Vapor Detection," *Journal of the American Chemical Society*, vol. 129, 2007, pp. 9366-9376.

Chapter Seven

[1] J. Huang, J. Miragliotta, A. Becknell, and H.E. Katz, "Hydroxy-Terminated Organic Semiconductor-Based Field-Effect Transistors for Phosphonate Vapor Detection," *Journal of the American Chemical Society*, vol. 129, 2007, pp. 9366-9376.
[2] J.B. Chang, V. Liu, V. Subramanian, K. Sivula, C. Luscombe, A. Murphy, J. Liu, and J.M.J. Frechet, "Printable polythiophene gas sensor array for low-cost electronic noses," *Journal of Applied Physics*, vol. 100, Jul. 2006, pp. 014506-7.
[3] F. Liao, C. Chen, and V. Subramanian, "Organic TFTs as gas sensors for electronic nose applications," *Sensors and Actuators B: Chemical*, vol. 107, Jun. 2005, pp. 849-855.
[4] F. Liao, S. Yin, M. Toney, and V. Subramanian, "Physical Discrimination of Amine Vapor Mixtures Using Polythiophene Gas Sensor Arrays," *Submitted for publication*.
[5] F. Liao, M. Toney, and V. Subramanian, "Thickness changes in polythiophene gas sensors exposed to vapor," *Submitted for publication*.
[6] F. Liao and V. Subramanian, "Experimental and theoretical studies for optimization of polythiophene gas sensor arrays," *ECS Transactions*, Honolulu, Hawaii: 2008, pp. 529-538.

[7] F. Liao, C. Chen, and V. Subramanian, "Organic TFT Gas Sensors for Electronic Nose Applications," *Materials Research Society Spring Meeting*, San Francisco: 2004.
[8] C. Chen, F. Liao, and V. Subramanian, "The role of film thickness in organic thin film transistor gas sensors," *Materials Research Society Spring Meeting*, San Francisco: 2004.

Appendix A: Additional 2D-GIXD Patterns of Spun Polythiophene Films

For the sake of brevity and clarity, not all 2D-GIXD patterns were included in Chapter Five. The remaining patterns are included here for reference. For convenience, Table I relists the material parameters that were varied in these samples.

Material	Side Chain Functionality	Side Chain Length	Anneal Time
poly-3-butylthiophene	Alkyl	4	5 min
poly-3-butylthiophene	Alkyl	4	24 hours
poly-3-octylthiophene	Alkyl	8	5 min
poly-3-octylthiophene	Alkyl	8	24 hours
poly-(3-ethyl-4-butanoate)thiophene	Ester	4	5 min
poly-(3-ethyl-4-butanoate)thiophene	Ester	4	24 hours
poly-(3-ethyl-4-heptanoate)thiophene	Ester	7	5 min
poly-(3-ethyl-4-heptanoate)thiophene	Ester	7	24 hours

Table I. The parameters of the different polythiophene materials investigated with GIXD.

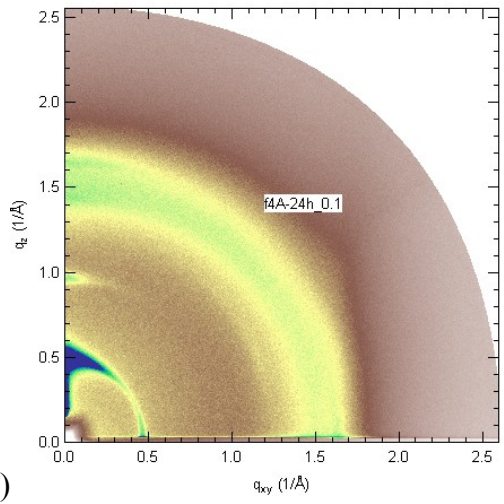

(a)

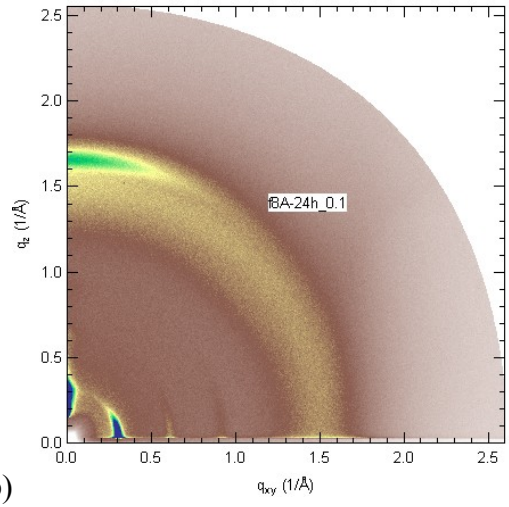

(b)

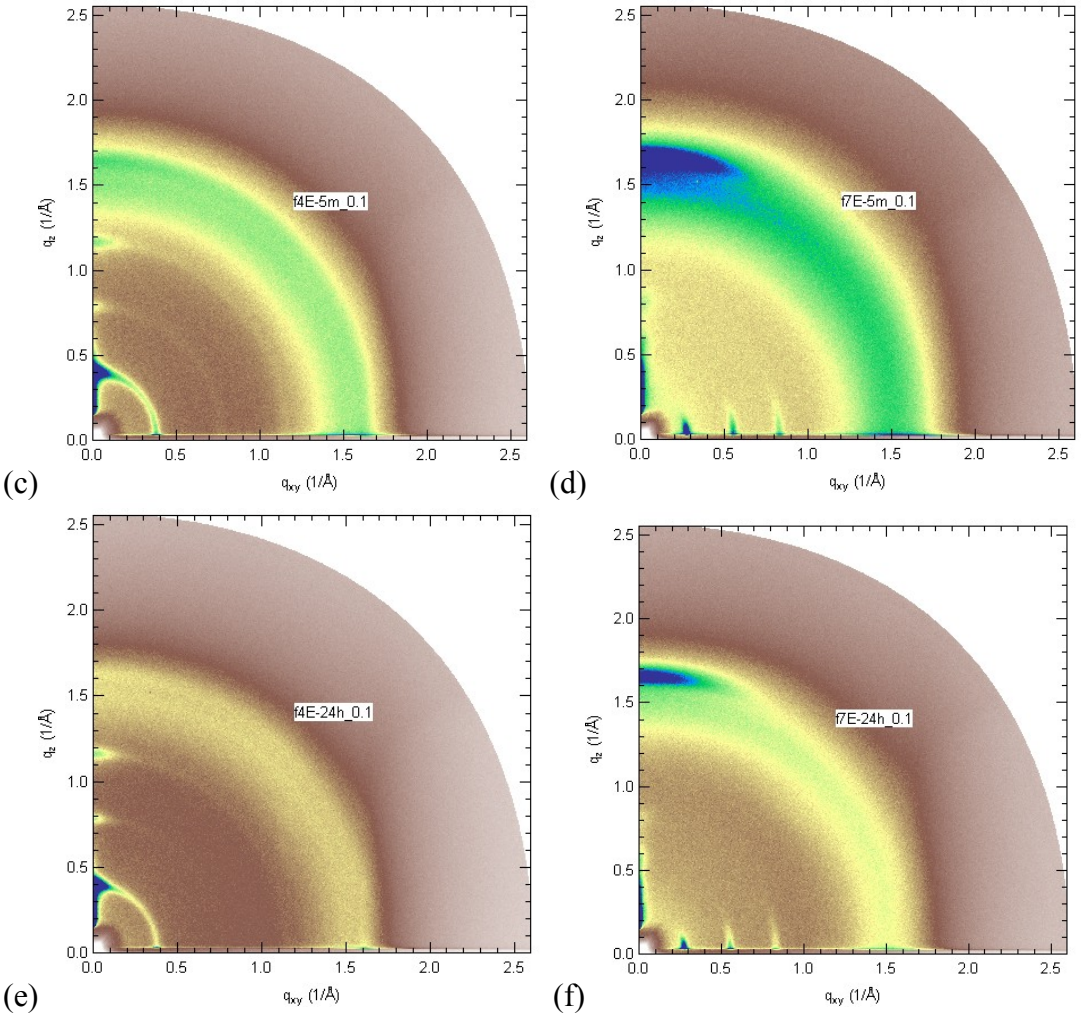

(c) (d)

(e) (f)

Figure 1. GIXD patterns of (a) poly-3-butylthiophene annealed for 24 hours, (b) poly-3-octylthiophene annealed for 24 hours, (c) poly-(3-ethyl-4-butanoate)thiophene annealed for 5 minutes, (d) poly-(3-ethyl-4-heptanoate)thiophene annealed for 5 minutes, (e) poly-(3-ethyl-4-butanoate)thiophene annealed for 24 hours, (f) poly-(3-ethyl-4-heptanoate)thiophene annealed for 24 hours.

Appendix B: Background on X-Ray Reflectivity for Thickness Measurements

This appendix covers some additional background of X-Ray Reflectivity (XRR) for thickness measurements, specifically the limits of the technique. The majority of this material is derived from "*High Resolution X-Ray Scattering: From Thin Films to Lateral Nanostructures*" by Ullrich Pietsch, Václav Holý, and Tilo Baumbach (Springer 2004 2nd Ed.) and the reader is recommended to consult this text for more details.

Additional Background on XRR

Accurate measurement of the thickness of a film can be determined by from the angular positions of the subsidiary maxima on the reflection curves. These maxima are caused by the interference of the waves reflected from the upper and lower interfaces of the layers. The appearance of this interference pattern depends on the reflectivities of both boundaries, which includes the x-ray refraction indices above and below the boundaries and the interface roughness.

From general dynamical formulae, the expression for reflectivity of a single layer deposited on a semi-infinite substrate is:

$$R = \left| \frac{r_1 + r_2 e^{-2ik_{0z}T}}{1 + r_1 r_2 e^{-2i_{0z}T}} \right|^2 \qquad \text{Equation A2.1}$$

where $r_{1,2}$ are the Fresnel reflectivity coefficients of the free surface and the substrate interface, respectively, k_{0z} is the vertical component of the wave vector of the beam transmitted through the layer, and T is the layer thickness. Therefore, the formula indicates that intensity maxima appear whenever $\exp(-2ik_{0z}T) = 1$, at angle positions aim. This condition can be expressed by

$$2T\sqrt{\boldsymbol{sin}^2\,\alpha_{im} - \boldsymbol{sin}^2\,\alpha_c} = m\lambda \qquad \text{Equation A2.2}$$

where m is an integer, $\boldsymbol{sin}\,\alpha_c = \sqrt{2(1-n)}$ and α_c is the critical angle of total external reflection of the layer and n is the layer refractive index. Equation A2.2 is analogous to the Bragg equation but modified by the influence of refraction. The subsequent fringes are called *Kiessig* fringes, in honor of their discoverer.

Limits and Accuracy of XRR Measurements

The range of layer thicknesses that can be measured by XRR depends on the intensity and divergence of the primary beam, on the angular resolution, and on the total angular range of the goniometer used, as well as on the wavelength λ.

In the case of a single layer film (which is the only structure that will be considered in this Appendix), the distance between the adjacent interference maxima is given by

$$\delta\eta_i = G\frac{\lambda}{2T} \qquad \text{Equation A2.3}$$

where G is a geometry factor, which is unity for XRR.

Therefore, the upper limit of the measurable thickness, T, is determined by the primary-beam divergence and/or the angular resolution of the diffractometer. For example, if the divergence of the primary beam 0.01° and λ = 0.15405 nm (CuKα_1 line), the maximum measurable layer thickness is smaller than about 0.43 μm.

$$T_{max} = G\frac{\lambda}{2\delta\eta_i} = 1\frac{0.154\cdot 10^{-9}}{2\cdot 0.01^{\circ}\cdot \pi/180} = 0.44\ \mu m \qquad \text{Equation A2.4}$$

The lower limit is given by the accessible angular range; in other words, the maximum incidence angle, α_i, that gives a measurable reflectivity. Therefore, the number of decades of intensity essentially determines the minimum layer thickness. If the intensity is too low, then the reflectivity will fall below detection before a maxima feature can be seen. For instance, the determination of a layer thickness of 1.5 nm requires measurements up to α_i = 3° at least. In order to detect one single fringe period corresponding to the thickness of a single atomic layer (T ≈ 0.3 nm), a dynamical range of up to ten orders of magnitude in intensity is required.

The accuracy of the thickness measurements depends on the smallest angular step $\delta\alpha_i$ of the goniometer and on the layer thickness T. Neglecting refraction the accuracy can be estimated from

$$\frac{\Delta T}{T} = \frac{\Delta\alpha_i}{\alpha} \approx \frac{\alpha_i}{m_{max}} \qquad \text{Equation A2.5}$$

This accuracy is of the order of 1% if the oscillation maximum measured at α_i = 1° is determined with an accuracy better than $\Delta\alpha_i$ = 0.01°. Equation A2.5 can be expressed in terms of the largest fringe order that is detected in the reflectivity curve with an accuracy of one-half of a fringe period. For example, if m_{max} = 45 at $2\alpha_i$ ≈ 5.0°, then the layer thickness t is determined

with a relative error of $\frac{\Delta T}{T} \approx 2\%$. The accuracy of the layer thickness can be preserved as long as a sufficient number of fringe maxima appear within the detectable angular interval.